National Library of Canada
Acquisitions and Bibliographic Services Branch
395 Wellington Street
Ottawa, Ontario
K1A 0N4

Bibliothèque nationale du Canada
Direction des acquisitions et des services bibliographiques
395, rue Wellington
Ottawa (Ontario)
K1A 0N4

Your file Votre référence

Our file Notre référence

NOTICE

The quality of this microform is heavily dependent upon the quality of the original thesis submitted for microfilming. Every effort has been made to ensure the highest quality of reproduction possible.

If pages are missing, contact the university which granted the degree.

Some pages may have indistinct print especially if the original pages were typed with a poor typewriter ribbon or if the university sent us an inferior photocopy.

AVIS

La qualité de cette microforme dépend grandement de la qualité de la thèse soumise au microfilmage. Nous avons tout fait pour assurer une qualité supérieure de reproduction.

S'il manque des pages, veuillez communiquer avec l'université qui a conféré le grade.

La qualité d'impression de certaines pages peut laisser à désirer, surtout si les pages originales ont été dactylographiées à l'aide d'un ruban usé ou si l'université nous a fait parvenir une photocopie de qualité inférieure.

Canada

Hot Working of High Temperature Rapidly Solidified Aluminum Alloys FVS1212 and 8009 (FVS0812)

David Shimansky

A Thesis

in

The Department

of

Mechanical Engineering

Presented in Partial Fulfilment of the Requirements

for the Degree of Master of Applied Science at

Concordia University

Montreal, Quebec, Canada

September 1995

ISBN 0-612-05138-2

ABSTRACT

Hot Working of High Temperature Rapidly Solidified Aluminum Alloys FVS1212 and 8009 (FVS0812)

David Shimansky

Isothermal hot torsion tests were performed on two rapidly solidified aluminum alloys FVS1212 (Al-12.4Fe-1.2V-2.3Si) and 8009 or FVS0812 (Al-8.5Fe-1.3V-1.7Si). Both of the above alloys are produced by Allied Signal Company. The materials were tested in torsion over the range of 300°C to 600°C and at a strain rate ($\dot{\varepsilon}$) ranging from 0.1 to 4.0 s^{-1}. Flow stress (σ) and strain-to-failure (ε_f) data were determined and compared with published results. The flow stress decreased gradually with increasing deformation temperature (T) and declining $\dot{\varepsilon}$, following the general trend for aluminum alloys. Due to deformation heating and possible localized dynamic recrystallization, stress peaks feature prominently in the equivalent σ-ε curves. Increase of fracture strain with rise in T and with decrease of $\dot{\varepsilon}$ at the same T have been observed in compliance with the general trend for aluminum alloys. However, FVS1212 and 8009 show very low ductility in comparison with conventional aluminum alloys, thus shaping conditions for these materials have to be carefully controlled.

The flow stress peak was found to fit the following constitutive equation

$$A[\sinh(\alpha\sigma)]^n = \dot{\varepsilon}\exp(Q/RT)$$

An almost constant stress exponent (n) at constant stress multiplier (α) governs the σ-ε relationship at a constant T. In the Arrhenius function, the activation energy (Q) for hot deformation was found to be much higher than that of pure aluminum and some powder-

consolidated rapidly-solidified aluminum alloys. This can be ascribed to the high volume fraction of very fine nearly spherical $Al_{13}(Fe,V)_3Si$ dispersoids which present major obstacles to dislocation motion. The hot working behaviour related to dynamic recovery mechanisms begins for FVS0812 (8009) at 300°C, while for FVS1212 it may only begin at 400°C due to much higher silicide concentration. Both alloys exhibited a linear correlation of slope s values in the Arrhenius plots with α. An inverse correlation between n and α is found As a net result of the above two relationships, Q is independent of α. The optimum coefficient values for both alloys were established for α = 0 020 MPa^{-1}.

PREFACE

The work described in this thesis was carried out by me in the Department of Mechanical Engineering, Concordia University and the Department of Mining and Metallurgy, McGill University between September 1990 and May 1995 Under the supervision of Dr. H.J. McQueen, this research was triggered by my interests in the high strength materials, as well as my affiliation with Allied Signal Company, where I held the position of Senior Mechanical Engineer from 1986 to 1991

No part of this thesis has been previously submitted for a degree at this or any other university. Data used in this thesis from other research work has been acknowledged in the text. A list of references is included at the end of the thesis

I would like to express my belief that it will not be very long that these very special materials will find their way not only in aerospace but also in rehabilitation and bioengineering applications As an engineer and designer, I feel that it is our privilege and obligation to design for humanity and I hope that this work will help to serve this purpose

ACKNOWLEDGMENTS

I wish to express my gratitude and appreciation to my supervisor Dr. Hugh J McQueen who provided guidance and encouragement throughout this research project He is a rare individual, whose commitment and dedication to science takes precedence over his personal needs

I also wish to thank my fellow student Peter Sakaris for his great and essential help in conducting the experiments and giving technical assistance with respect to the hot torsion testing machine and helping organize the data

Special words of gratitude to Dr. Paul Gilman of Allied Signal Company who has provided the machined samples of 8009 and FVS1212 aluminum alloys, as well as various technical publications on these materials

I would also like to thank my family, my wife Charlene Wald-Shimansky, who has supported me through the long hours of my studies and my daughters Beverley and Michaela for understanding

I would also like to acknowledge the honorable chairman, Dr. T. Krepec and the members of the examining committee, Dr. X. Xia, Dr. J V. Svoboda and Dr. D. Feldman for taking their precious time to review the thesis and participate during my thesis defense.

DEDICATION

To the memory of my teacher and friend, Dr. Jaan Aaron Saber,
who had inspired me on the never ending path of learning.

To my father, Shlomo Shimansky,
for showing me the meaning of true values in life.

To the memory of my mother, Brocha (Bronia) Shimansky,
whose greatest gift to me was the lesson of courage and spiritual strength

David Shimansky

For They Conquer
Who Believe They Can

John Dryden (1631-1700)

TABLE OF CONTENTS

Page

LIST OF FIGURES x

LIST OF TABLES xiv

NOMENCLATURE xv

CHAPTER

1 INTRODUCTION 1

2 CHARACTERISTICS OF HIGH TEMPERATURE RAPIDLY SOLIDIFIED ALUMINUM ALLOYS 2

2 1 Brief History 2

2 2 General Information 5

2 3 Rapid Solidification Processing 8

2 4 High Temperature Aluminum Alloys 21

2 5 Applications 44

2.6 Future Trends 54

3 HOT WORKING CHARACTERISTICS 56

3 1 General Information 56

3.2 Stress-Strain Curves 57

3.2.1 Dynamic Recovery (DRV) and Recrystallization (DRX) 59

3.2.2 Deformation Heating 60

3 2.3 Structural Changes 62

3.3 Ductility 62

3 4 Strain Rate Sensitivity 65

3.5 Interdependence of Stress, Strain Rate and Temperature 66

Page

4 EXPERIMENTAL PROCEDURE 71

4 1 Torsion Testing... 71

4 2 Testing System and Equipment 72

4 3 Test Materials. 74

4.4 Test Procedure. .. 74

5 EXPERIMENTAL RESULTS . . 77

5.1 Stress-Strain Curves. .. 77

5.2 Ductility..... 80

5.3 Constitutive Plots.. 80

6 DISCUSSION..... 95

6.1 Stress-Strain Curves.. . . 95

6.2 Ductility.. 99

6.3 Strain Rate Sensitivity and Superplasticity 100

6.4 Interdependence of Stress, Strain Rate and Temperature 104

7. CONCLUSIONS..... 109

REFERENCES.... 111

LIST OF FIGURES

Page

FIGURE

2.1 Development of High Strength Aluminum Alloys During the Past 20 Years (2) 4

2.2 Rapid Solidification Yields Powder Formed by (a) Hot Extrusion and (b) Ramming in Shaped Container (10) 6

2.3 Merchant's Shot Tower in Baltimore (12) 10

2.4 Schematic representation of Roller Atomization: a = Liquid Metal Stream; b = Heat Source, c = Rolls; d = Metal Powder (11). 12

2.5 Rapid Solidification Powder Fabrication Using (a) Centrifugal Atomization or (b) Inert Gas Atomization (10) 13

2.6 Allied RST Powder Process (13). 16

2.7 Allied Planar Flow Casting (13) 16

2.8 Allied Planar Flow Casting for Crystalline Alloys (13) 16

2.9 Comparison of Elevated Temperature Tensile Yield Strengths of Various High Temperature and Standard Aerospace Aluminum Alloys (26). 25

2.10 Comparison of Coarsening Rates of Dispersoids in Various Rapidly Solidified Al-TM alloys, r = average particle size at time t (26) 29

2.11 Fracture Toughness K_{IC} vs. Yield Strength Relationship for High Temperature Aluminum Alloys (26) 30

2.12 Microstructures of RSP Al-8Fe-1V-2Si Alloys (a) In As-Quenched Melt-Spun Ribbon and (b) After Extrusion (18 to 1) at 375°C (26) 31

2.13 Corrosion Rates of Rapidly Solidified Al-8Fe-1V-2Si and Rapidly Solidified Al-Li Compared with Aluminum Alloy 2014-T6 and other Powder Metallurgy Aluminum Alloys (26) 33

Page

FIGURE

2.14 Tensile Properties of Rapidly Solidified High Temperature Al-Fe-V-Si Alloys (42).. 34

2.15 Tensile Properties of Alloys FVS0812 and FVS1212 After 425°C Exposures Up To 1000 Hours (42) 35

2.16 Creep Rupture Strength as a Fuction of the Larson-Miller Parameter for Alloy FVS0812 (42) 36

2 17 Specific Stiffness of Alloys FVS0812 and FVS1212 as a Function of Temperature (42) 37

2 18 Creep Curves for Alloy FVS1212 (a) At 479°C Plotted as Strain Rate vs Strain and (b) Stress Dependence of the Creep Rate with Stress Exponent, n (39) 39

2.19 Diffusion Normalized Strain Rate Versus Modulus Compensated Stress for Creep Tests Assuming An Activation Energy for Creep of (a) 360 kJ/mol and (b) 150 kJ/mol (39).... . . . 40

2.20 Variation of Coarsening Rates as a Function of Applied Stress (a) Linear and (b) Log-Log (39).. 41

2 21 Temperature Dependence of the Elastic Modulus for FVS1212 (39) 42

2 22 Comparison of Predicted Coarsening Behavior of Alloy FVS1212 (39) 43

2.23 Flight Control Actuator (44) 46

2.24 Bulkhead Component (44) 47

2.25 Strength/Fracture Toughness Combinations of Rapidly Solidified Al-Fe-V-Si Alloys (32) 48

2.26 Tensile Strength at Temperature of Alloy FVS0812 Compared to Aluminum Alloy 2014-T6 (32)..... 49

2.27 Fatigue Crack Growth Rates of Alloy FVS0812 (32) 51

2.28 Corrosion Performance of Alloy FVS0812 in a Salt Fog (ASTM B-117) (32)..... 52

Page

FIGURE

3 1 Selection of Equivalent Stress-Strain Curves Obtained from Torsion Tests of Al-20Si-7.5Ni-3Cu-1Mg at (a) 400°C and (b) 0.083 s^{-1} (59). 58

3 2 Microstructures of Al-20Si-7 5Ni-3Cu-1Mg at 400°C and 2.49 s^{-1} (a) General Structure; (b) Interaction Between Particles and Subgrain Boundaries; (c) Outcrop of Recrystallization at a Particle (59). 61

3 3 Strain to Fracture at Different Temperatures and Strain Rates for Al-20Si-7 5Ni-3Cu-1Mg (59). 64

3 4 Application of the Hyperbolic Sine Equation at the Given Temperatures to Determine the Constitutive Constant n(in Equation 3 3 for Al-20Si-7 5Ni-3Cu-1Mg (59) 67

3 5 Determination of the Activation Energy for Al-20Si-7 5Ni-3Cu-1Mg at the Peak Stress, Surface Equivalent Strain Rates (59) 68

3 6 Applicability of the Zener-Hollomon Parameter to Torsional Deformation for Al-20Si-7 5Ni-3Cu-1Mg (59). 70

4 1 Torsion Testing Machine (80).. 73

4.2 Torsion Specimen Design 76

5 1 Stress-Strain Curves: (a) 8009 and (b) FVS1212.. 78

5.2 Peak Stress vs Temperature: (a) 8009 and (b) FVS1212 79

5 3 Strain-To-Fracture versus Temperature: (a) 8009 and (b) FVS1212. . . . 81

5 4 Arrhenius Plots for 8009 at (a) $\alpha = 0.020$ MPa^{-1}; (b) $\alpha = 0.040$ MPa^{-1}; (c) $\alpha = 0.052$ MPa^{-1} and (d) $\alpha = 0.080$ MPa^{-1}. 85

5 5 Arrhenius Plots for FVS1212 at (a) $\alpha = 0.020$ MPa^{-1}; (b) $\alpha = 0.040$ MPa^{-1}; (c) $\alpha = 0\ 052$ MPa^{-1} and (d) $\alpha = 0.080$ MPa^{-1}. 86

5.6 Slope versus Stress Multiplier: (a) 8009 and (b) FVS1212.. 87

5.7 Log Strain Rate Versus Log Sinh($\alpha\sigma$) for 8009 at (a) $\alpha = 0.020$ MPa^{-1}; (b) $\alpha = 0.040$ MPa^{-1}; (c) $\alpha = 0.052$ MPa^{-1} and (d) $\alpha = 0.080$ MPa^{-1}. 88

Page

FIGURE

5.8 Log Strain Rate Versus Log Sinh($\alpha\sigma$) for FVS1212 at (a) α = 0.020 MPa^{-1}; (b) α = 0.040 MPa^{-1}; (c) α = 0.052 MPa^{-1} and (d) α = 0.080 MPa^{-1} 89

5.9 Stress Exponent Versus Stress Multiplier; (a) 8009 and (b) FVS1212 91

5.10 Activation Energy Versus Stress Multiplier, (a) 8009 and (b) FVS1212 92

5.11 Log Zener-Hollomon Parameter versus Log Sinh($\alpha\sigma$) for 8009 at (a) α = 0.020 MPa^{-1}; (b) α = 0.040 MPa^{-1}, (c) α = 0.052 MPa^{-1} and (d) α = 0.080 MPa^{-1} 93

5.12 Log Zener-Hollomon Parameter versus Log Sinh($\alpha\sigma$) for FVS1212 at (a) α = 0.020 MPa^{-1}; (b) α = 0.040 MPa^{-1}; (c) α = 0.052 MPa^{-1} and (d) α = 0.080 MPa^{-1} 94

6.1 Strain Rate Sensitivities for (a) 8009 and (b) FVS1212 102

LIST OF TABLES

TABLE		Page
2 1	Rapidly Solidified Powder Processes (26)	20
2.2	Explosivity of Rapidly Solidified Aluminum Alloy Powders (26)	22
2.3	Diffusivity, Liquid and Solid Solubility of Some Transition Metals in Aluminum (26)	24
2 4	Mechanical Properties of Rapidly Solidified Al-Fe-V-Si Alloys FVS 0611, 0812 and 1212 (32)	27
4 1	Chemical Compositions of Test Materials	75
5 1	Constitutive Constants for Alloy 8009	83
5 2	Constitutive Constants for Alloy FVS1212	84

NOMENCLATURE

a:	Specific Stress Constant [MPa]
A.	Material Constant [s^{-1}]
b:	Specific Slope Constant [MPa]
L:	Specimen Gauge Length [mm]
m:	Strain Rate Sensitivity Exponent
N:	Strain Hardening Rate
n.	Stress Exponent
Q:	Activation Energy for Hot Working [kJ/mol]
R:	Universal Gas Constant [8.314 J/mol-K]
r:	Specimen Gauge Radius [mm]
s	Slope
Z:	Zener-Hollomon Parameter [s^{-1}]
α:	Stress Multiplier [MPa^{-1}]
ε:	Equivalent Strain
$\dot{\varepsilon}$:	Strain Rate [s^{-1}]
θ:	Twist [rad]
σ:	Equivalent Flow Stress [MPa]

1. INTRODUCTION

The object of this research is to determine the hot working behavior of two high temperature rapidly solidified aluminum alloys under continuous deformation conditions. The literature review will provide a background against which the experimental work and results can be compared and analyzed. Torsion is the method of testing employed and has the advantage compared to tension and compression in that large strain can be applied to a specimen at a relatively constant rate. The drawback of the torsion test is that strain and strain rate vary from zero at the axis to a maximum at the surface.

Characteristics of rapidly solidified aluminum alloys are examined in Chapter 2. The literature which describes the general hot working characteristics of these alloys then follows in Chapter 3. A description of the hot torsion machine along with its operating procedure are presented in Chapter 4. A full description of the experimental procedures adopted in the present study is also given. Chapter 5 details all experimental results and a discussion of the results follows in Chapter 6. Finally, in Chapter 7, conclusions are drawn concerning the hot deformation characteristics of the two aluminum alloys based on the present work.

2. CHARACTERISTICS OF HIGH TEMPERATURE RAPIDLY SOLIDIFIED ALUMINUM ALLOYS

2.1 Brief History

Aluminum was little more than a chemical novelty until the metal was first produced commercially in 1854 by Sainte Claire Deville (1). In 1886, Héroult in France and Hall in USA, working independently, made the same discovery, and in that year, they obtained patents for a new process for producing aluminum. This invention was made possible by the progress in electricity production. That ingenious process was the basis for all modern methods of aluminum production and is still the leading process internationally, the only modifications it has undergone being of a technological nature and connected with the changes in production scale (2).

Technological research in the aluminum field has today developed along many different lines on account of the versatility of the application of this metal. Aluminum is the first of the new metals. It belongs to the modern metal age and has been developed on the basis of research and experimental work rather than by craftsmanship. This particular strategy of development was adopted as a result of the pressing needs of aeronautics, just as, many years later the nuclear and aerospace industry resulted in the development of considerable and coordinated efforts with regard to new materials. The new developments resulted in discoveries of lighter, more corrosion resistant, stronger and more temperature resistant materials. In the area of structural efficiency, evolutionary changes have taken place which have provided significant weight savings in airframe structures, and it is in this

area that major increases in efficiency in the future are possible. The concepts of fail-safe and damage tolerant structures are related through design to the fundamental material properties, new concepts of fracture toughness, crack growth propensity of materials and the design philosophy needed to ensure structural integrity (3).

The major material of construction of modern aircraft is aluminum alloys (about 80%). These alloys possess high strength, fracture toughness, and resistance to stress corrosion cracking - the high strength affords minimum weight structures; the high fracture toughness ensures fail-safe design in the presence of flaws or cracks; and the resistance to stress corrosion cracking ensures the ability of the alloy to operate in aggressive environments without premature failure (3).

The chronological pattern of the development of the high-strength alloys over the 40-year period from 1920 to 1960 as described by Hunsicker (4) is depicted in the bar chart shown in Figure 2.1. During this period, alloys were introduced having steadily increasing tensile and yield strengths. New developments in wrought high-strength aluminum alloys have been aimed at improving corrosion resistance, especially to stress corrosion. In aggressive environments, some high-strength aluminum alloys can be subject to a type of corrosive attack, which is characterized by blistering and apparent delamination at or near the metal surface. The path of attack is generally along grain or grain fragment boundaries and frequently initiates at an exposed edge (5-7).

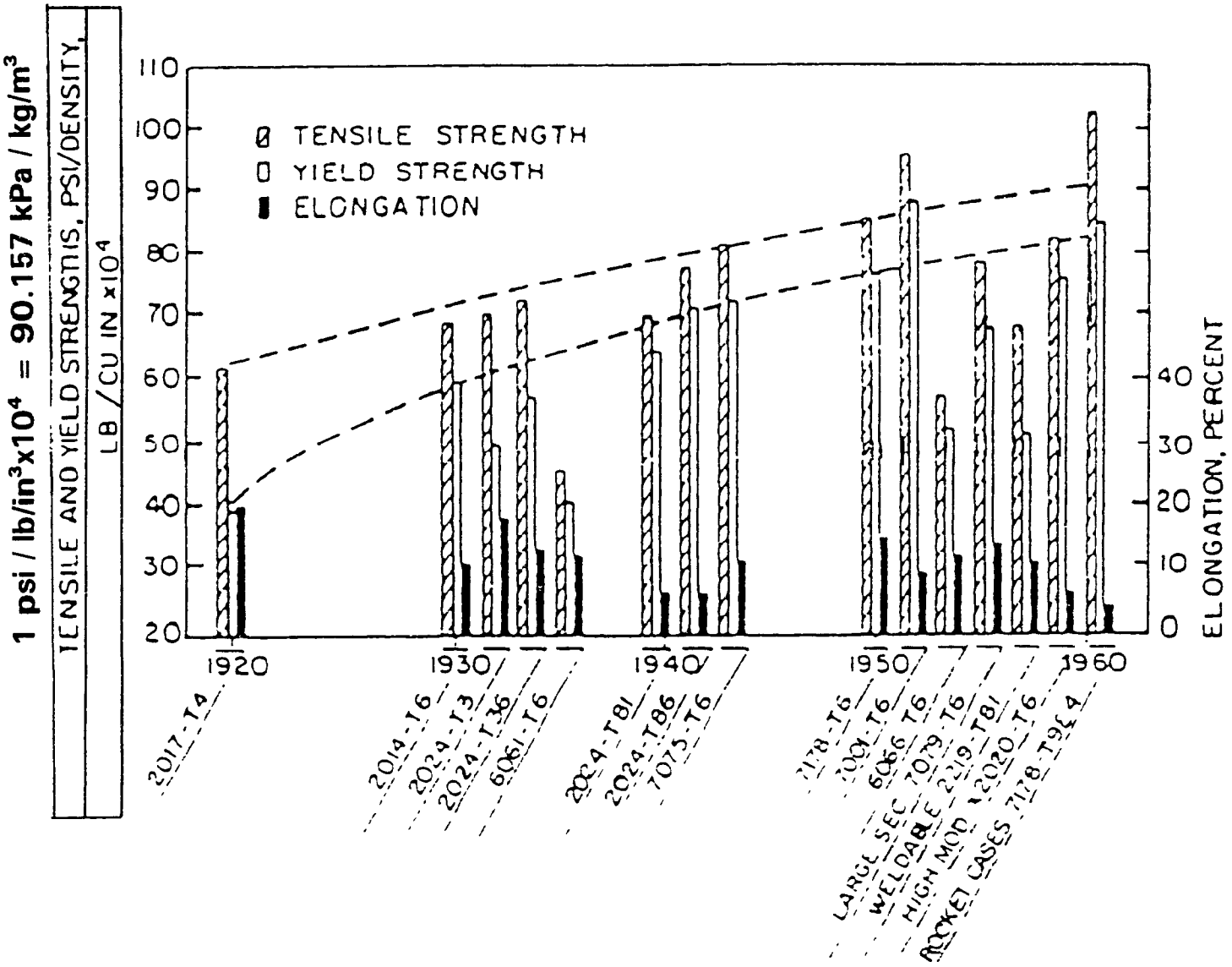

Figure 2.1: Development of High Strength Aluminum Alloys During the Past 20 Years (2)

2.2 General Information

Since the discovery of the rapid solidification process and especially in the past decade, a considerable effort went into development of high-temperature aluminum alloys capable of competing with titanium and steel on a specific strength basis up to 375°C These alloys achieve their strengthening by transition metal intermetallic compounds Various amounts of iron, vanadium and silicon, as well as other alloying elements are combined with aluminum altering strength, rigidity and other properties of the end product The elements are added to molten aluminum, which is fed through an extremely narrow nozzle onto a water-cooled casting wheel There it is quenched at the rate of 1,000,000°C/s and cast at high speed into a very thin ribbon. The ribbon is then pulverized, gases and moisture are removed and the resulting powder is compacted by a vacuum hot press into "billets" which are metal cylinders weighing from 100 to 250 kg (7,8) Consolidation of the metal powder into billets can also be achieved by extrusion. It is also possible to ram into a shaped container as shown in Figure 2 2 in what is called near-net shape forming requiring no subsequent machining, This process therefore offers great technological benefits as a very economical method of fabrication of various parts (9)

From a metallurgical point of view, the metal produced by consolidation, are able to retain the properties of the individual powder particles. General process of fabrication of consolidated billets from powder involves preliminary cold compaction of powder to the density of 70 to 80% The billet is then placed into an aluminum cylinder, is outgased and sealed. The outgased billets undergo hot compaction at 300 to 500°C to the density

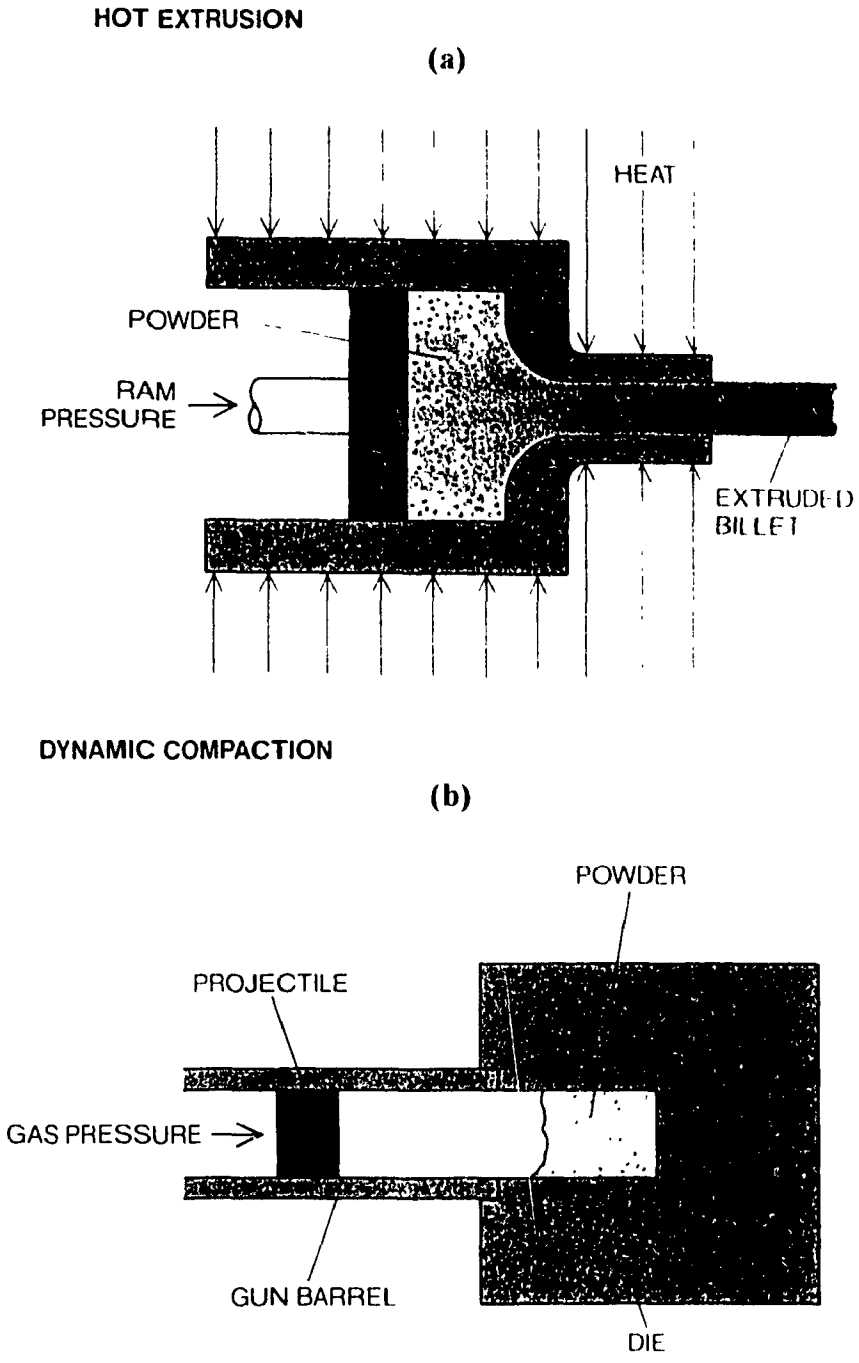

Figure 2.2: Rapid Solidification Yields Powder Formed by (a) Hot Extrusion and (b) Ramming in Shaped Container (10)

of 100%. The aluminum cylinder or capsule is shaved off after the compaction. Immediately after rapid solidification, the powder particles are covered by amorphous aluminum oxide that contains crystals of magnesium oxide (impurities), moreover on the surface of the powder there is a layer that contains water and oxygen If one outgases the powder, the hydroxides disappear while the layer containing aluminum and magnesium oxide become thinner After outgassing the material the thickness of oxide layer drops to 40 A During the further hot processing (hot pressing and stamping) the magnesium oxide decomposes, while the components diffuse into the matrix after the outgasing, the hydrogen content in the powder metal alloy depending on the level of the vacuum, temperature and duration of the outgasing is approximately equal to 0 5 cm^3/100 g of metal which is about the same content as in the cast metal The practice of outgasing the powder and sealing of aluminum capsules reduces the cost of production of the semi-finished product To decrease the cost of consolidating the material, it is conducted in an argon or nitrogen atmosphere In this case the content of the gas in the semi-finished material is 2 to 5 cm^3/100 g (9)

The presence of the oxide film on the surface of the powder prevents the sintering of the powder and production of high quality billets. During the hot pressing the oxide film is destroyed as a result, one may obtain the billets with the necessary properties. It was established that an extrusion ratio (billet to extrudate radius) of 8 or more is required to obtain high quality powder consolidated billets In the event that the extrusion ratio is lower, the level of the strength and relative ductility is much lower than optimal. Once such difficulties have been overcome these alloys possess superior mechanical properties

such as a combination of good room temperature ductility and fracture toughness coupled with excellent elevated temperature strength. The alloys also exhibit high modulii, excellent thermal stability and corrosion resistance. The alloys can be fabricated into sheets, extrusions, forgings and other end products destined for a wide range of aerospace applications including structural airframe, gas-turbine and missile applications (7-9)

2.3 Rapid Solidification Processing

Initial results indicated that a highly metastable structure resulted from the rapid quench; analysis of the structure indicated glassy alloy. Direct measurements of the quench rates were reported to be 10^7 to 10^8 K/s, providing confirmation that such quench rates could result in sufficient undercooling of the liquid droplets to result in glass formation. Clearly, quenching and solidification rates as high as 10^9 K/s opened many doors for investigations of metastable structures and structural refinements The first of a number of international conferences held on the subject of rapid solidification was held in 1970, entitled Proceedings of the International Conference on Metastable Metallic Alloys. Rapid quenching (for all materials) and rapid solidification (for crystalline metals) arbitrarily include rates of heat extraction from about 10^2 K/s to the maximum rate reported of 10^{10} K/s. These high rates are attainable by providing particulates in which at least one dimension is very small The smaller that dimension, the greater the potential quench rate, all other factors being constant (11).

It is worth devoting some short time to an archival example which provides insight into the development of a superior engineering alloy, and results from work on the

production of lead shot from the early part of the last century. Figure 2.3 shows the merchant's Shot Tower in Baltimore, built in 1828 and in continuous operation producing some half-million 10 kg bags of spherical lead shot each year until 1892. The tower is roughly 40 m tall. The production of shot involved various lead alloys, and the beneficial influence of several alloying elements was broadly appreciated at that time. Arsenic encouraged the formation of spherical shot, presumably through the modification of surface tension. Antimony and copper produced harder shot. Relatively simple heat-transfer calculations show that 2 mm diameter spherical particles, achieving a velocity of 30 m/s under free-fall conditions over 50 m (Reynolds Number = 4000, Prandtl Number = 0.9) experience a heat transfer coefficient of 3 kW/cm^2-K, leading to a droplet cooling rate greater than 10^4 K/s. One can conclude that such lead droplets were rapidly solidified some 150 years ago. Although the solid solubility of antimony in lead is substantial 3.5 wt. % at 252°C... without further direct evidence, one may speculate that the improved hardening produced by copper was an early example of increased solid solubility produced by rapid solidification (12)

Conventional gas-atomization of liquid metals is a relatively mature technology, having been used since the 1930's to produce a wide variety of metallic powders for diverse applications. Each space shuttle launch, for example, consumes 160,000 kg of atomized aluminum powder as part of the solid fuel propellant mixture (12). In atomization processes alloy melts are finely divided into roughly spherical particles of 10 to 50 μm average diameter, although the size distribution may vary from 1 to 200 μm, depending on the particular process. Some atomization processes are depicted in the

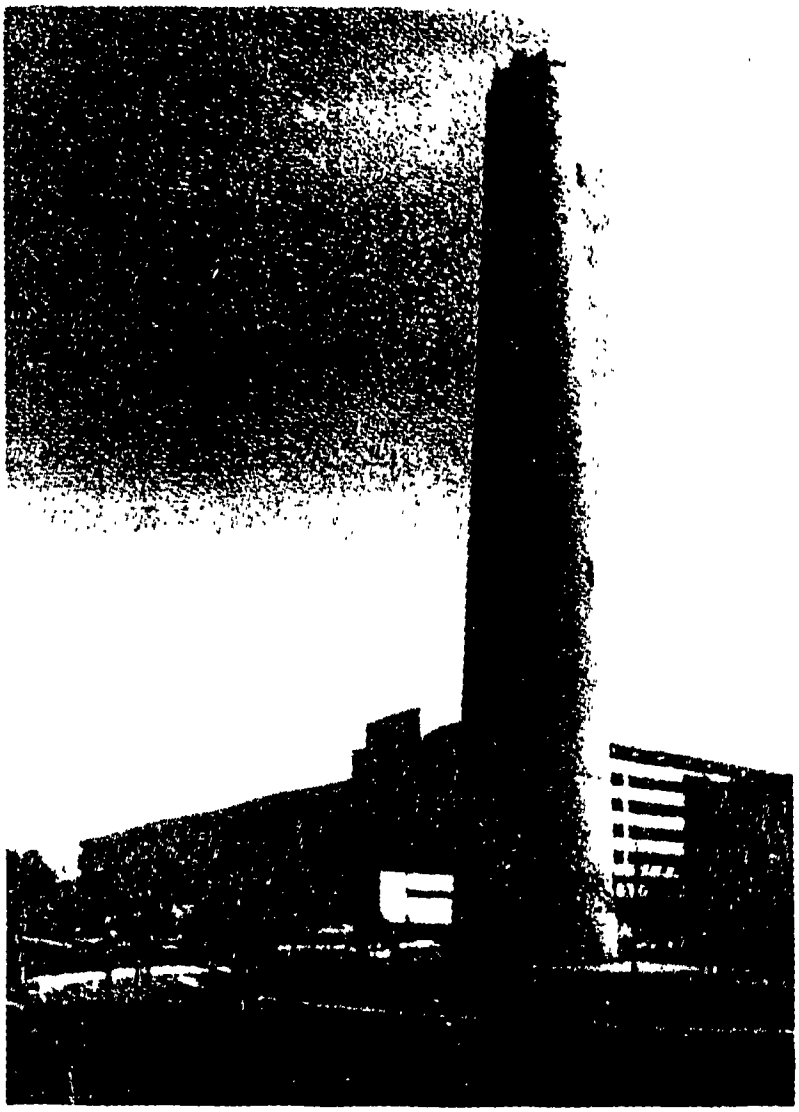

Figure 2.3: Merchant's Shot Tower in Baltimore (12)

schematic diagrams. Figure 2.4 shows the roller atomization principle while Figure 2.5 illustrates the centrifugal atomization process using different configurations Centrifugal atomization by a rotary disk is shown on Figure 2.5(a). Another method called inert gas atomization is shown on Figure 2.5(b) where annular-ring configuration provides gas jets to impinge on a liquid metal stream (11).

One of the problems associated with this process is welding of fine droplets onto coarser particles (satellites) due to repeated collisions among liquid or semi-liquid coarse particles and fine solidified particles in a turbulent atmosphere. Packing densities suffer from these conditions; surface area measurements become much less meaningful and increased contamination occurs; and separation of fine and coarse particles becomes impossible This means that powder particles with significantly different dendrite sizes and phase distribution are incorporated into the final product with negative effects on structure and properties. A second major problem with gas atomization is the entrapment of gas in powders. Even with an inert gas, argon for example, the gas becomes part of the final product. The gas pores are sealed in hot extrusion, but reform gas pockets on high temperature use (11)

As with gas atomization, water atomization is a two-fluid process, with the important difference that water has a high quench capability. Various jet configurations are used but the metal is always in the free fall configuration. A converging cone arrangement for the water is the preferred configuration Process variables which are taken into consideration are similar to those for gas atomization. A choice of conditions intermediate between those of gas and water atomization is attainable by steam

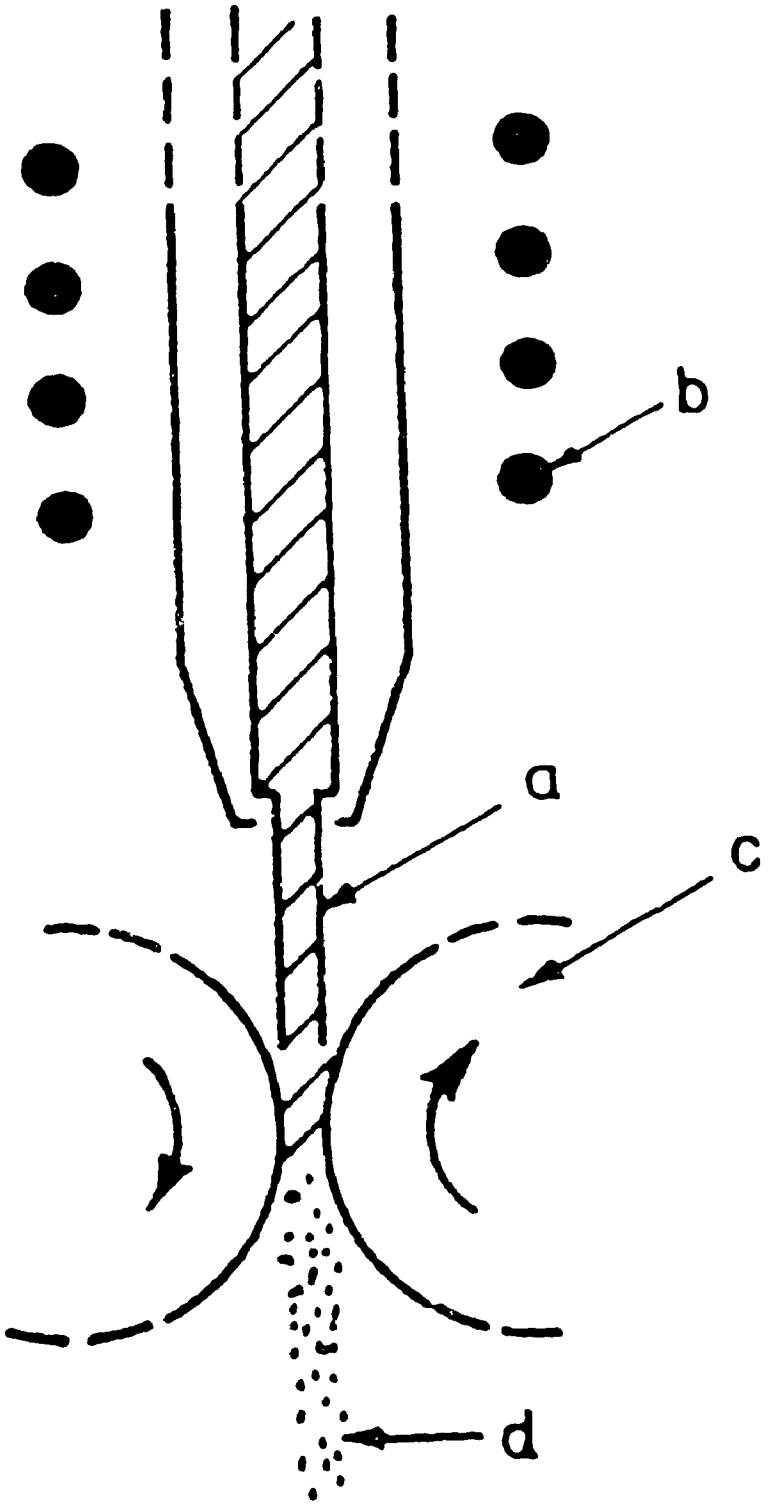

Figure 2.4: Schematic representation of Roller Atomization: a = Liquid Metal Stream; b = Heat Source; c = Rolls; d = Metal Powder (11)

(a) CENTRIFUGAL ATOMIZATION

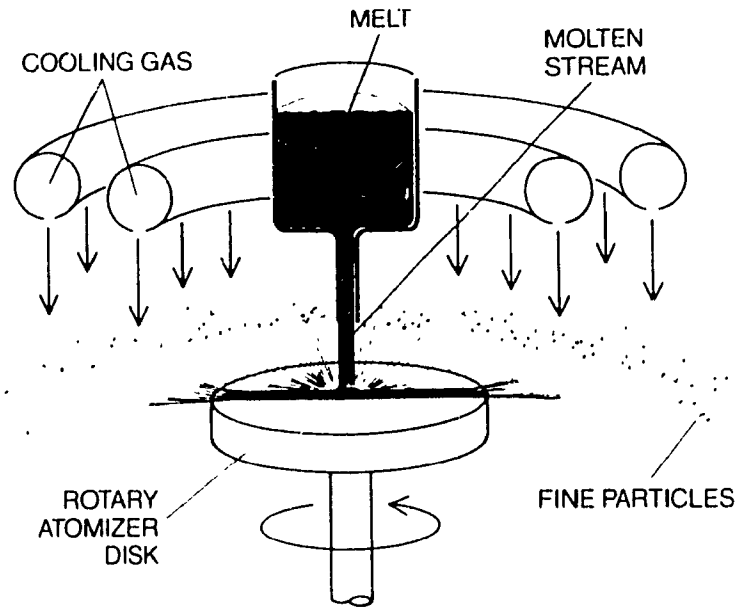

(b) INERT GAS ATOMIZATION

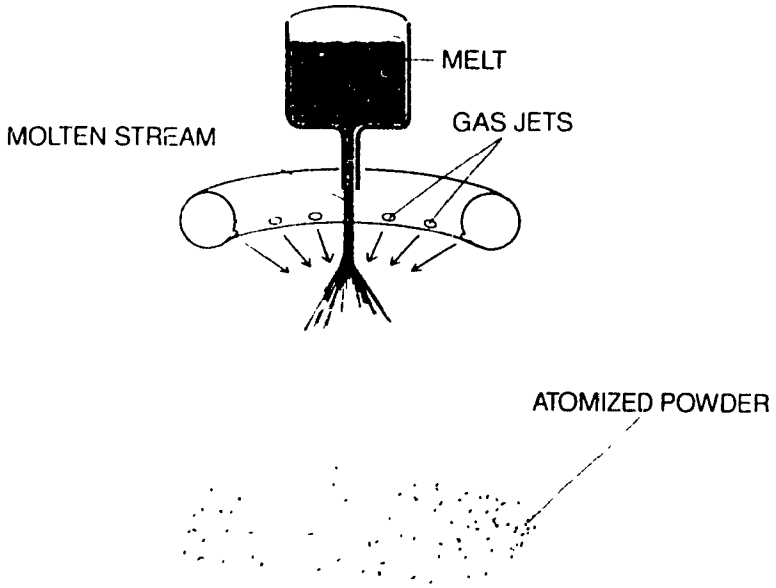

Figure 2.5: Rapid Solidification Powder Fabrication Using (a) Centrifugal Atomization and (b) Inert Gas Atomization (10)

atomization. Low pressure steam, passed through geometrically arranged nozzle configurations, can be brought to resonance to produce relatively coarse powders, of less than spherical shape (irregular, spheroidal) with relatively high quench rate response. Various metals have been successfully atomized this way, however, there have not been reports of aluminum being among them (11).

Numerous configurations of rotary atomizing have been tried and are undergoing further development. The spinner may be a dish or a cup, a crucible, a flat or curved plate, or some variation of these. Disintegration can take place over a lip, off a surface or through holes; energy requirements are relatively low; particle size can be varied from spherical to flattened and elongated shapes; and powder size can be varied over significant limits, but on average powders tend to be coarse A number of difficulties are associated with this process such as erosion and dissolution of the spinner and atomizer devices, creep or deformation of the dish, cup or crucible for high melting alloys is troublesome. In the case of centrifugal atomization, vacuum could be used but quench rates in vacuum could be low. If high quench rates are desired, a quenching fluid or metallic impact-substrate must be provided, at increased cost to the system Dynamic helium quenching is the process used in one facility to achieve high quench rates of coarse powders (11)

The rotating electrode process is also a centrifugal atomizer A rod of the alloy to be atomized is rotated at high speed, usually in an argon atmosphere, the tip is melted gradually either by the arc struck to a tungsten electrode, or by plasma, or by electron beam, etc. The thin film of liquid metal is spun off and forms smooth spherical powders Powders are coarse, very smooth and of high purity. Quench rates are on the low side of

10^2 K/s. Yields of powder are high. Two negative features, related to cost are electrode production is expensive and production rates are relatively low (11).

When solidification rates greater than about 10^4 to 10^5 K/s are desired or required, one turns to the various splat quenching or metallic substrate quenching techniques which have been developed over the past 20 years. The particulates produced by substrate quenching are flakes, foils, ribbons, strip and sheet with thickness dimensions under about 50 μm. The most commonly and most broadly used technique is melt spinning, followed by melt extraction and the twin roller technique (11).

The development of equipment to produce rapidly solidified continuous filaments commenced with the work of Pond (14) in 1958. This melt spinning process was subsequently used during the 1960s to produce amorphous ribbons of several alloys. The process consisted of casting a thin free jet of liquid metal onto the inner surface of a rotating drum, and the prevailing design allowed centrifugal force to maintain adequate heat transfer between the ribbon and the quenching surface. Main problem of this method was small quantity of material produced. Work at Allied Corporation commenced in the early 1970s and the development of various processes to produce large quantities of high quality amorphous ribbon has led to a commercial success (see Figures 2.6, 2.7 and 2.8) (13).

During 1973 work at Allied Corporation was successful in jet casting thin liquid streams onto the external surface of a water-cooled copper drum of some 100 mm diameter, rotating with a surface speed of approximately 30 m/s. This was, to some degree, unexpected, since it had been anticipated that the liquid jet would simply "bounce" off the cooling substrate. This jet casting process demonstration provided significant

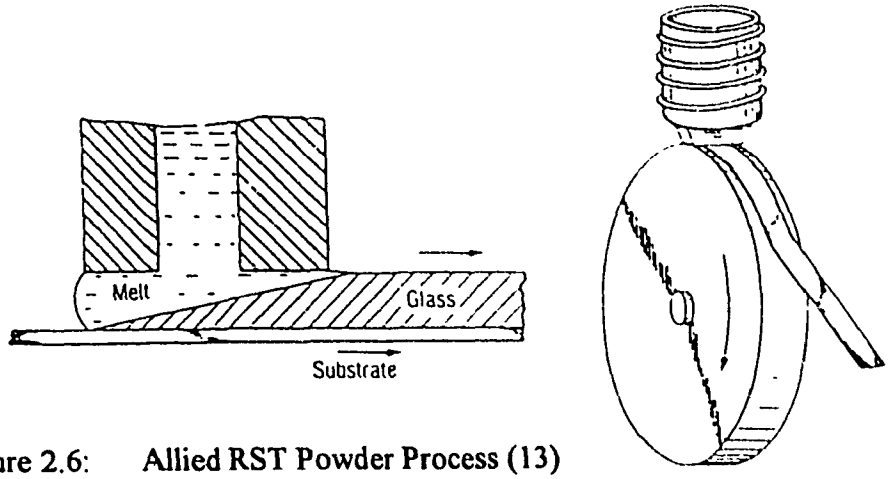

Figure 2.6: Allied RST Powder Process (13)

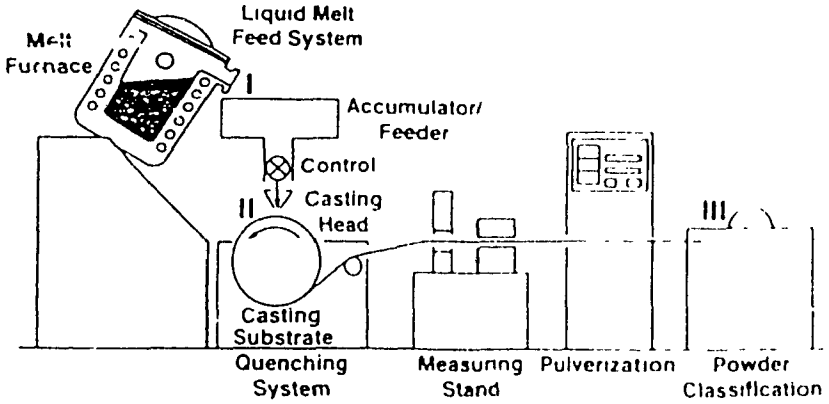

Figure 2.7: Allied Planar Flow Casting (13)

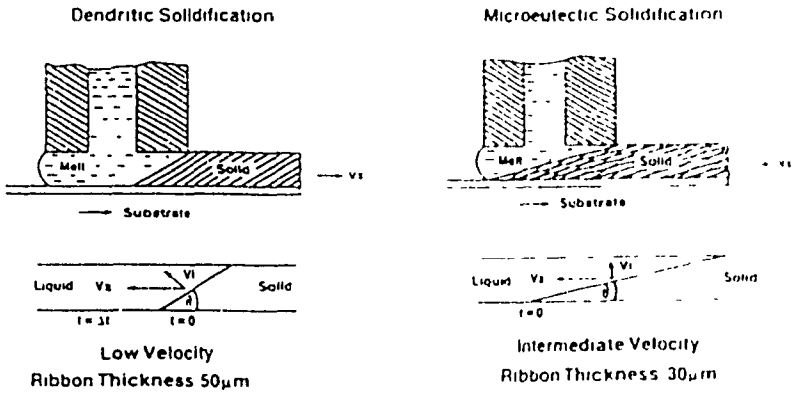

Figure 2.8: Allied Planar Flow Casting for Crystalline Alloys (13)

impetus to Allied's decision to produce metallic glass alloys in large scale and to ultimately offer them for sale commercially after the further development of its planar flow casting process. The jet casting process was successful in producing a wide range of amorphous alloys; however, the melt-puddle was not particularly stable and, as a result, the progress is restricted to the production of ribbon less than 5 mm wide (15). This potentially serious production deficiency was solved by M.C. Narasimhan (16) who invented the planar flow casting (PFC) process and provided the practical basis for what is now a routine production capability of 100 mm and 180 mm wide strip of 20 to 30 μm thickness. This PFC process (see Figure 2.7), Interalia, positions the casting nozzle in close proximity to the rotating chill block and employs a rectangular slot orifice. The molten pool of metal is constrained into a stable shape, as it is now understood, by balancing surface tension forces with the applied liquid metal pressure, to achieve a dynamically stable melt pool on the rotating substrate. Several parameters for stable operation include substrate velocity, liquid metal surface and prevention of air entrapment under the liquid film. Normally, reactive iron and aluminum base alloys have been routinely planar flow cast into magnesium and titanium base alloys have been cast in vacuum. At present it does not appear to be economically feasible to produce large quantities of reactive alloys in large vacuum chambers; however, there appears to be no practical limit to the width of PFC strip cast in air (13).

In the materials world, the key issue is structure. Microstructure in turn determines properties, whether mechanical, physical, chemical, electronic or magnetic. In the world of ingot and casting technology, there is limited potential to further manipulate

structure through chemistry because of road blocks directly associated with severe segregation of elements and impurities (which worsen with increasing concentrations), formation of coarse often brittle phases, coarse grain structure, porosity, etc (17).

Metallurgical research have shown that the rapidly solidified aluminum alloys (at the rate above 10^4 °C/s) possess the following structural characteristics (9).

- Fine grained crystalline microstructure
- Reduction in spacing between the axis of dendrites to about 1 μm as compared to 20 to 30 μm during casting into the billets
- Reduction in size of intermetallic phase particles to less than 0 5 μm and less as compared to 1 to 10 μm for as cast aluminum alloys
- Substantial increase of the solubilty limits of alloying elements in the solid state, for example, the solubility of Fe in the aluminum in the equilibrium near the solidification condition does not exceed 0.05% while during rapid solidification it reaches up to 8 or 10%
- Drop in liquidity of alloying elements, firstly in the section of the particle; at specific conditions and speeds of crystallization structures, in which the segregation of alloying elements is absent
- Creation of new metastable second phase particles

Industrially produced aluminum and its alloys always consisted of aggregates of crystals It is only in the most recent twenty years that metallic glasses have been known (that is, super-cooled metal liquids with non-crystalline structures). These materials are obtained by quenching liquid alloys so fast that they do not have time to crystallize. For only about

10 years has it been possible to do the fast-quenching continuously to obtain glasses with the useful shapes of ribbons and wires (17).

More recently this same rapid solidification ribbon casting technology with subsequent communition of the ribbon to powder, has been applied to the development of new microcrystalline structural alloys. In a sense, the ribbon approach to rapid solidification processing (RSP) of materials has now merged with the more conventional approach of powder atomization, although ribbon casting offers clear advantages when high solidification rates are critical. Developments of microcrystalline materials by both methods have been evolutionary, rather than revolutionary, but each offers crystalline alloys unobtainable by other processing routes. Both methods are compared in Table 2.1 (18,19).

RSP methods offer practical means for achieving refined grain size, increased chemical homogeneity, extended solid solubility and metastable phase formation. The microstructural refinement provided by modest solidification rates has led, for example, to improved mechanical properties in a wide range of aluminum alloys, including improved toughness. Grain refinement via dispersions and thermomechanical treatment has also provided ductility enhancement (18,19).

An important issue arises when dealing with reactive alloys, such as aluminum. To approach the desired properties for these alloys via gas atomization, very fine powders must be dealt with and these present a potential explosion hazard. The powder particles produced by ribbon casting comminution, irrespective or particulate size; accordingly, coarser powders (typically, platelets of the order of 100 μm square by 25 μm thick) can be

Table 2.1: **Rapidly Solidified Powder Processes (26)**

	Atomization	*Planar flow casting-ribbon comminution*
Cooling rate	$< 10^4$ K s^{-1}	$> 10^5$ K s^{-1}
Atmosphere	Inert atmosphere	Carried out in air
Morphology	Nearly spherical	Irregular flakes
Microstructural uniformity	Limited to finest particle sizes	Uniform, irrespective of particulate size
Economics	Depends on atomization process used	Low cost
Safety	Extreme precaution needed in handling of fine (-325 mesh) powder	Less hazard associated with coarse (-30 mesh) powder particulate

processed and these are limited only by the need to achieve reasonable packing densities when filling dies or cans. The influence of powder size on explosion hazard for aluminum alloys is reviewed in (20) (see Table 2.2) (18,19).

2.4 High Temperature Aluminum Alloys

The RSP of aluminum-based alloys has addressed a broad range of systems, including a variety of commercial alloys (e.g. aluminum alloy 2024) with or without minor additional elements. In dealing with the traditional alloys, it is possible to achieve improved levels of chemical homogeneity and grain refinement, which can lead to reduced solutionizing times. Such an advantage is not a sufficient economic value, however, for powder processing technology to replace direct chill ingot casting technology for standard or slightly modified aluminum aerospace alloys. RSP addresses, therefore, alloy combinations which, for one reason or another are inaccessible to direct chill casting technology; Al-TM (transition metals) chemistries represent particularly important examples of such alloys (21).

Transition metals typically have very low equilibrium solid solubilities in aluminum and very low diffusive fluxes. The former point means that iron, for example, is a contaminant in direct chill casting since, at very low concentrations it precipitates in the melt to form very coarse Al-Fe-Si intermetallic phases. However, low diffusive fluxes mean that, once retained in solid solution or in the form of dispersed phases, the nucleation of new phases and/or the growth of existing dispersoids will be rather slow.

Table 2.2: Explosivity of Rapidly Solidified Aluminum Alloy Powders (26)

	Al-Fe-V-Si alloy	*Al-Fe-V-Si alloy*	*Al-Li-Cu-Mg-Zr alloy*	*Al-Li-Cu-Mg-Zr alloy*	*Typical atomized Al*
Particle size	−60 mesh	−200 mesh	−60 mesh	−200 mesh	−200 mesh
Minimum ignition energy (J)	>1500	1.53	305	66	100
Minimum explosive concentration (g m^{-3})	No explosion	1.05	595	45	60

The relative resistance of aluminum alloys to diffusion of transition metal elements are indicated in Table 2.3 (21).

Beginning with the work of Jones (22) and Tonejc et al. (23), it was demonstrated that rapid cooling of liquid to solid could result in the extension of the solid solubility of iron in aluminum by orders of magnitude (from 0.05 to about 10 wt. %). It was further shown by Thursfield and Stowell (24) that controlled nucleation and growth of metastable second phases (e.g. Al_6Fe) (25) during extrusion of splatcooled Al-Fe alloys leads to high stiffness and high strength, because of the obstacles provided to dislocation motion by dispersoids, and to the retention of high levels of strength at high temperatures (about 350°C), because of the relative resistance of the Al-Fe dispersoids to Oswald Ripening (26).

Since all the binary Al-TM alloys are moderately soft and/or they possess only moderate thermal stabilities, continuing development of optimized high temperature alloys has focused on ternary and quaternary alloys, with the most prominent of these being Al-Fe alloys, containing additions of cerium (27), molybdenum (21) or vanadium and silicon (29) to promote the formation and retention of favorable metastable phases. The latter alloys all possess good to excellent strength at high temperatures; their strength-temperature relationships are shown in Figure 2.9 (28-31) and indicate, in each case, a strength which is three to ten times higher than for standard aerospace alloys in the vicinity of 350°C. As indicated in this figure on a specific strength basis, these alloys match the performance of titanium at temperatures of 200 to 230°C (26).

Table 2.3: **Diffusivity, Liquid and Solid Solubility of Some Transition Metals in Aluminum (26)**

Transition metal	D (cm^2/s)	Liquid solubility at 1400 K		Maximum equilibrium solid solubility at indicated temperature (wt % (at %))		
Fe	[illegible]	32	(1.52)	0.04	(0.025)	at 928 K
V	[illegible]	6	(0.45)	0.6	0.32	at 934 K
Zr	[illegible]	[illegible]	(0.7)	0.28	(0.085)	at 934 K
Cr	[illegible]	5	[illegible]	0.77	(0.40)	at 934 K
Mn	[illegible]	41.5	21	0.95	0.91	at 910 K
Mo	[illegible]	3	1.7	0.25	0.056	at 934 K
Ti	[illegible]	0.3	3.6	1.3	(0.57)	at 938 K

[illegible]

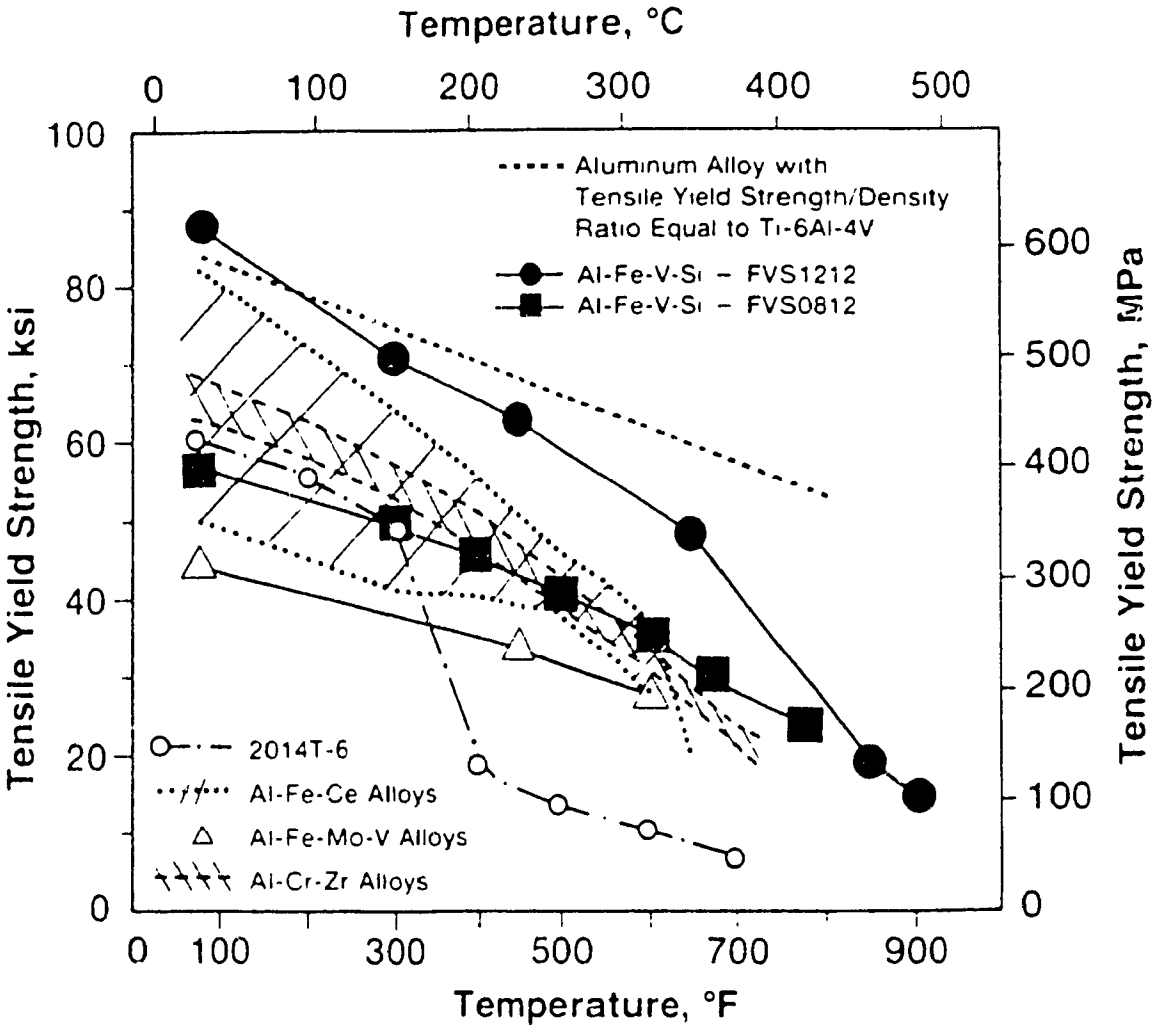

Figure 2.9: Comparison of Elevated Temperature Tensile Yield Strengths of Various High Temperature and Standard Aerospace Aluminum Alloys (26)

In all practical alloys of the aluminum-transition metal systems, rapid solidification produces either cellular-dendritic, microeutectic or icosahedral ("O phase" in the Allied system) solidification structures which are capable of subsequent decomposition during thermomechanical processing, to produce alloys with quite different toughness and strength properties. The Al-Fe-V-Si alloys consist of very fine, nearly spherical $Al_{12}(Fe,V)_3Si$ (Silicide) dispersoids formed from the decomposition of the rapidly solidified microstructures, uniformly distributed throughout the aluminum matrix. The superior elevated temperature strengths and stability of these alloys are due to the much slower coarsening rates of the silicides compared to the dispersoids found in other high temperature aluminum alloys. Also these alloys are devoid of any coarse needle or plate-like intermetallic phases which degrade alloy ductility and fracture toughness The Al-Fe-V-Si alloys contain high transition element concentrations (5 5 to 12 5 wt % Fe) that form high volume fractions of silicides and their desirable microstructural morphology essentially controls the mechanical properties of these alloys (32)

The three most advanced Al-Fe-V-Si alloys are FVS0812 (Al-8.5 wt % Fe-1 3 wt.% V-1.7 wt.% Si), FVS1212 (Al-12.4 wt.% Fe-1 2 wt % V-2 3 wt.% Si) and FVS0611 (Al-5.5 wt.% Fe-0.5 wt.% V-1.1 wt.% Si) The tensile properties of the three alloys are listed in Table 2 4. Alloy FVS0812, now designated as 8009 by the Aluminum Association is the alloy most appealing to overall aerospace applications because it suits applications that require light-weight in combination with advantageous elevated temperature mechanical properties and in particular, fracture toughness/strength levels of conventional 2000 and 7000 series aluminum aerospace alloys Alloy FVS1212 is directed

Table 2.4: Mechanical Properties of Rapidly Solidified Al-Fe-V-Si Alloys FVS 0611, 0812 and 1212 (32)

	FVS0611			FVS0812			FVS1212		
Temp. °C(F°)	YS MPa(ksi)	UTS MPa(ksi)	El. (%)	YS MPa(ksi)	UTS MPa(ksi)	El. (%)	YS MPa(ksi)	UTS MPa(ksi)	El. (%)
24(75)	310(45)	352(51)	16.7	414(60)	462(67)	12.9	531(77)	559(81)	7.2
150(300)	241(35)	262(38)	10.9	345(50)	379(55)	7.2	455(66)	469(68)	4.2
230(450)	234(34)	248(36)	14.4	310(45)	338(49)	8.2	393(57)	407(59)	6.0
315(600)	172(25)	193(28)	17.3	255(37)	276(40)	11.9	297(43)	303(44)	6.8

at service that requires superior ambient and elevated temperature strengths and stiffnesses. Alloy FVS0611 combines the elevated temperature strength and stabilities of the Al-Fe-V-Si alloys with room temperature formability

A further intercomparison of the Al-Fe based alloys properly focuses on their long term thermal stabilities, i.e. on their resistance to microstructural coarsening at long times and on their fracture toughness For Al-12Fe-1V-2Si (FVS1212) and Al-8Fe-1V-2Si (FVS0812) alloys, the coarsening rates observed at 425°C are two to three orders of magnitude lower than for the Al-Fe-Mo and Al-Fe-Ce alloys (Figure 2 10) (33) As a consequence of their low coarsening rates, Al-Fe-V-Si alloys exhibit no degradation of strength after exposure to a temperature of 425°C for 1000 h (34) This excellent thermal stability is achieved because of the presence of an $Al_{12}(Fe,V)_3Si$ phase, which remains in metastable equilibrium to temperatures in excess of 500°C (35) This phase has a bcc structure and, as a result, has no propensity for the formation of needle-shaped precipitates; rapid needle elongation, for example, of equilibrium monoclinic Al_3Fe, leads to rapid coarsening in the cerium and molybdenum-containing alloys (21)

Needle formation is also detrimental to obtaining a high fracture toughness Plane strain fracture toughness of the order of 25 to 30 MPa-$m^{1/2}$ may be achieved in Al-8Fe-1V-2Si (28,30), the toughness observed for Al-Fe alloys with acicular dispersoids are less than 20 MPa-$m^{1/2}$ at high strength levels (Figure 2 11) The microstructure of as-cast Al-8Fe-1V-2Si is shown in Figure 2.12, it is a microcellular structure, comprised of intermetallic dispersoids of $Al_{12}(Fe,V)_3Si$, about 50 nm in diameter, present in a volume fraction of about 24%. This fine-scale uniform structure provides a high toughness The

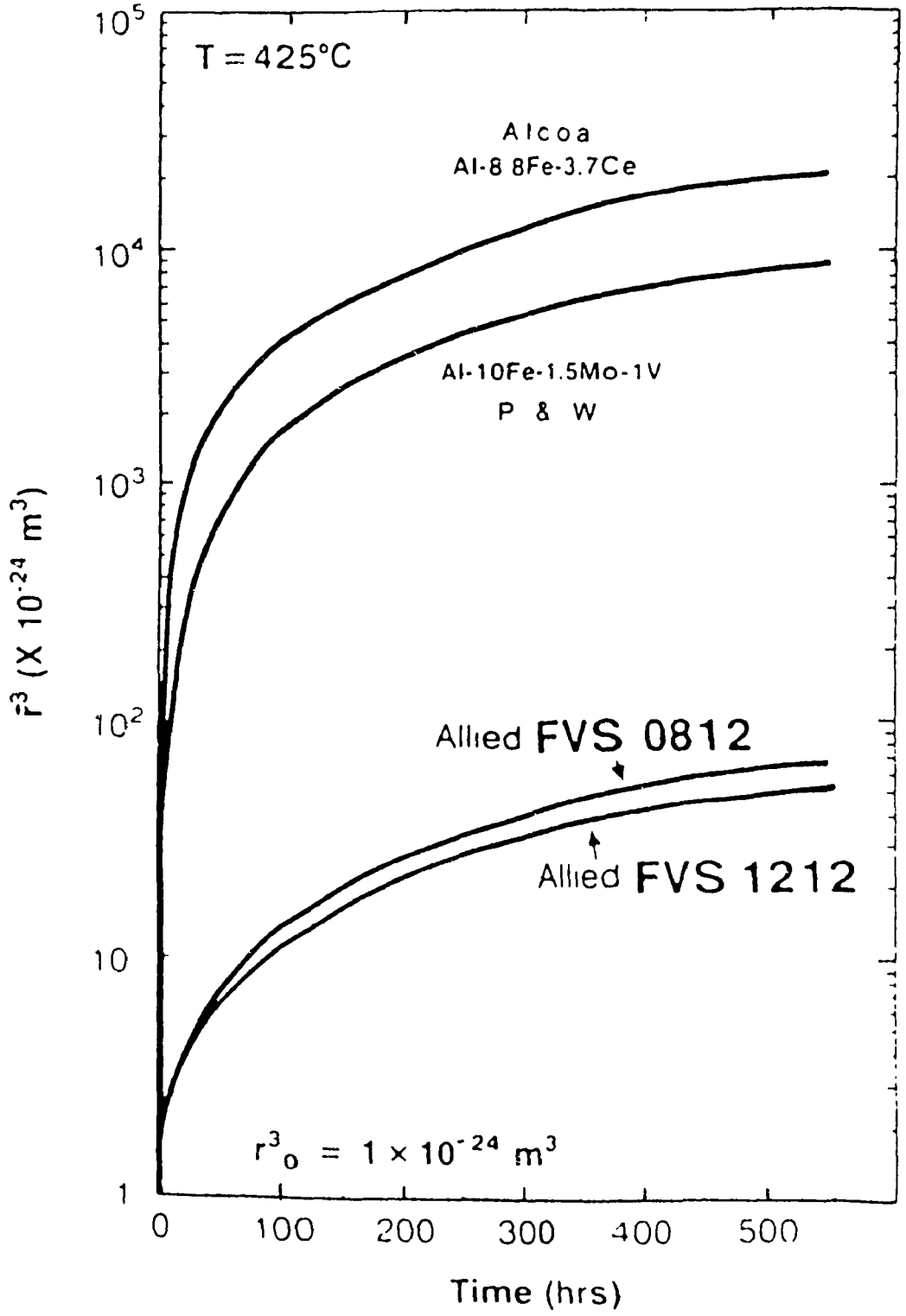

Figure 2.10: Comparison of Coarsening Rates of Dispersoids in Various Rapidly Solidified Al-TM alloys; r = average particle size at time t (26)

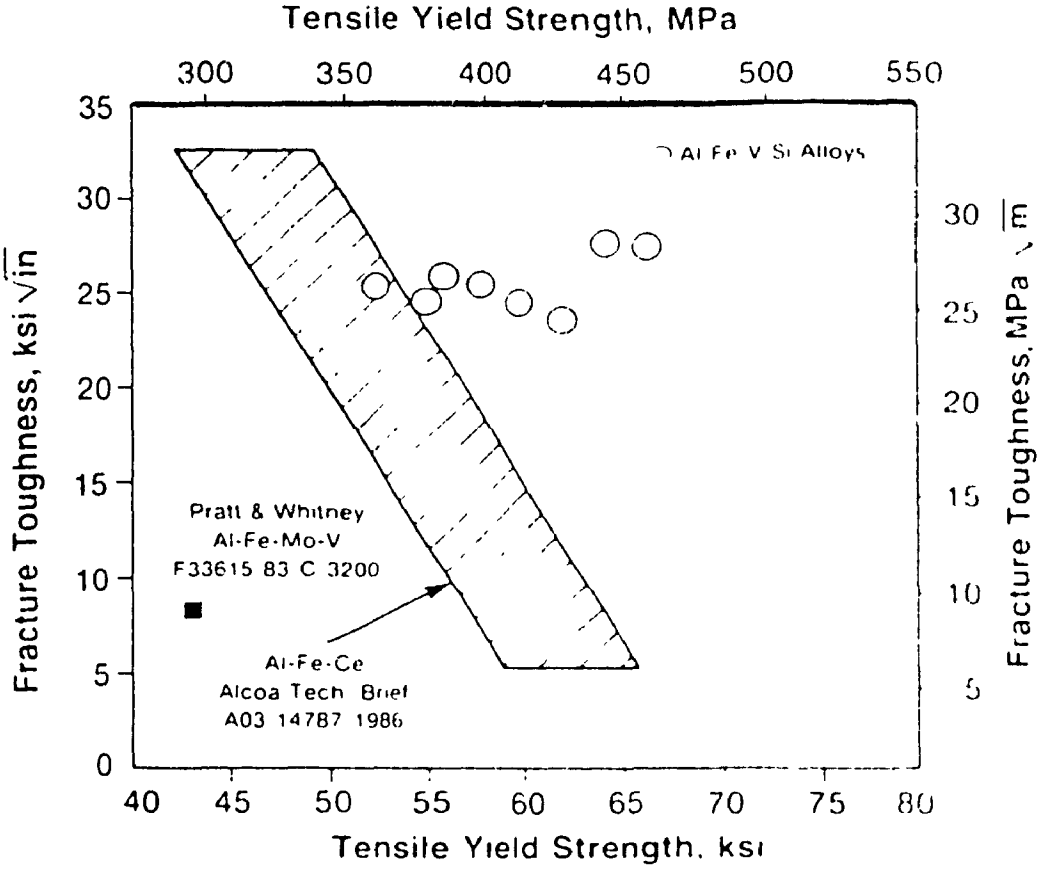

Figure 2.11: **Fracture Toughness K_{IC} vs. Yield Strength Relationship for High Temperature Aluminum Alloys (26)**

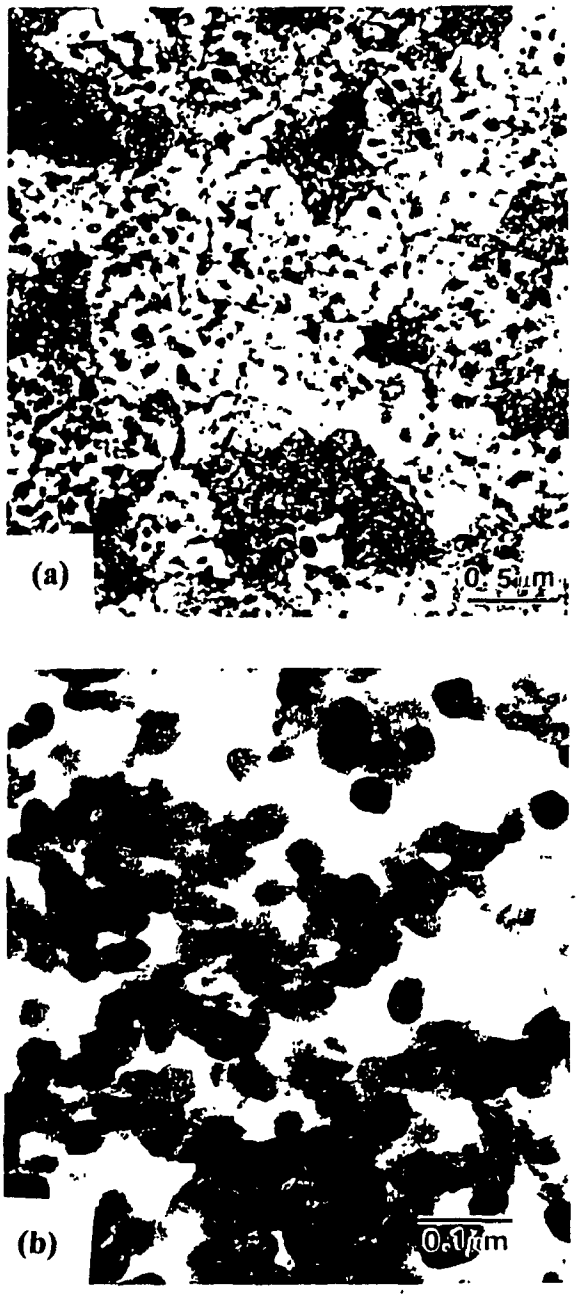

Figure 2.12: Microstructures of RSP Al-8Fe-1V-2Si Alloys (a) In As-Quenched Melt-Spun Ribbon and (b) After Extrusion (18 to 1) at 375°C (26)

presence of a large volume fraction of dispersoids also leads to a marked increased in elastic stiffness. Young's modulus of 96.5 GPa is observed at room temperature for Al-12Fe-1V-2Si containing about 37 vol. % of dispersoids; it is about 82 8 GPa for Al-8Fe-1V-2Si containing about 24 vol. % dispersoids. In general the modulus of elasticity for pure Al is 70 GPa. Such high stiffness render Al-Fe-V-Si alloys useful for stiffness critical applications, as well as for high temperature applications In many applications, their outstanding corrosion resistances will prove equally valuable in comparison to other aluminum alloys (Figure 2.13) (31,36).

The tensile properties of the three high temperature FVS aluminum alloys are depicted in Figure 2.14 One may note that the strength of these alloys increases with increasing volume fraction of silicide with a corresponding decrease in ductility The alloys also show excellent stability at elevated temperature (Figure 2 15) After 1000 h at 425°C neither FVS0812 nor FVS1212 shows any reduction in the tensile properties The excellent high temperature properties of the FVS alloys is also reflected in their creep strengths (Figure 2.16) At the same Larson-Miller parameter, alloy FVS0812 has approximately a 50% greater creep strength than conventional aluminum alloy 2219-T6 Because of the high volume fraction and stability of the silicides in the FVS alloys the alloys have higher moduli as a function of temperature compared to conventional aluminum alloys. Also the specific stiffness (modulus/density) of alloys FVS0812 and FVS1212 are greater than those of Ti-6Al-4V and 17-4 precipitation hardened steel at temperatures up to 480°C (Figure 2.17) (37).

Rapid solidification processing, in the manufacture of elevated temperature aluminum alloys, results in significant supersaturation of solute elements in the aluminum

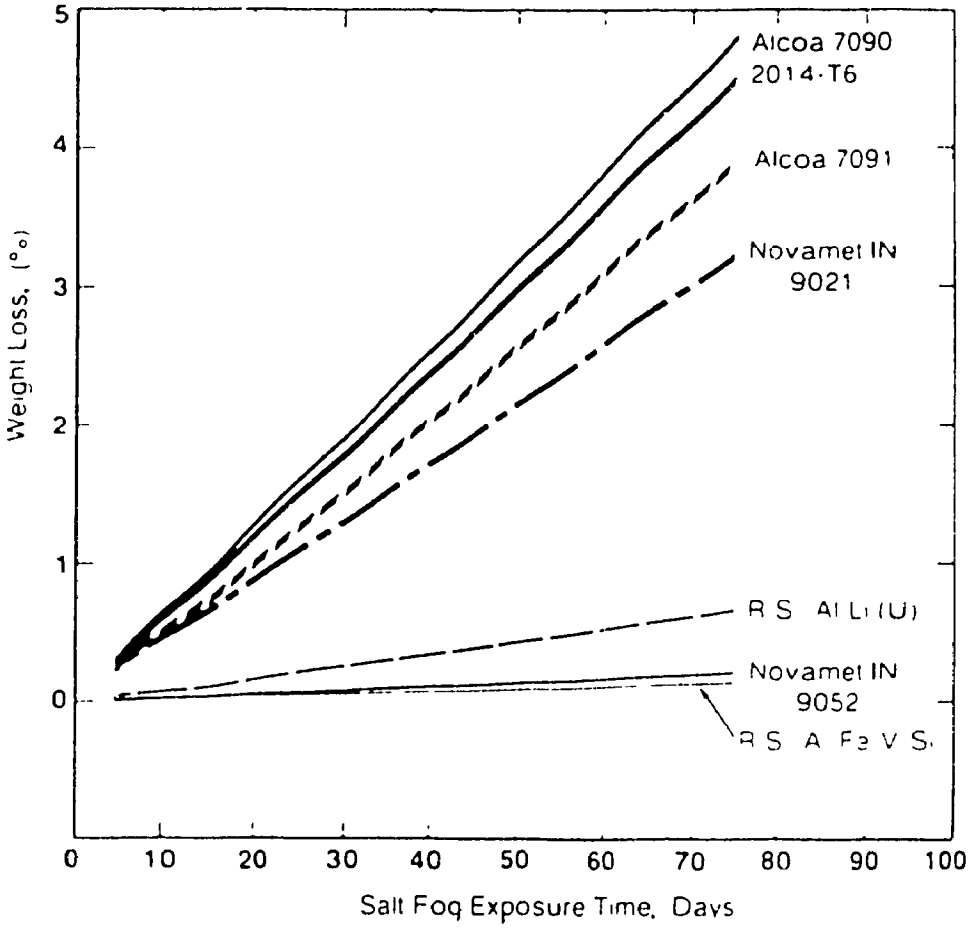

Figure 2.13: Corrosion Rates of Rapidly Solidified Al-8Fe-1V-2Si and Rapidly Solidified Al-Li Compared with Aluminum Alloy 2014-T6 and other Powder Metallurgy Aluminum Alloys (26)

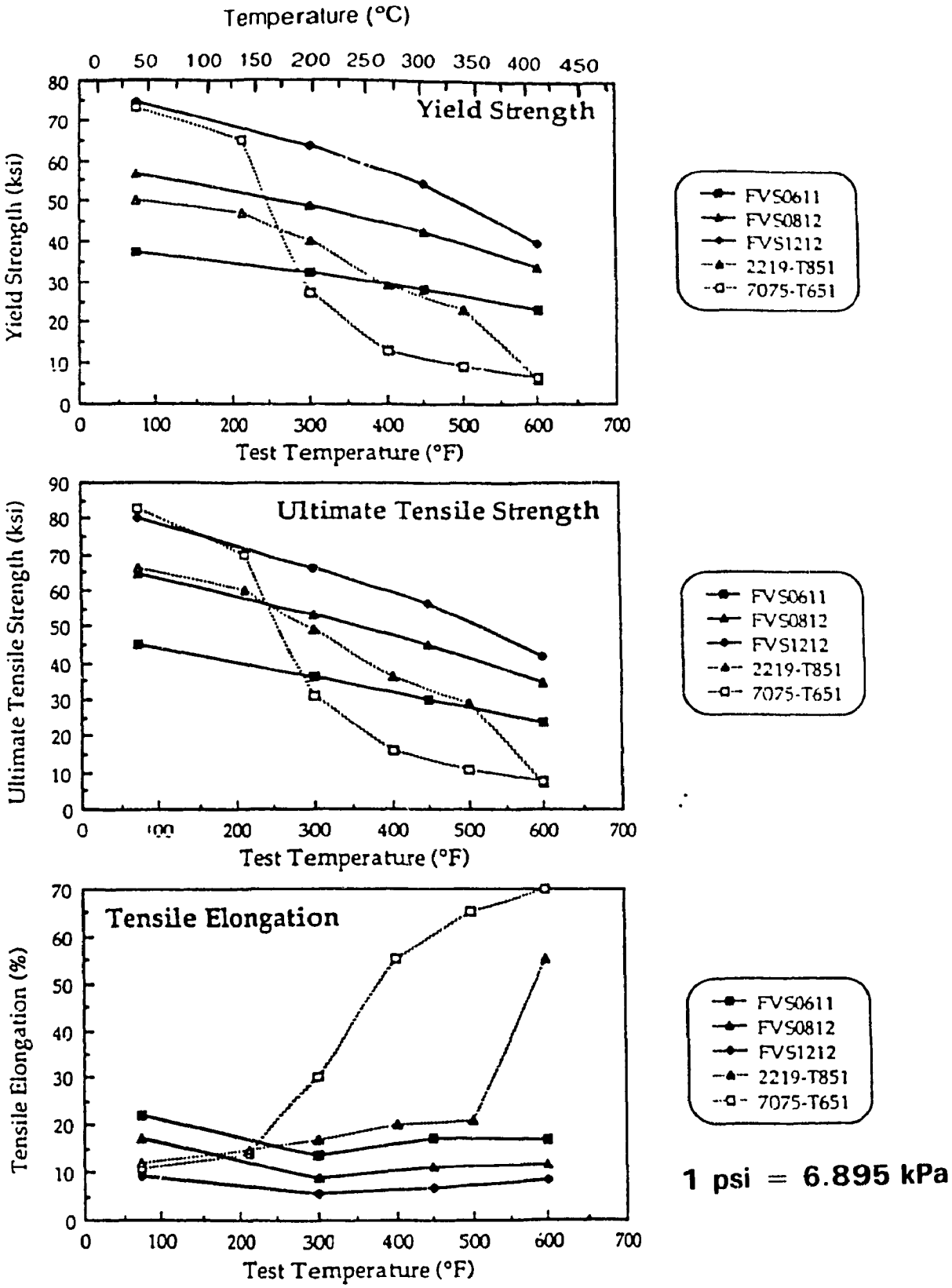

Figure 2.14: Tensile Properties of Rapidly Solidified High Temperature Al-Fe-V-Si Alloys (42)

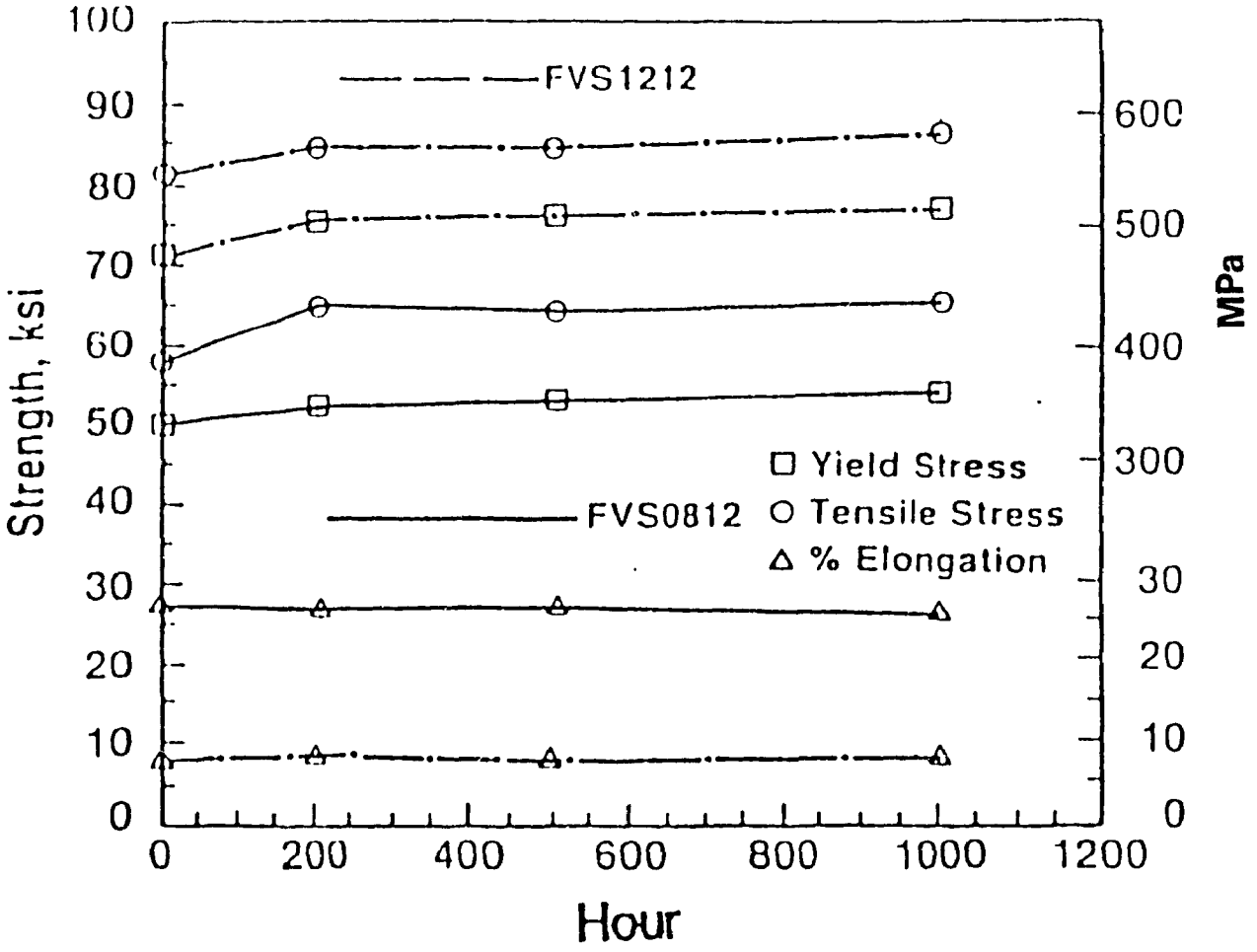

Figure 2.15: Tensile Properties of Alloys FVS0812 and FVS1212 After 425°C Exposures Up To 1000 Hours (42)

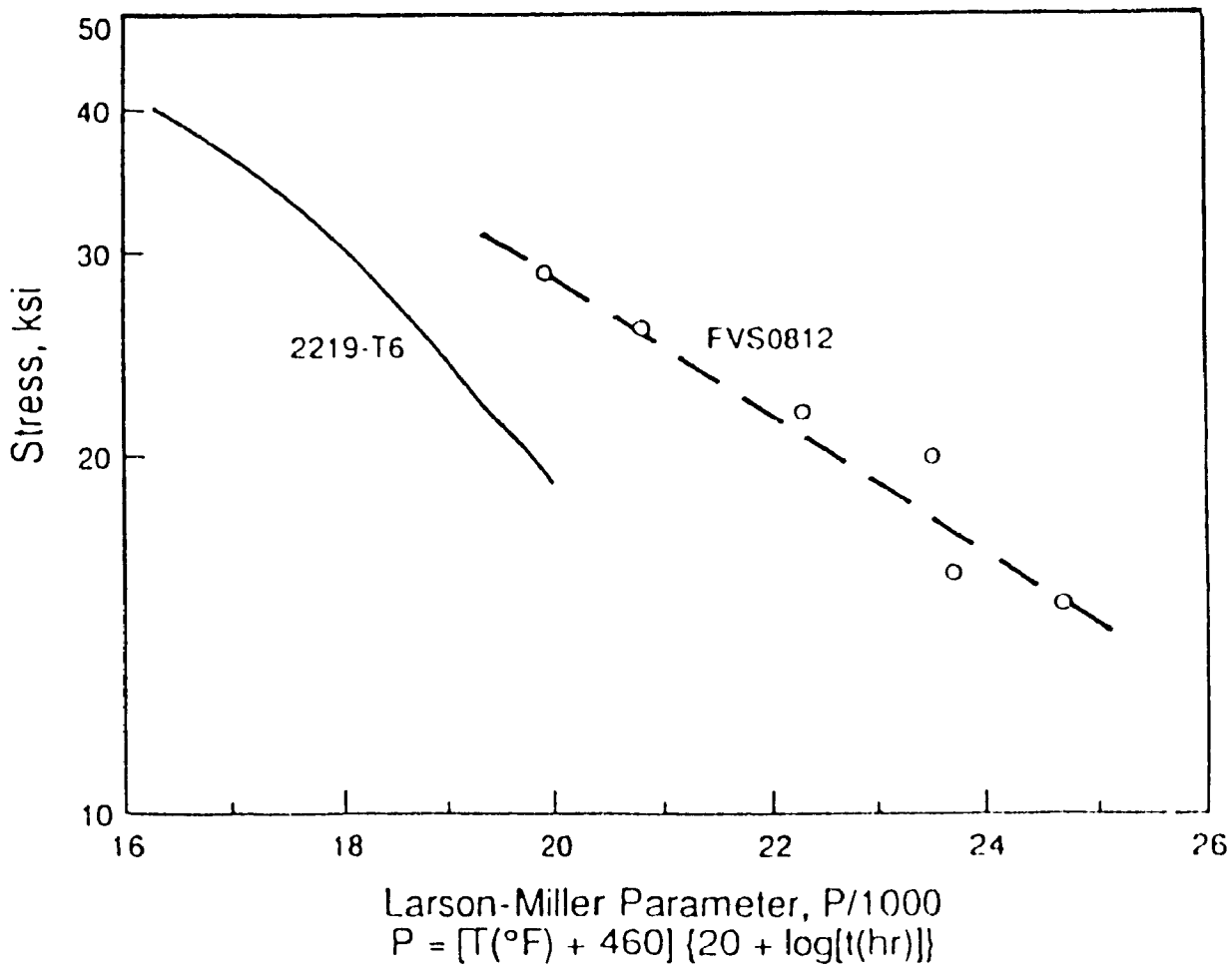

1 psi = 6.895 kPa

Figure 2.16: Creep Rupture Strength as a Fuction of the Larson-Miller Parameter for Alloy FVS0812 (42)

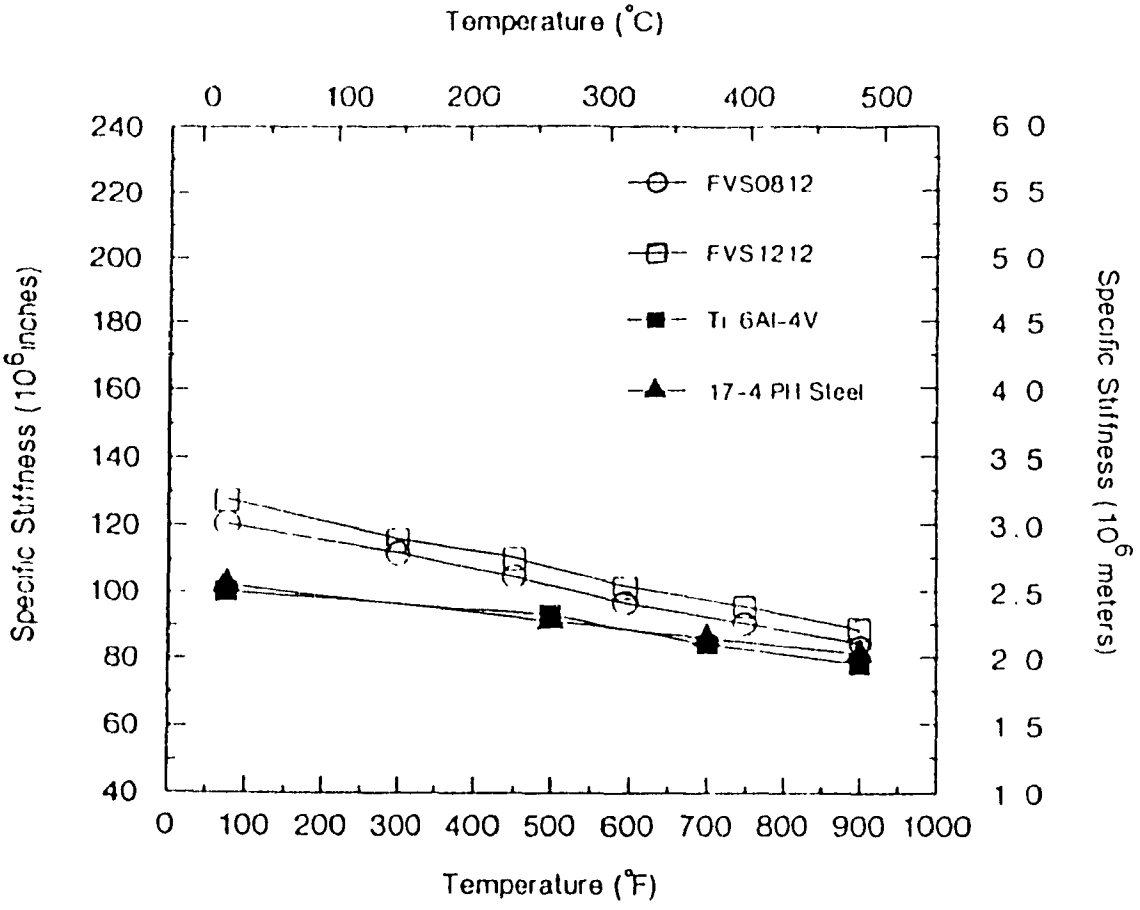

Figure 2.17: Specific Stiffness of Alloys FVS0812 and FVS1212 as a Function of Temperature (42)

matrix solid solution. These levels were shown to alter significantly the deformation characteristics of this class of alloys through the phenomenon of dynamic strain aging (DSA) which DSA reduces tensile ductility at intermediate temperatures The temperature ranges were found to be dependent on the solute element in solid solution and the strain rate of testing (38). The attractive high temperature creep properties and stabilities of alloy FVS1212 are due to the high volume fractions (36%) of thermally stable fine (30-80 nm diameter) spherical $Al_{12}(Fe,V)_3Si$ particles uniformly distributed in an aluminum solid solution matrix with ultra-fine grain size (0 5 μm). Results of coarsening analysis were discussed and correlated to the creep results and possible mechanisms It has been shown that the creep rate varies as a function of temperature and stress (Figure 2.18(a)) being dependent with stress exponent n (Figure 2 18(b)). It is possible to depict diffusion normalized strain rate versus modulus compensated stress for creep tests (Figure 2.19), the fit is much better by assuming a special activation energy for creep instead of the standard 150 kJ/mol. The temperature and the applied stress also affect the coarsening rates (Figure 2.20) which in turn affect the creep. The elastic modulus shows a reduction with increase in temperature. For the material FVS1212 the relationship shows linear regression:

$$E(GPa) = 95.6 - 0.0523T(^{\circ}C) \qquad (2\ 1)$$

as depicted in Figure 2.21. The coarsening behavior of the rapidly solidified alooy as a function of time temperature have been analyzed showing the sizes of the particles increase with stress increase and decrease with temperature decrease (Figure 2 22) (39).

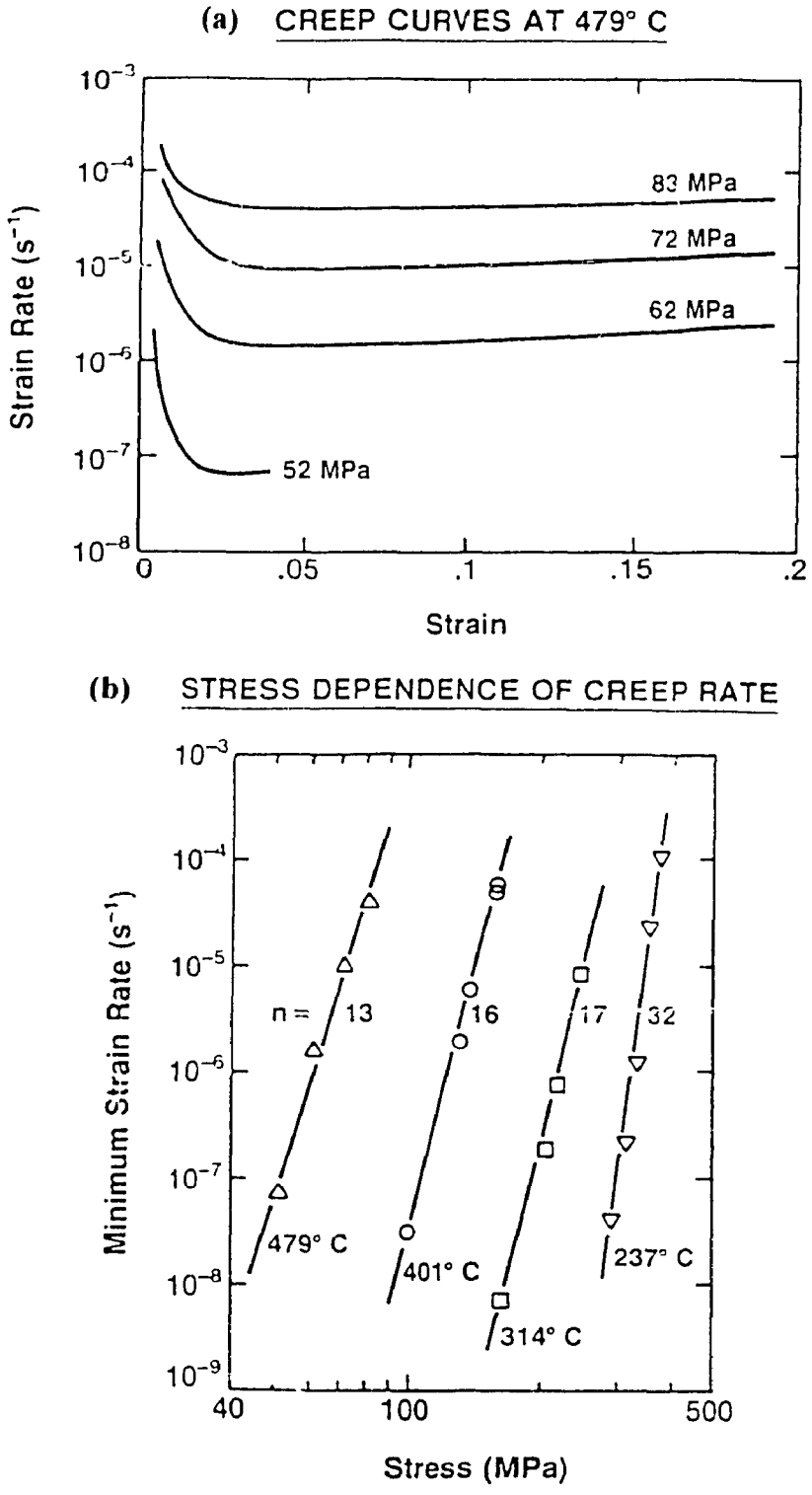

Figure 2.18: Creep Curves for Alloy FVS1212 (a) At 479°C Plotted as Strain Rate vs. Strain and (b) Stress Dependence of the Creep Rate with Stress Exponent, n (39)

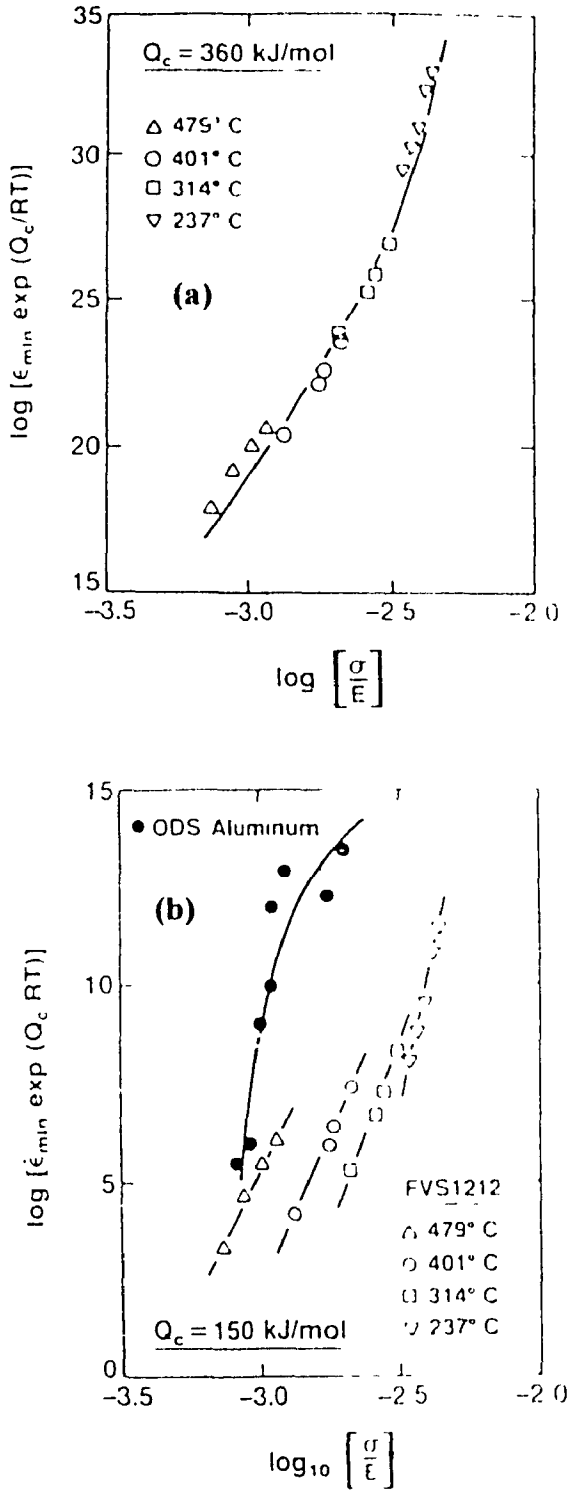

Figure 2.19: Diffusion Normalized Strain Rate Versus Modulus Compensated Stress for Creep Tests Assuming An Activation Energy for Creep of (a) 360 kJ/mol and (b) 150 kJ/mol (39)

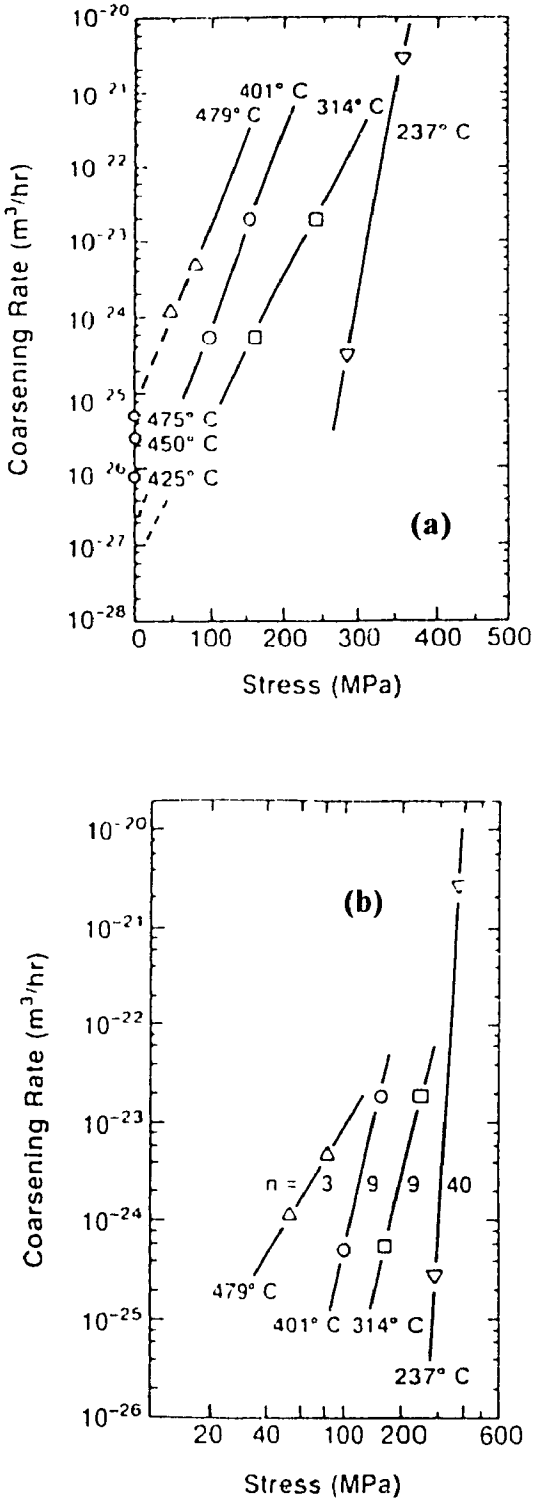

Figure 2.20: Variation of Coarsening Rates as a Function of Applied Stress: (a) Linear and (b) Log-Log (39)

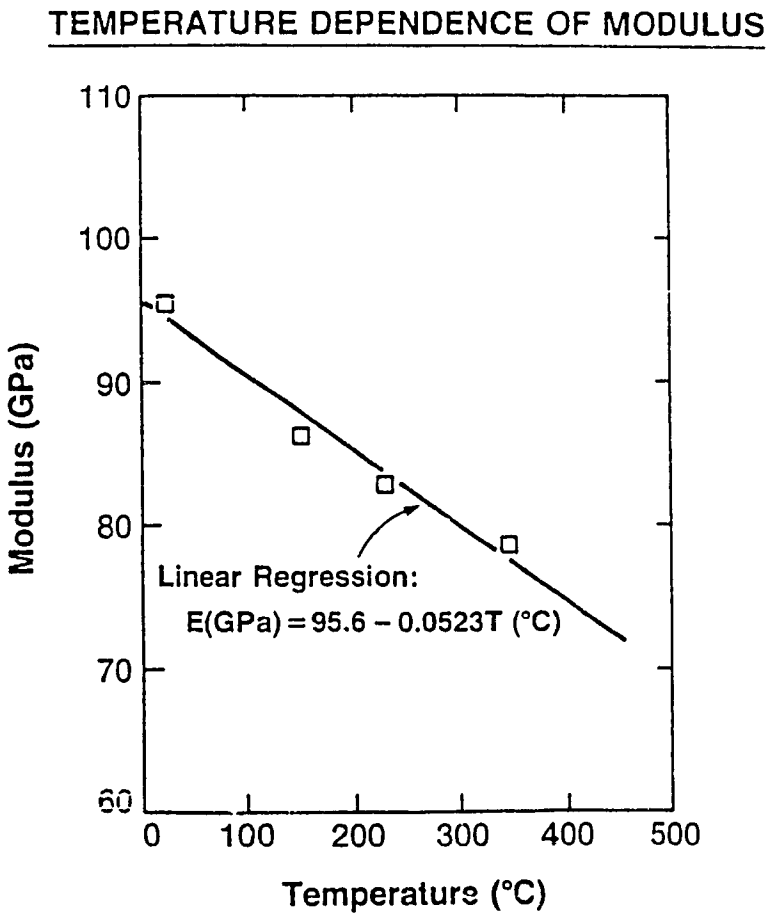

Figure 2.21: Temperature Dependence of the Elastic Modulus for FVS1212 (39)

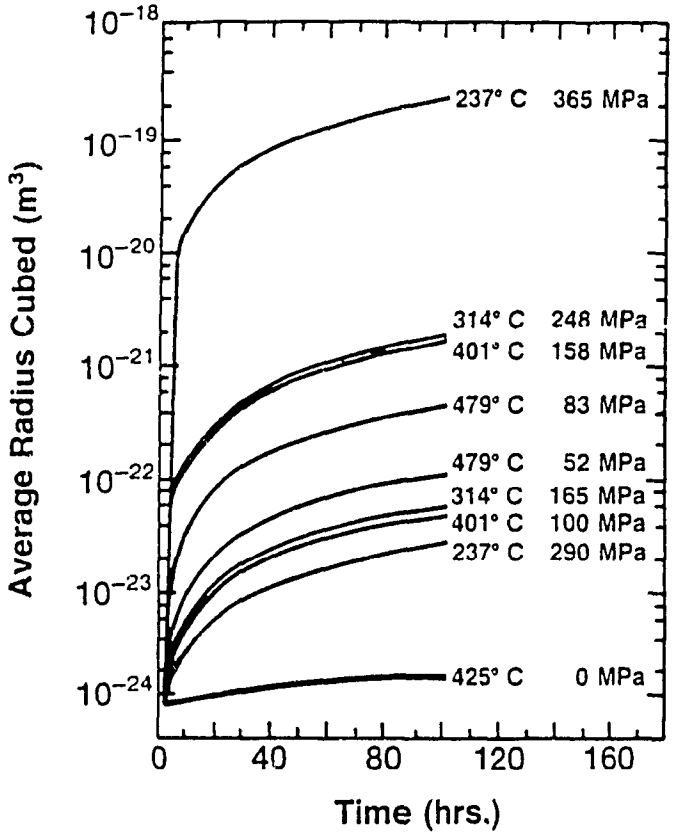

Figure 2.22: Comparison of Predicted Coarsening Behavior of Alloy FVS1212 (39)

The work of Mukherjee, Bird and Dorn (40) showed that a general characterization of creep behaviour is given by the relation

$$\dot{\varepsilon} = A(\sigma / E)^n \exp(Q_c / RT) \qquad (2.2)$$

where C is the minimum creep rate, A is a material constant, σ is the applied stress, E is the elastic modulus, n is the stress exponent, Q_c is the activation energy for creep, R is the universal gas constant and T is the absolute temperature. The stress exponent, n, for most metals is in the range of 3 to 6 and can be explained by well understood creep mechanisms (38). However, stress exponents greater than 6 have been found when either the testing is performed at $\sigma > 10^{-3}$ E, or a threshold behaviour (a lower stress limit for creep) exists for a material being tested (41). A breakdown from power law creep occurs in the FVS0812 alloy which indicates that if creep is being controlled by a diffusional process, it is more complex than what can be predicted by simple diffusion in aluminum. Al-Fe-V-Si alloys are being studied further in order to examine the possible threshold behaviour and to fully explain the mechanisms and processes governing the creep deformation of these rapidly solidified Al-Fe-V-Si alloys (40).

2.5 Applications

The first use of high-temperature alumninum alloys was to be aircraft wheels. The new braking systems increased wheel heat, and designers needed an alloy that was lighter and more heat- and corrosion-resistant. Dr. Paul Gilman, research associate in charge of Allied's high-temperature aluminum program, said "A major driving force in alloy development has been our internal uses for aircraft wheels through our Bendix Aircraft

Brake and Strut Division" (43) Since its discovery, the FVS0812 alloy has been forged into various aerospace and automotive forms, including aircraft wheels, structural members and engine components Sheet, plate and profiled extrusions have also been made Alloy FVS1212 has been fabricated into product forms that utilize the alloy's high strength and modulus combinations such as sheet, large extrusions and closed die forgings Wire and light-weight fasteners were produced from FVS0611 (43) The advantages of this FVS0611 high-temperature aluminum alloy are light weight, ease of shaping, elevated temperature strength, thermal stability, higher formability and better corrosion resistance Applications of FVS0611 include flight control actuators (Figure 2 23), variable geometry actuators, bulkhead components (Figure 2 24) and precision forgings (42).

Aircraft components must be light and strong and sometimes operate at high temperature Consequently, FVS aluminum alloy sheet for various aircraft applications such as skins, leading edges and structural members are being carefully studied The critical properties for the utilization of these alloys for structural applications include strength at temperature and fracture toughness which FVS aluminum alloys possess (Figure 2 25) Alloy FVS0812 has the design requirement of strength/fracture toughness levels equivalent to 2000 series aluminum alloys, and superior elevated temperature strengths compared to them (Figure 2 26) These desirable elevated temperature strengths and fracture toughness levels result from the high, 27 volume fraction of fine spherical and thermally stable silicides (32)

Flight Control Actuator Component

Application	Thrust vector actuator shaft for enhanced fighter maneuverability X-31A demonstrator aircraft
Rationale	Reduce components weight
Team	Electrodynamics Division (Nor. Hollywood) Rockwell/MBB Research and Technology

System

	Conventional	HTA
Material	Steel (1505)	FVS0812
Size (D x L) [in]	3 L x 10	3 L x 10
Weight (Lbs)		
Maximum Use Temp (°F)	350	350
Expected Life (cycles)	2 Million	2 Million
Thermal Cycle (°F)	65 to 350	65 to 350

Key Results:

- FVS0812 component passed "safety of flight" tests (Al 2014 marginal)
- Excellent dimensional stability and corrosion resistance
- Lighter material allows heftier component design
- Component judge to be flight worthy
- Scheduled to fly on X-31 aircraft in late spring

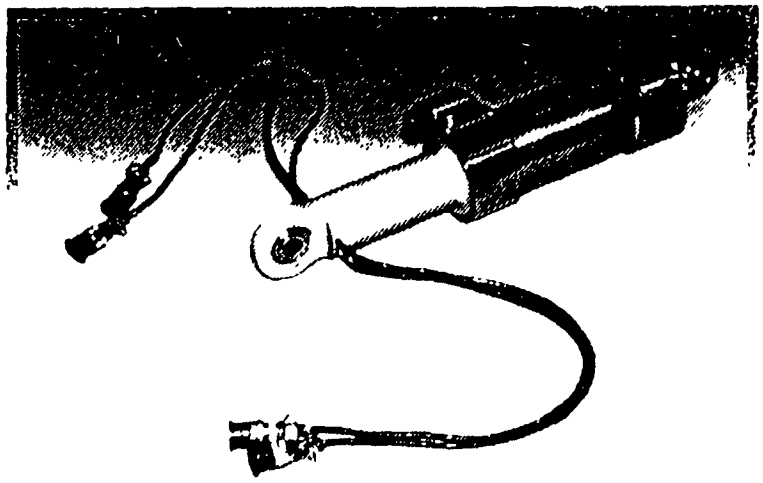

Figure 2.23: Flight Control Actuator (44)

Bulkhead Component

Application	Bulkhead Component
Rationale	Minimize Manufacturing/Assembly Costs and Component Weight
Team	Northrop Aircraft Company Research and Technology

System

	Conventional	HTA
Material	Ti 6-4	FVS0812
Size (W x L) [in]	24 x 48	24 x 48
Ease of Machining	Moderate	High
Inspection Req	High	Moderate
Finishing Costs**		30% Lower

** Note: Restricted from Chem Milling Ti 6-4 In House. No Restriction for Chem Milling FVS0812

Key Results:

- Finished Cost of FVS0812 Component About 30% Less Than Ti 6-4 Counterpart
- Overall Machinability Higher for FVS0812

Status:

- Complete Design of lightweight FVS0812 Component

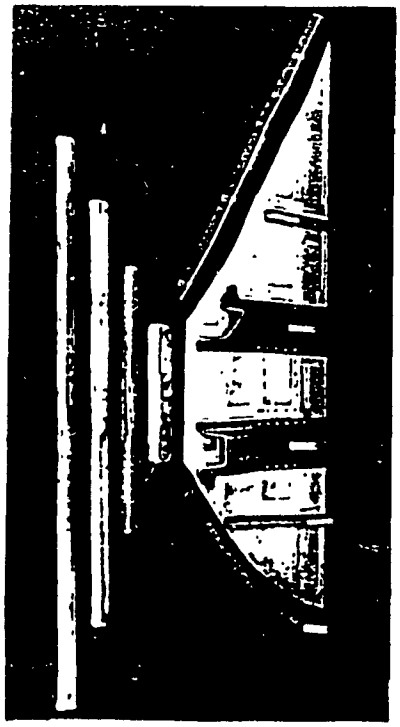

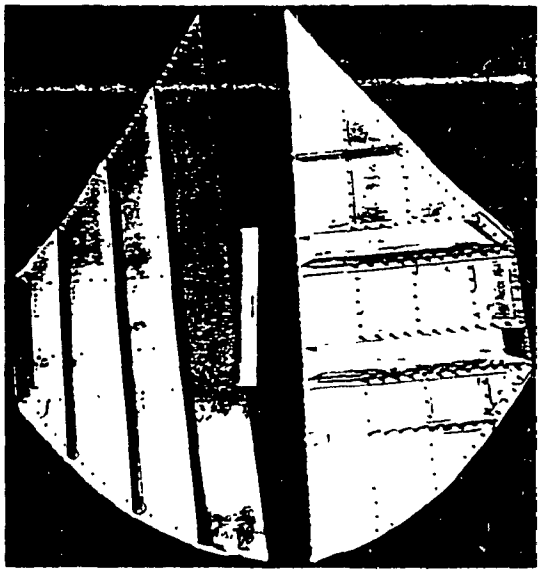

Figure 2.24: Bulkhead Component (44)

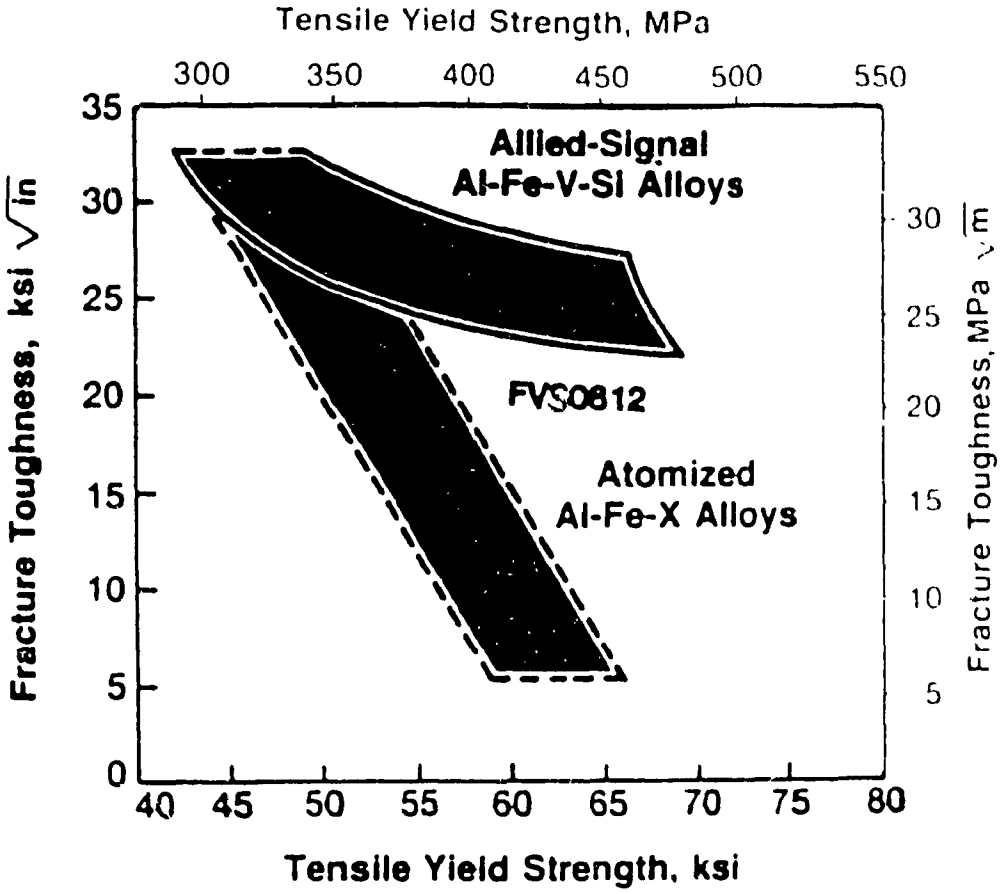

Figure 2.25: Strength/Fracture Toughness Combinations of Rapidly Solidified Al-Fe-V-Si Alloys (32)

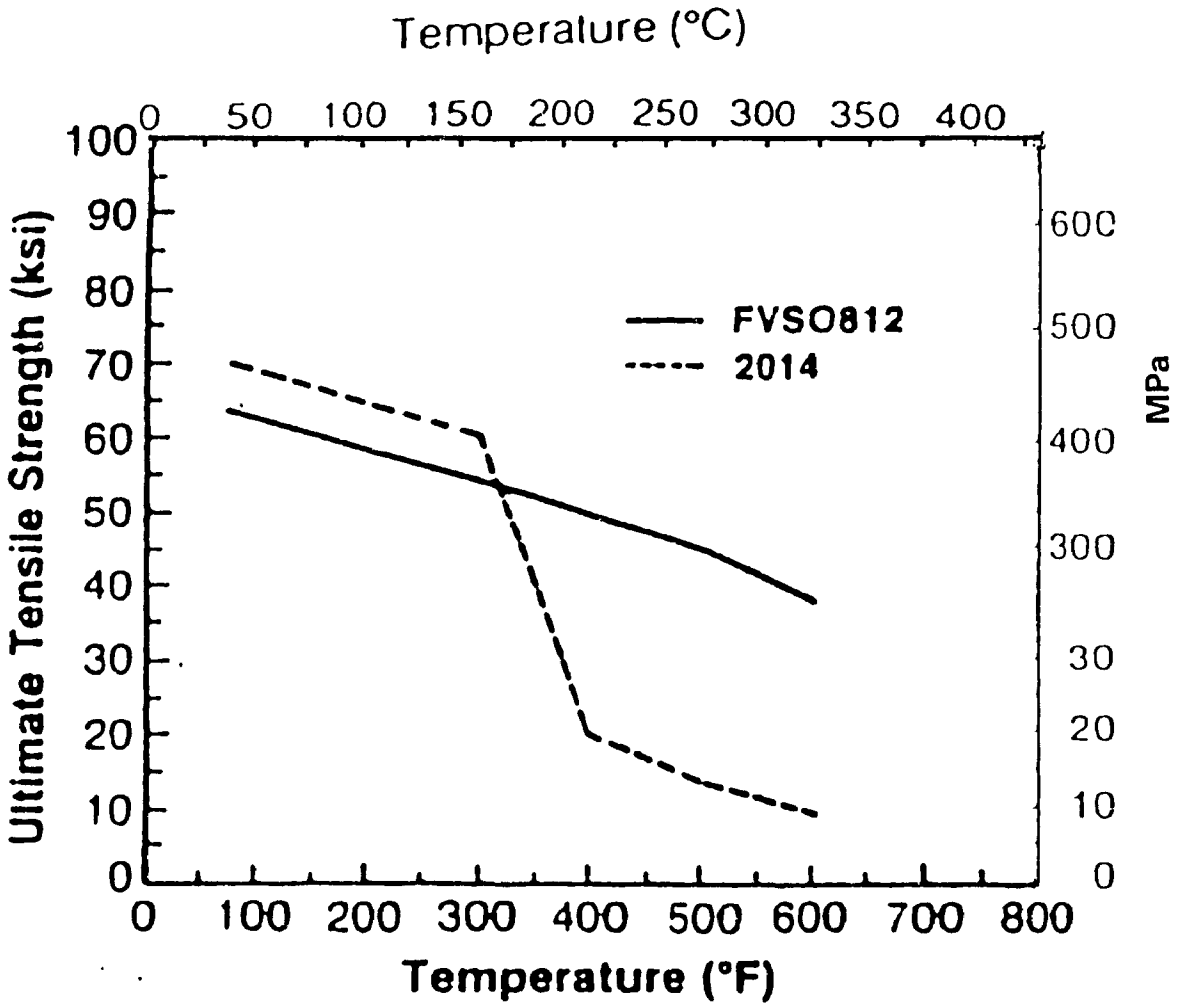

Figure 2.26: Tensile Strength at Temperature of Alloy FVS0812 Compared to Aluminum Alloy 2014-T6 (32)

The fatigue crack growth rates of alloy FVS0812 approaches that of alloy 2014-T6, (see Figure 2.27), even though the grain size of alloy FVS0812 is much finer than that of the wrought 2000 series alloy which should facilitate crack growth By carefully controlling the composition and processing of the alloy to form only the spherical silicides and avoid the coarse flake and plate-like aluminum-iron intermetallics, the alloy's resistance to excessive fatigue crack growth rates is optimized Moreover, the high cycle fatigue strength of alloy FVS0812 is equivalent to the 2000 series alloy because the less than one micron grain size of the rapidly solidified alloy delays fatigue crack initiation (32).

Advances in composite aircraft brake design produced requirements for advanced aircraft wheel forgings that are able to operate at temperatures above that of aluminum alloy 2014, the alloy which is used most often for aircraft wheels The better corrosion resistance than that of 2014 alloy was another performance advantage The FVS0812 has been specifically developed for advanced aircraft wheel applications Prototype wheels have already been manufactured out of the above alloy using commercial forging practices (43). FVS0812 have been found to possess excellent corrosion resistance properties (see Figure 2.28) which may be explained as a result of fine uniform distribution of the silicides (46).

Some engine components have been produced from FVS alloy forgings, rolled rings and thick-section extrusions. The gas turbine engine static structures may operate at temperatures up to 300°C either in ambient air or the operating fluid which exerts pressures ranging from 40 to 55 MPa. An increasingly important design criterion is the

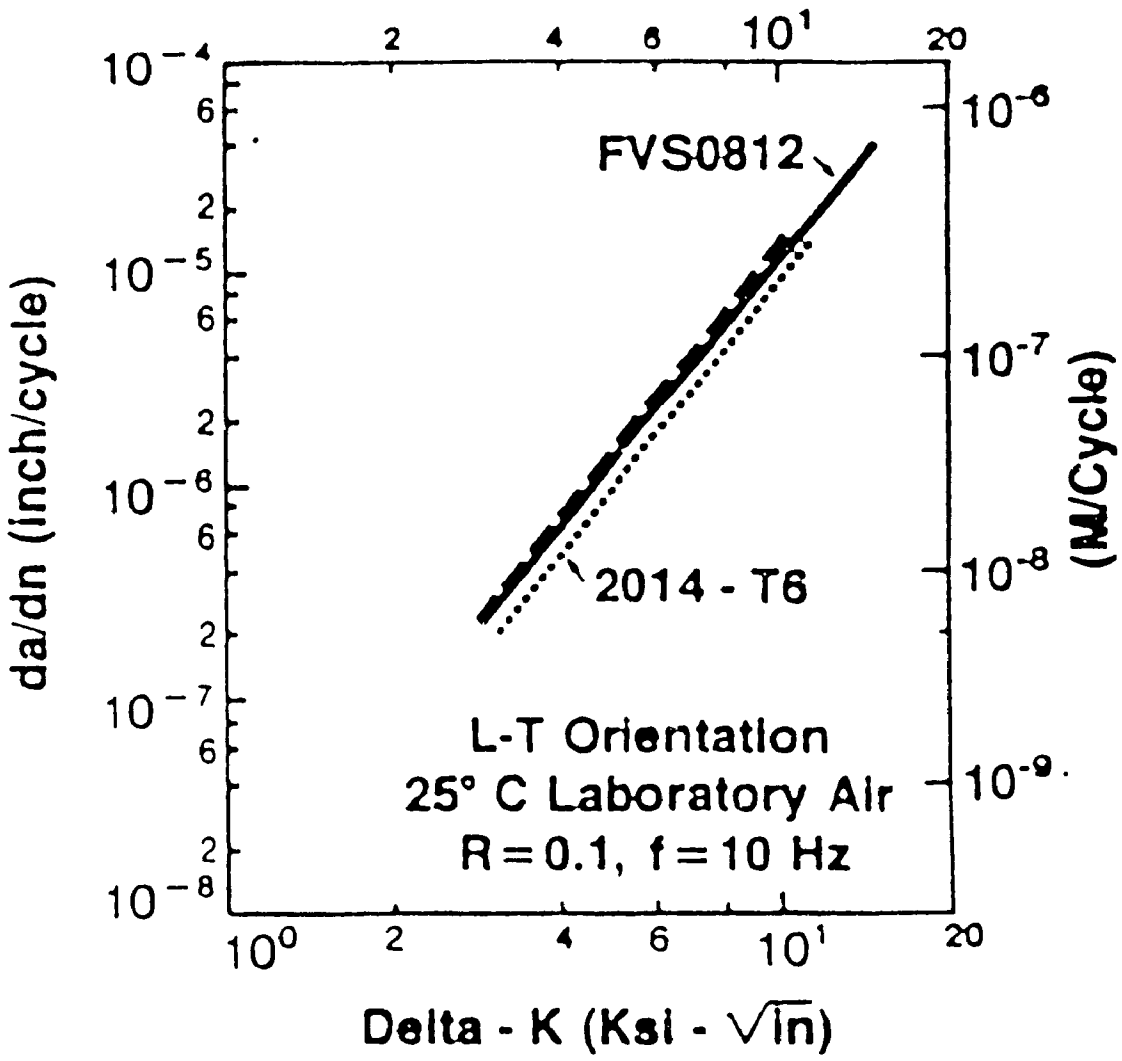

Figure 2.27: Fatigue Crack Growth Rates of Alloy FVS0812 (32)

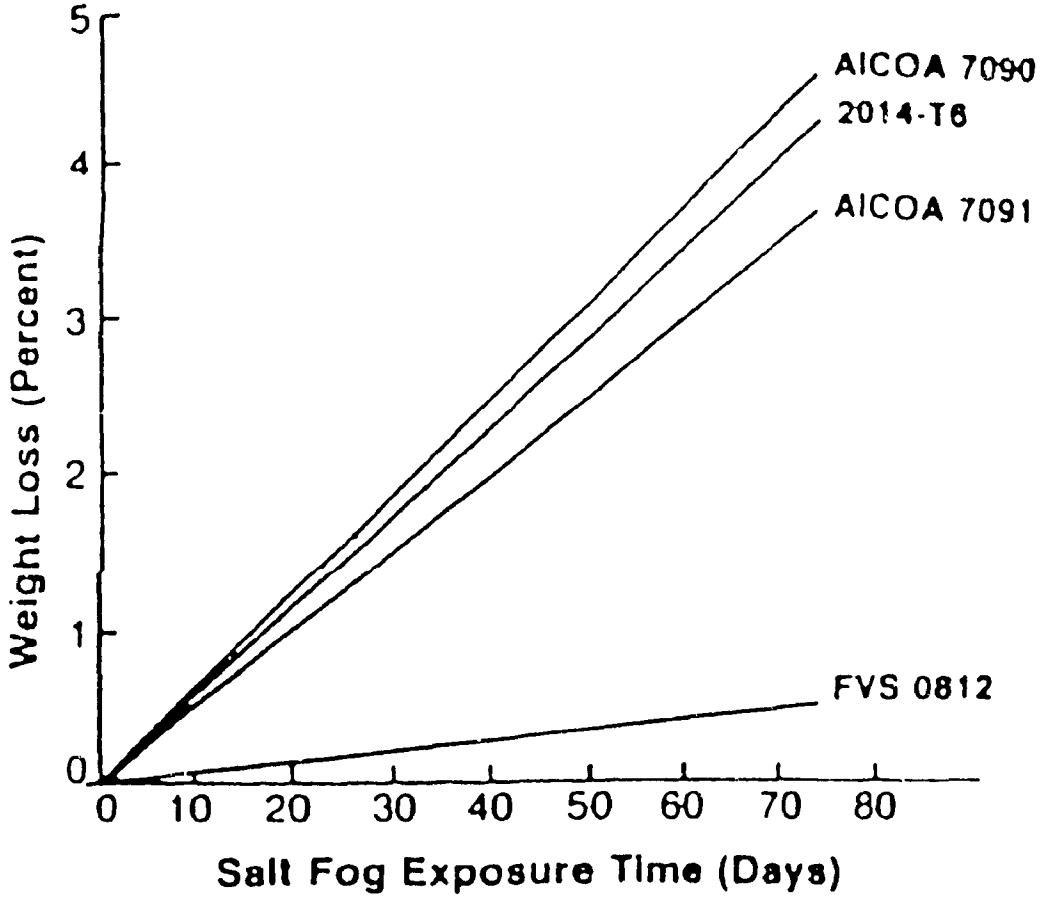

Figure 2.28: Corrosion Performance of Alloy FVS0812 in a Salt Fog (ASTM B-117) (32)

weight savings over titanium, the material that outperformed the conventional aluminum alloys as far as specified temperature/pressure regimes are concerned. Both alloys FVS0812 and FVS1212 are excellent candidates for engine components, since they offer thermal stability and creep resistance. Exposed to 425°C for times up to 1000 hours, these alloys show no degradation in room temperature tensile properties (47). As was mentioned before, the FVS0611 alloy is finding applications rapidly in aircraft structures in the form of rivets, replacing the heavier stainless steel A286 rivets. The FVS0611 rivets are similar in their thermal expansion, galvanic properties and strengths with the aluminum alloy aircraft structures. Alloy FVS0611 has been fabricated into 3 mm diameter rivet wire, with excellent surface finish The wire exceeds the rivet formability requirements and has a room temperature shear strength greater than 225 MPa (32).

Property requirements for advanced missile fin design include: ability to withstand high temperature, high temperature stability and creep resistance. Weight savings as well as cost competitiveness are also of prime concern Alloy FVS1212 has been specifically identified for missile fin applications because of its excellent strengths up to 450°C and its high modulus. Both alloys FVS1212 and FVS0812 are being evaluated for various missile components including sheet for missile fin skins, plate for machined fins and forged fins (30).

Alloys FVS0812 and FVS1212 have Young's modulii of 88 GPa and 97 GPa, respectively, which are approximately 15 to 30% greater than widely used aerospace aluminum alloys. Above 175°C, the specific stiffness of FVS1212 is greater than that of most silicon carbide particulate reinforced aluminum matrix composites. Alloy FVS1212

is truly attractive when its excellent specific stiffness is considered along with its excellent strength at temperature. Alloy FVS1212 not only has superior elevated temperature strength/specific stiffness properties compared to present-age hardened elevated temperature aluminum alloys, i.e., 2618, but also when compared to aluminum-based metal matrix composites which are expensive and difficult to fabricate and machine Alloy FVS1212 derives its elevated temperature strength and high modulus from its 36% volume fraction of fine silicide dispersoids. This alloy does not require special machine tools and techniques for fabrication, nor complex heat treatment to achieve optimum strength levels as required for aluminum-based silicon carbide reinforced composites (32)

2.6 Future Trends

As research into rapidly solidified aluminum alloys continues, new and improved alloys will emerge. The utilization of these advanced aluminum alloys will depend on the property requirements of the application and sufficiently advanced technologies to fabricate the alloys with sufficient understanding of the physical metallurgy of the alloys so that subsequent processing will be tailored to attain particular property requirements (48)

Some of the new materials that are being developed are very promising composites which use rapidly solidified high temperature aluminum These materials utilize high-temperature Al-Fe-V-Si alloy matrix which is reinforced by silicon carbide high strength/modulus continuous fibers. This material, called continuous fibre reinforced high-temperature aluminum (CFRHTA) is expected to reach operating temperatures up to 500°C. In 1990 production of sheets rolled to the size of 2 mm x 450 mm x 900 mm has

started. The effort is on process optimization and consistency as well as on the development of alternate product forms (48)

3. HOT WORKING CHARACTERISTICS

3.1 General Information

Recently, much attention has been focused on replacing ingot casting traditional alloys with powder fabrication of rapidlly solidified, high temperature aluminum alloys. At present, many of the alloys are fabricated by atomization, as described in Chapter 2, followed by hot extrusion as an integrated process of consolidation and forming. These alloys are then subjected to a secondary forming process such as forging to produce mechanical components (49). Therefore, it is very critical to understand the deformation behavior of the alloys produced through powder metallurgy in order to determine a suitable hot working condition to be used in fabrication Unfortunately, limited research has been done in developing the forming technology of these alloys although a great number of hot worked components are used in the automotive industry (50). They show that rapidly solidified high temperature aluminum alloys are quite different from conventional aluminum alloys primarily due to the heavy alloying. Still, the workability of these alloys has not been fully understood because the testing techniques used have been limited to uniaxial tension and compression, each of which has some inherent disadvantages (51-54).

Determination of material properties such as flow stress, strain rate sensitivity and activation energy for deformation requires high strain tests Hot torsion is a suitable method because it has the advantage in comparison to tension and compression of covering a large range of strains as used in extrusion and forging. Also, the large strain

before the start of fracture is very important since the present alloys have limited hot ductility. However, it should be noted that because the hot torsioned material has already been consolidated from powder by hot extrusion, its behaviour in the laboratory tests cannot be expected to be exactly the same as that in extrusion of the powder. Nevertheless, hot torsion tests provide basic information on workability which is currently not available and is also an important guide to secondary forming such as forging. (55-58).

3.2 Stress-Strain Curves

In the work of Zhou et al. (59), hot torsion tests were performed on Al-20Si-7.5Ni-3Cu-1Mg rapidly solidified aluminum alloy. They aimed at determining the hot working characteristics of the material over a range of temperatures and strain rates in order to establish a constitutive equation.

It was generally observed that, under most of the deformation conditions applied, the stress-strain curves were characterized by distinct stress peaks followed by considerable softening particularly at low temperatures (< 400°C) and high strain rates (> 1.0 s^{-1}) (Figure 3.1); such peaks and high softening are usually absent from the curves of conventional aluminum alloys. Aluminum alloys usually display a gradual increase and then a plateau in stress until fracture due to the balance between work hardening and softening by dynamic recovery (DRV). The degree of softening is dependent on the temperature and strain rate applied. Assuming there are no other microstructural changes, a distinct peak stress can be an indication of softening by dynamic recrystallization during deformation. However, this softening mechanism is usually not operative in aluminum

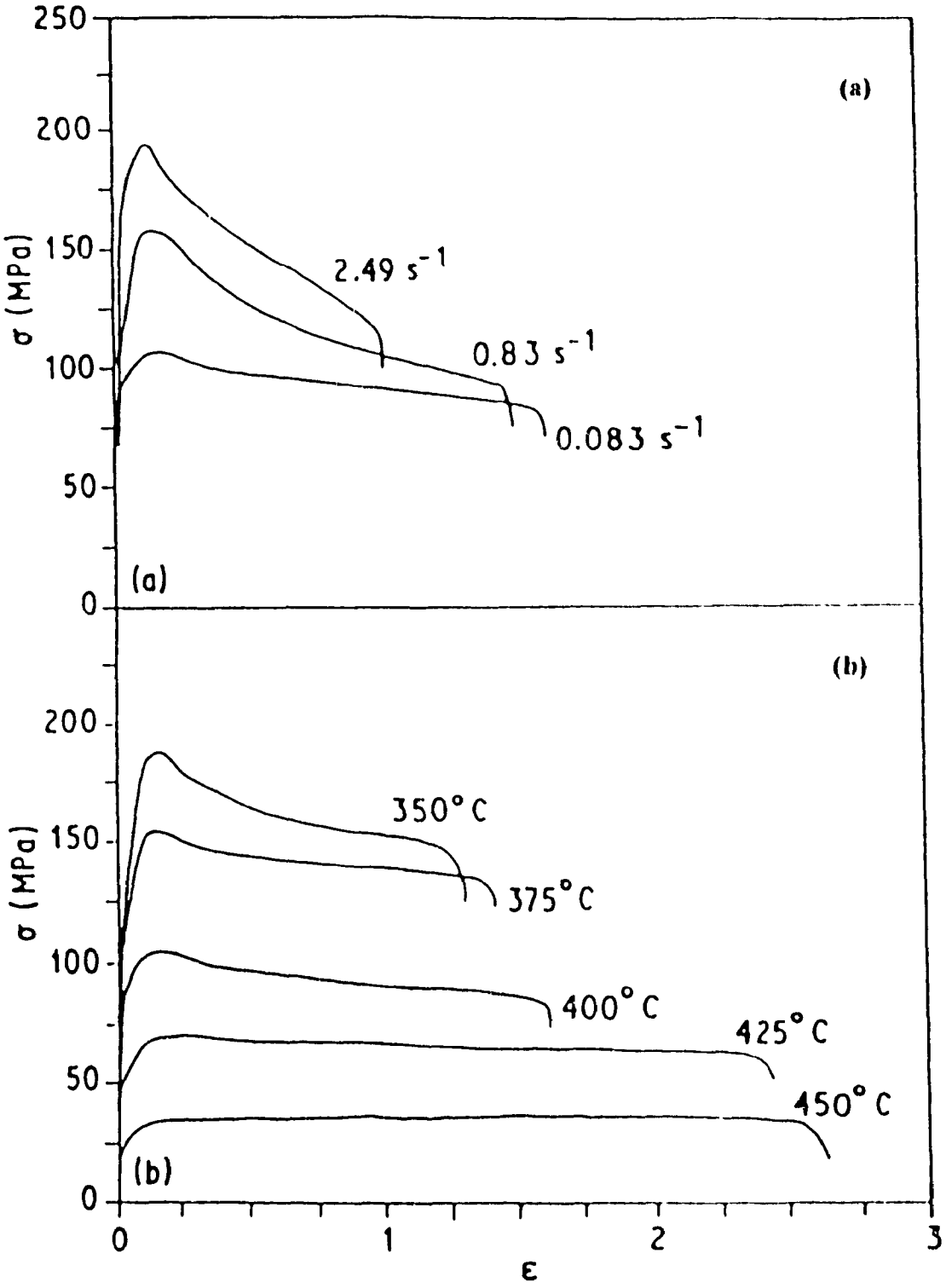

Figure 3.1: Selection of Equivalent Stress-Strain Curves Obtained from Torsion Tests of Al-20Si-7.5Ni-3Cu-1Mg at (a) 400°C and (b) 0.083 s^{-1} (59)

alloys with high stacking fault energy which allow dislocations to cross-slip and climb easily so that dynamic recovery can occur The appearance of the stress peak can be attributed to the following effects (59,60)

- Dynamic Recrystallization (DRX)
- Deformational Heating
- Structural Changes

3.2.1 Dynamic Recovery (DRV) and Recrystallization (DRX)

DRX is generally observed in metals with low stacking fault energy (SFE) whereas in metals with high SFE, it seldom occurs because dynamic recovery produces a low dislocation density When the dislocation density builds up to a critical level, the nucleation of DRX occurs At lower strain rates, nucleation possibly occurs by the bulging of existing grain boundaries Migrating grain boundaries leave behind dislocation-free regions in which the dislocation density once again increases as strain proceeds until recrystallization is again nucleated At high strain rates, a fine and dense tangled cellular structure is developed throughout the grains but more strongly at the grain boundaries and deformation bands Nuclei develop initially along grain boundaries where there are high misorientations between the subgrains, with further strain DRX spreads to the center of the old grains to complete one wave The dislocation densities at the centres of the first new grains increase sufficiently that nucleation occurs again before any wave of recrystallization is complete As a result, there is a distribution of DRV dislocation

substructures which maintains the average flow stress at a steady state between the initial yield stress and the peak stress (61,62).

Zhou et al. (59) found that the degree of DRX is sensitive to strain rate and temperature. The stress peaks disappeared at low strain rates (0.083 s^{-1}) and high temperatures (425°C to 450°C) (Figure 3.1). Under these deformation conditions, the stress-strain curves appear to be typical of a material that is being restored by DRV, that is work hardening followed by steady state deformation. This is thought to differ from the condition at lower temperatures and higher strain rates where stress and dislocation concentrations are built up causing nucleation of DRX. With increasing strain rate at a given temperature, softening by DRX becomes more significant as indicated by the sharp peaks in Figure 3.1 and evidenced by the microstructures shown in Figure 3.2 DRX is stimulated in the vicinities of large particles due to local strain concentrations (63,64)

3.2.2 Deformation Heating

The work of defomation is transferred into heat; the effect is more significant when the stress is high at high strain rate or low temperature. This effect leads to thermal softening in the gauge section of a test specimen particularly at high strain rates as the deformation approaches an adiabatic process. As seen in the review, rapidly solidified, high temperature aluminum alloys may have high hot strength which are strongly dependent to temperature and strain rate. When the strain rates are not too high, the temperature rise is insignifcant, so that deformation heating effect is unlikely to be fully responsible for the stress peaks. This is supported in Zhou et al (59) by the fact that at

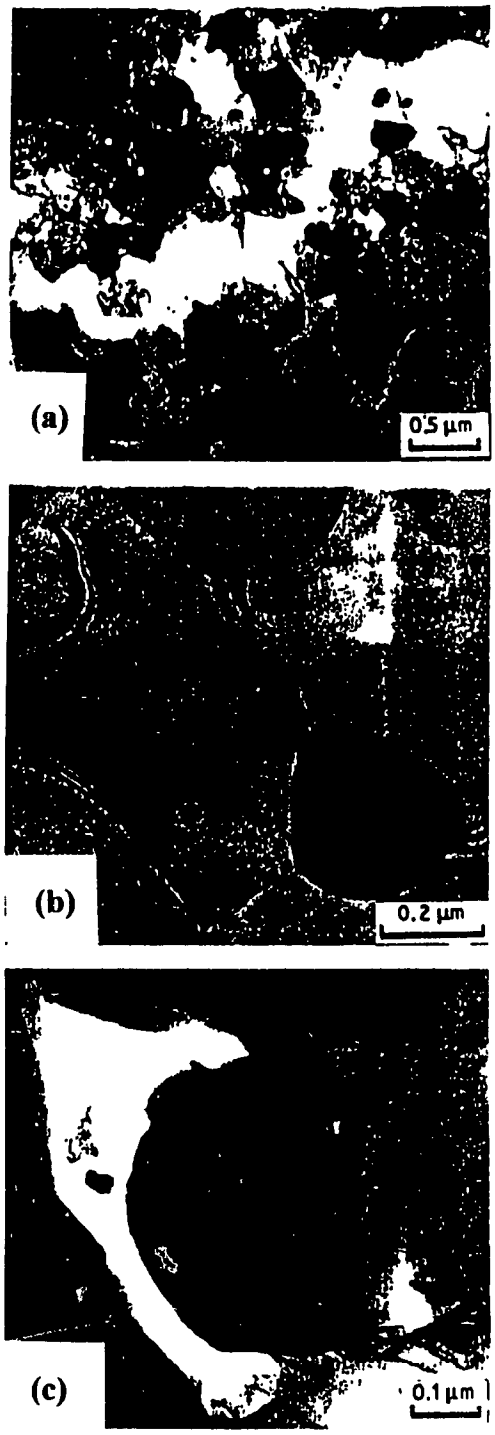

Figure 3.2: Microstructures of Al-20Si-7.5Ni-3Cu-1Mg at 400°C and 2.49 s^{-1}: (a) General Structure; (b) Interaction Between Particles and Subgrain Boundaries; (c) Outcrop of Recrystallization at a Particle (59)

the low strain rate (0.083 s^{-1}) when deformational heating would be less significant, the stress peaks were also observed at 350°C to 400°C as shown in Figure 3.1. This suggests that effects such as DRX or other structural changes might be at play (62,64).

3.2.3 Structural Changes

Structural changes such as loss of solute to precipitates, transformation and second phase coarsening have been known to cause softening during deformation. The initial dynamic precipitation and subsequent coarsening of second phase particles has been considered to be responsible for stress peak exhibited by a 2024 aluminum alloy in torsion (57,58,67,68). The Mg_2Si phase had a tendency to coalesce while the other constituent phases dispersed in the aluminum matrix. Hence, the coarsening of Mg_2Si phase might be relevant to the observed peak in the stress-strain curves. However, Zhou et al (59) used X-ray diffractometry for Al-20Si-7.5Ni-3Cu-1Mg which revealed little change in the aluminum matrix lattice parameter and phase constituents during deformation indicating that neither precipitation or transformation did occur. Even if there was undetectable precipitation, it would be highly unlikely to have an impact on the flow stress of the material because a loss in solutes would be balanced by an increase in precipitate density (66-69).

3.3 Ductility

The ductility of rapidly solidified, high temperature aluminum alloys are found to be very low in comparison with that of conventional aluminum alloys. At low

temperatures and high strain rates, steady state could not be reached before failure as shown in Figure 3.1. The flow only reached steady state at relatively low strain rates indicating that ductility is dependent on the strain rate. Figure 3.3 shows the variation of the strain to fracture (ε_f) with temperature and strain rate of Al-20Si-7.5Ni-3Cu-1Mg. The increase of ε_f at higher temperature and lower strain rate is due to the reduced stress concentrations at second phase particles where crack initiation and propagation takes place. This argument has been regarded as an indication that dynamic recovery is the principal restoration mechanism in single phase aluminum alloys. On the other hand, in dynamically recrystallizing metals, ε_f increases with rising strain rate because the rate of DRX increases, isolating and blunting any crack nuclei. If this were the case, the results presented by Zhou et al. (59) would suggest that DRX is not the major restoration mechanism. However, the ductility of an aluminum alloy is dependent not only upon restoration mechanisms but also upon fracture mechanisms. In the above rapidly solidifed, high temperature aluminum alloy, fracture starts by the cracking of silicon crystals and the decohesion between aluminum and dispersed phase particles which are enhanced by deformation at a higher strain rate. The volume fraction of these particles is usually about 30% which gives a high interface area and an easy path for linking of cracks inside the material. The increased density of recrystallized nuclei resulting from deformation at high strain rate will probably not prevent any decohesion, thus leading to failure at an earlier stage of deformation (70,71).

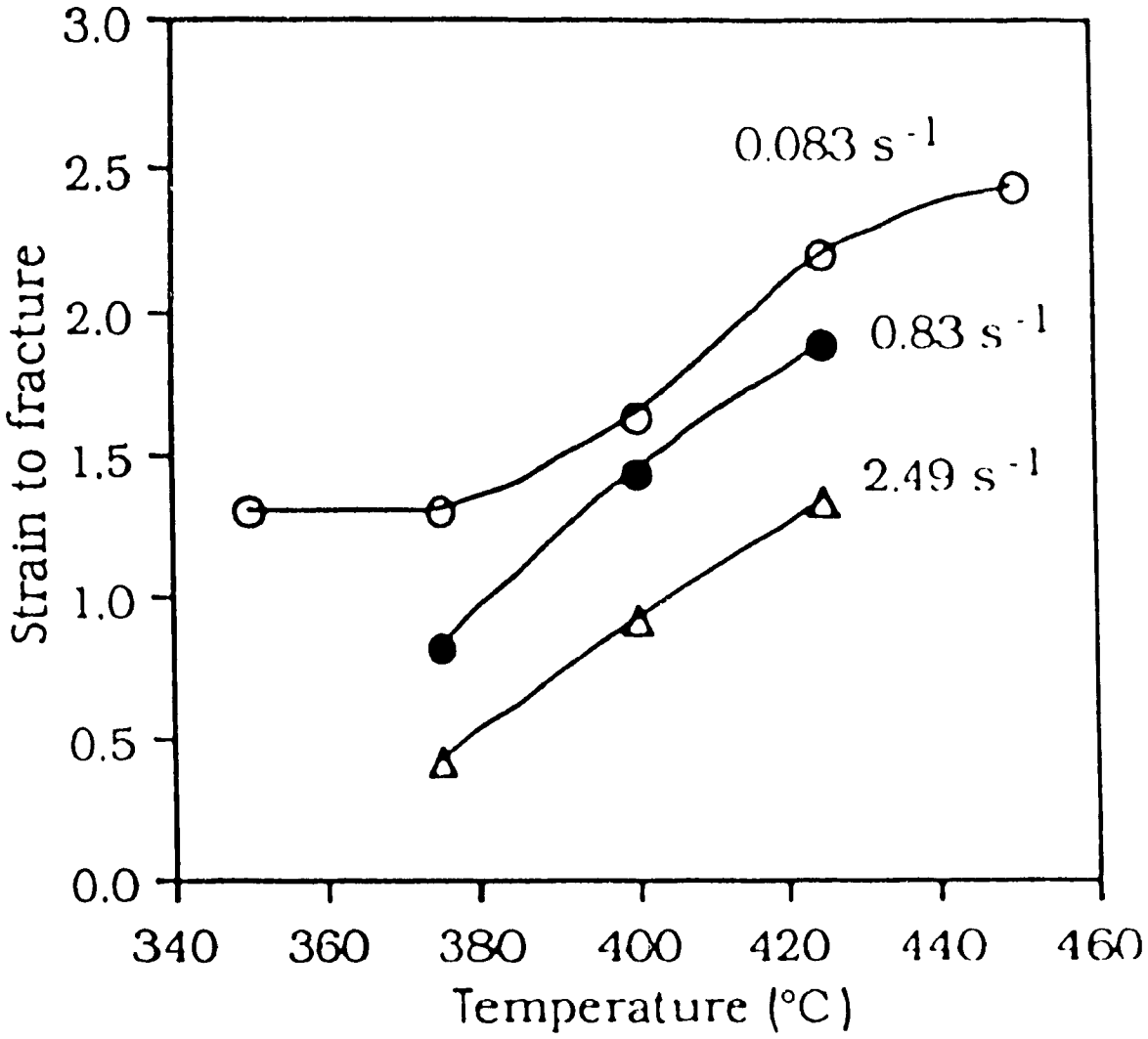

Figure 3.3: Strain to Fracture at Different Temperatures and Strain Rates for Al-20Si-7.5Ni-3Cu-1Mg (59)

3.4 Strain Rate Sensitivity

The strain rate sensitivity (m) of rapidly solidified, high temperature aluminum alloys is high in comparison to various grades of conventional aluminum alloys. As determined from the slope of plots of the peak torque against strain rate, values range from m = 0.13-0.24 at 300-425°C to m = 0.026-0.227 at 300-500°C (72). High m values mean that the material can be strain rate hardened. A pratical implication is a reduction in previous strain rate can considerably reduce the flow stress of the material so that a reduced temperature or an increased strain can be applied; however in commercial production, it is usually desirable to have large deformation rates for economic reasons. The relationship between the m values and the structure of the material is yet to be understood thus not explaining the high m values for these alloys. Zhou et al (59) pointed out that one of the causes may be the high silicon crystal content in the material (about 20 vol. %). Silicon has a linear thermal expansion coefficient about one-eighth of aluminum resulting in imposed stresses in the neighbouring aluminum matrix when the temperature is raised. It has been observed that imposed random internal stresses would help plastic flow of the aluminum matrix and lead to a low stress exponent and a high m at low applied stresses. The higher m value may be due to an increase of the resistance to instability of the metal flow resulting from the pre-exisiting stresses. Thus, the m value is regarded as a measure of the capacity of the material to resist plastic instability. This has led to aluminum alloys having superplasticity by adding silicon carbide whiskers. Therefore, the stresses imposed by silicon crystals are a factor for the high m values found in rapidly solidified, high temperature aluminum alloys (72-74).

3.4 Interdependence of Stress, Strain Rate and Temperature

A number of mathematical expressions have been proposed to describe the relationship between flow stress (σ), strain rate (ε) and temperature (T). It is generally accepted that the deformation behaviour of an aluminum alloy in hot working is similar to that in creep and the correlations between σ and ε can be described by (60,73-76)

$$\varepsilon = A_1\sigma^n \text{ (for low stress)} \qquad (3.1)$$

$$\varepsilon = A_2 \exp(\beta\sigma) \text{ (for high stress)} \qquad (3.2)$$

or

$$\varepsilon = A_3[\sinh(\alpha\sigma)]^{n'} \qquad (3.3)$$

where A_1, A_2 and A_3 are temperature dependent functions and α, β, n and n' are material constants. It is found that the hyperbolic sine equation (Equation 3.3) usually gives the most satisfactory fit to hot working of aluminum alloy data. To show that α and n' are independent of temperature in Equation 3.3, plots of the natural logarithmic strain rate against ln sinh($\alpha\sigma$) are made. In Zhou et al (59), the best fit to the parallel straight lines was obtained with the constitutive constants: α = 0.015 MPa^{-1} and n' = 2.46 (see Figure 3.4). The linearity in Figure 3.4 confirms the validity of Equation 3.3 describing the relationship between the peak stress and strain rate at a constant temperature.

In order to fully establish a constitutive equation, a temperature factor must be included. To do this, ln sinh($\alpha\sigma$) is plotted against the reciprocal absolute temperature which is shown in Figure 3.5. The observed linearity at the different strain rates incorporates an Arrhenius activation energy term in Equation 3.3 leading to (62,75-78)

$$\varepsilon = A'[\sinh(\alpha\sigma)]^{n'} \exp(-Q/RT) \qquad (3.4)$$

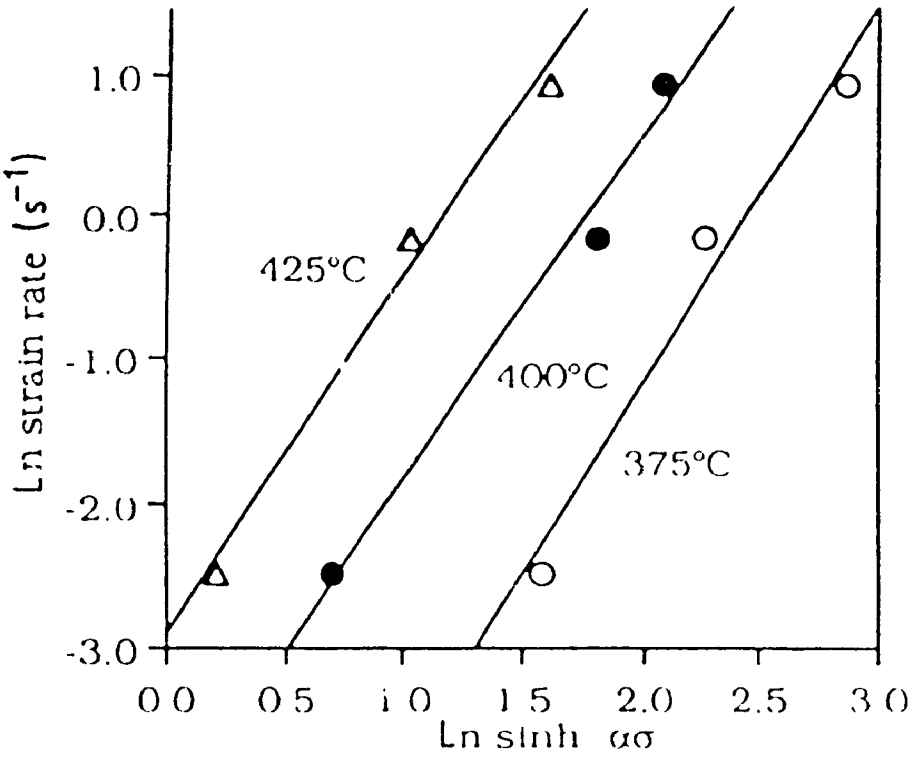

Figure 3.4 Application of the Hyperbolic Sine Equation at the Given Temperatures to Determine the Constitutive Constant n(in Equation 3.3 for Al-20Si-7.5Ni-3Cu-1Mg (59)

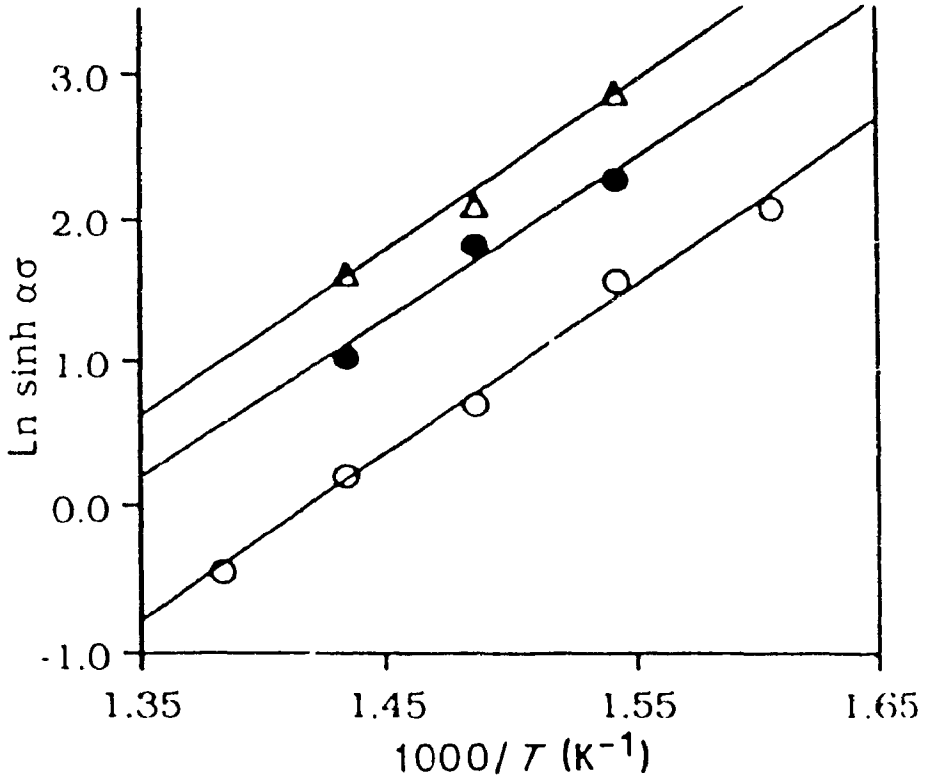

Figure 3.5: Determination of the Activation Energy for Al-20Si-7 5Ni-3Cu-1Mg at the Peak Stress, Surface Equivalent Strain Rates (59)

where A′ is a temperature independent constant and Q is the activation energy for hot working. Zhou et al. (57) found an averge Q and A′ value of 233 kJ/mol and 1.58×10^{16} s^{-1} respectively. Since the constitutive constants in Equation 3.4 are graphically determined, errors can be incorporated in the procedure. As a further check on this equation, all the stress data obtained for all temperatures and strain rates can be correlated to an expression as the temperature compensated strain rate or Zener-Hollomon parameter (Z):

$$Z = \dot{\varepsilon} \exp(Q / RT) = A[\sinh(\alpha\sigma)]^n \tag{3.5}$$

A single linear relationship between ln Z and ln sinh(ασ) is obtained as shown in Figure 3.6. It is clear that the constants derived in Figures 3.4 and 3.5 are not in significant error. Figure 3.6 also verifies that Z is applicable to the description of the material properties in relation to deformation conditions. This verification is of great significance for the control of a metal forming process of the material with the Z parameter (62,75-78).

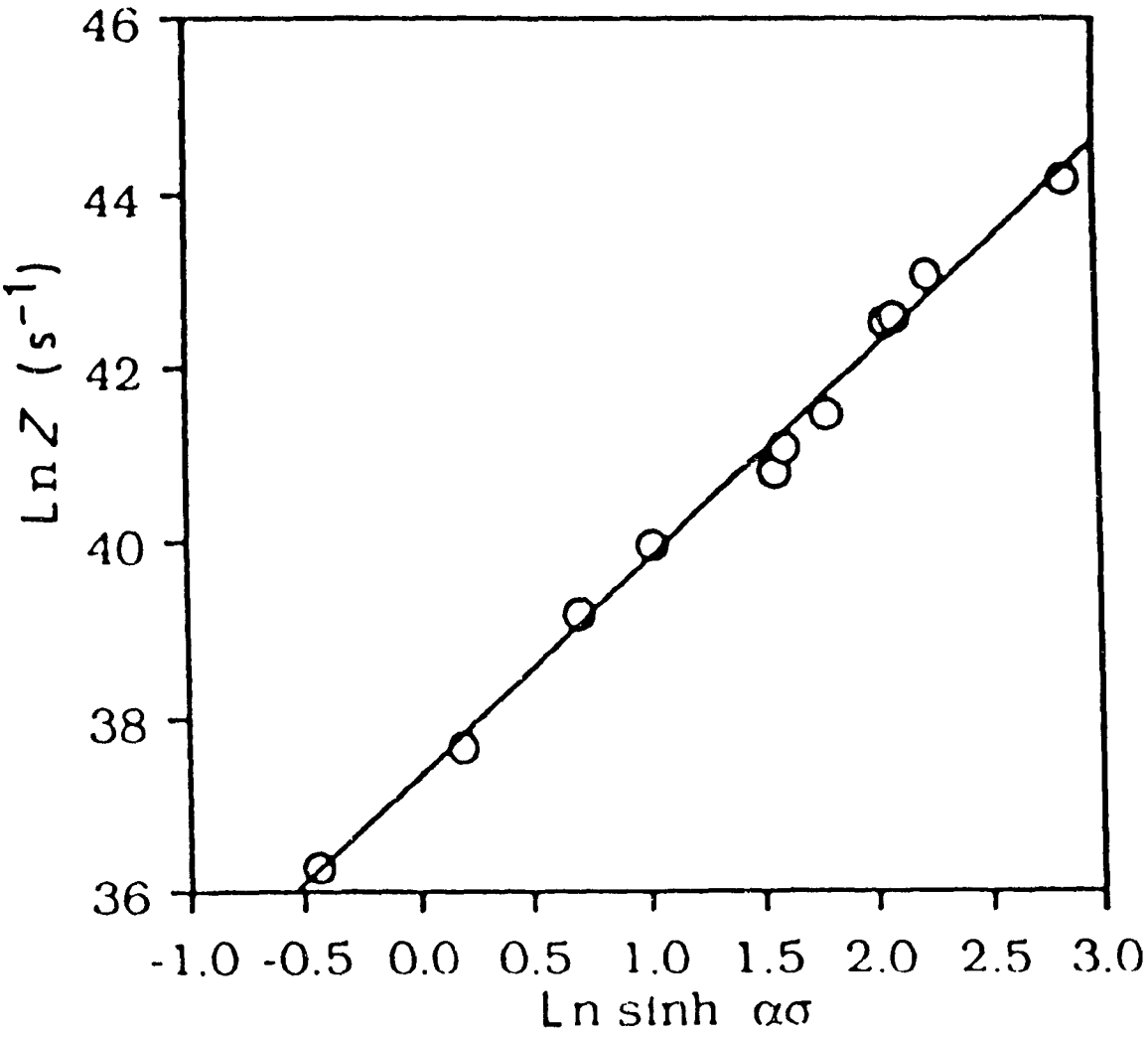

Figure 3.6: Applicability of the Zener-Hollomon Parameter to Torsional Deformation for Al-20Si-7.5Ni-3Cu-1Mg (59)

4. EXPERIMENTAL PROCEDURE

4.1 Torsion Testing

In recent years, hot torsion testing of solid cylindrical specimens has become more reliable in determining optimum hot working parameters such as strain, strain rate and temperature (55,58,62). Although high strains can be achieved at a constant strain rate, there is a linear variation of strain and strain rate from zero at the centre to maximum at the surface If necessary, the effects of this variation can be reduced by use of a specimen with a tubular cross section The major advantage of torsion over tension and compression testing is that there is no change in geometry of the specimen during deformation In light of this fact, true strain and strain rate are equal to the engineering strain and strain rate in torsion Moreover in tension, a sample undergoes localized necking, while a compression specimen suffers from barrelling due to frictional forces at the anvils In the present work, the torsion test was used to determine the hot working properties of two FVS alloys.

Torsion testing data are usually recorded in the form of torque (M) versus angle of twist (θ) diagrams These curves are converted to stress (σ)-strain (ε) curves, equivalent to those in uniaxial compression or tension, using the following equations (79):

$$\sigma = \sqrt{3}M(3+m+N)/(2\pi r^3) \quad (4.1)$$

$$\varepsilon = r\theta/\sqrt{3}L \quad (4.2)$$

where r and L are the gauge radius and gauge length of the specimens, respectively and m and N are strain rate sensitivity and strain hardening rate

4.2 Testing System and Equipment

Specimens were deformed in a servo-controlled, closed loop torsion machine designed by Sandor Fulop (80) and located in the Department of Mining and Metallurgy of McGill University (Figure 4 1) In this MTS electro-hydraulic system, torque is applied to a specimen through a rotary hydraulic actuator mounted on a converted lathe bed Hydraulic power for the system is provided by a 20 MPa supply On the torsional frame, the test piece is held by two coaxial superalloy bars with attached grips One end of the test piece is twisted a measured amount by the hydraulic motor controlled by a servo-valve while the other end is held fixed by a torque cell (80)

The specimen is heated by a quadruple elliptical radiant furnace connected to programmable controller with varied power input. The furnace is water-cooled and capable of temperatures up to 1200°C with rapid heating rates A transparent quartz tube runs through the furnace enclosing the specimens, grips and bars Argon is circulating through the tube during heating and testing to prevent oxidation The temperature is measured by an alumel-chromel (K-type) thermocouple, insulated with double bore ceramic tubing, extending along the stationary test piece shoulder and attached to the specimen with alumel-chromel wire to maintain thermal contact The location of the thermocouple tip on the gauge section at the fixed end of the specimen was determined to be satisfactory since the thermocouple could be rigidly fixed to the specimen yet undergo only a small fraction of its total revolutions without suffering damage (80)

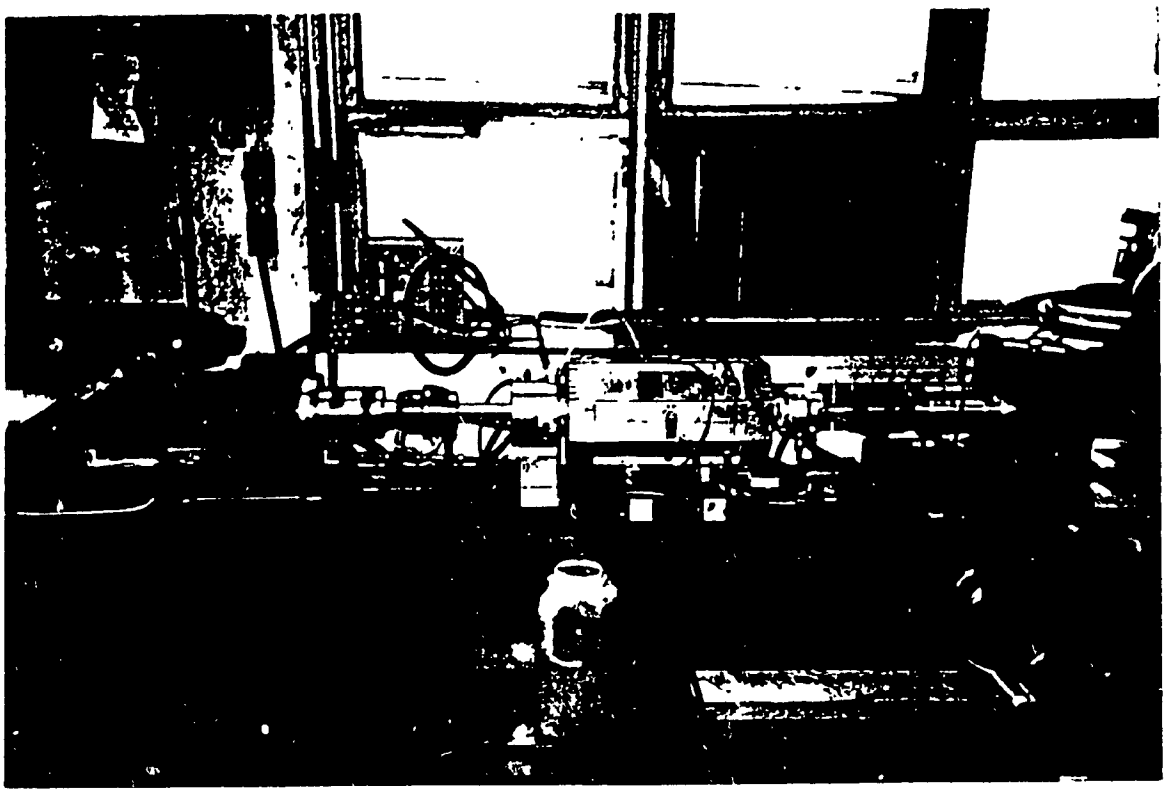

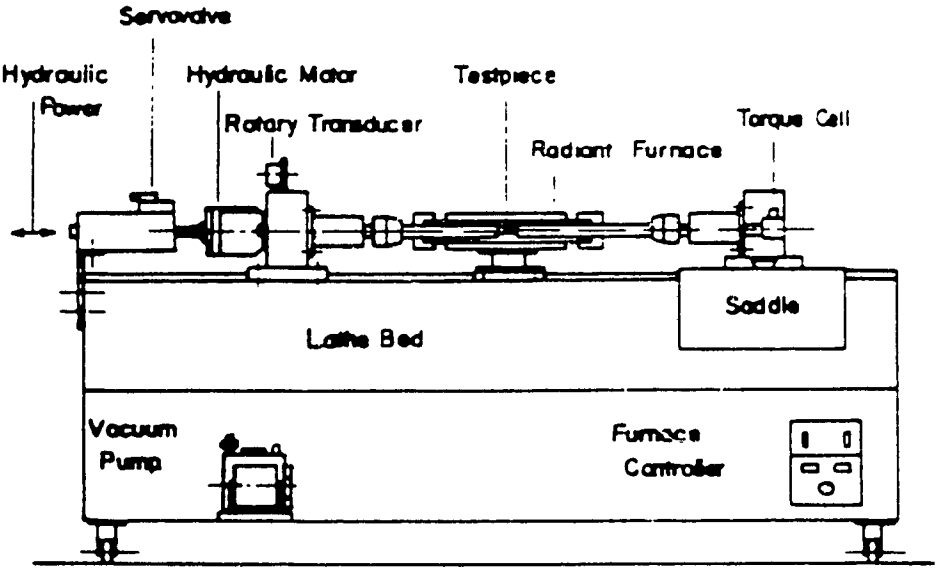

Figure 4.1: Torsion Testing Machine (80)

4.3 Test Materials

Two materials were used in the present study which are commercially designated as FVS1212 and 8009. The chemical composition of the materials are shown in Table 4.1. Torsion specimens with axes parallel to the rolling or casting direction were machined to close tolerances, especially in the gauge section, in order that twisting would be uniform. The test specimen design is shown in Figure 4.2. One end of the test piece is threaded, while the other end has a rectangular section which fits into a slot. This arrangement allows for easy mounting and removal without accidentally straining the specimen

4.4 Test Procedure

Before starting any test, the reflecting surfaces of the furnace were cleaned with gauze so that the test temperature would be reached as quickly as possible For both materials, isothermal continuous tests were conducted at 300 to 600°C at torsional shear strain rates of 0.1, 1.0 and 4.0 s^{-1} to a strain of appoximately 2.5 or to fracture The samples were twisted without interruption to fracture. All tests were carried out in a controlled atmosphere of high purity argon. Every specimen was heated to desired temperature and held constant ten minutes prior to deformation All specimens were quenched in water less than ten seconds after deformation was completed

Table 4.1 Chemical Compositions of Test Materials

Alloy	wt.% Fe	wt % V	wt % Si	wt.% Al
FVS1212	11.7	1.2	2.4	Balance
FVS0812 (8009)	8.5	1.3	1.7	Balance

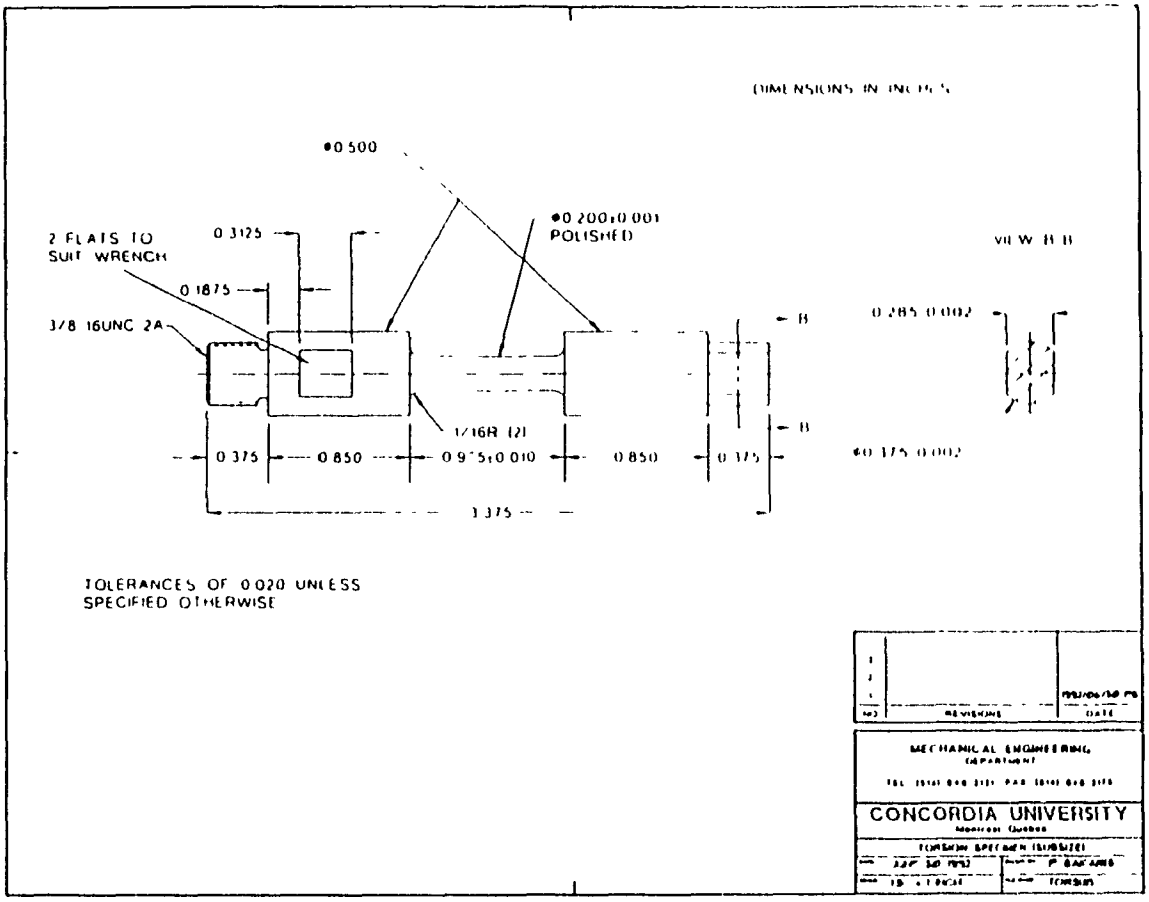

Figure 4.2: Torsion Specimen Design.

5. RESULTS

5.1 Stress-Strain Curves

The equivalent stress (σ) - equivalent strain (ε) graphs that were produced by the plotter interfacing with the signal processor during the hot torsion testing were redrawn to a common scale to facilitate the possibility for analogous comparison. The conversion from torque to equivalent stress by means of Equation 4.1 was carried out using an average value of $m = 0.3$ and $N = 0$ which is accurate only for the peak stress. We notice that for 8009, the peak stress values gradually drop from about 350 MPa at 300°C to 250 MPa at 400°C, 150 MPa at 500°C and as low as 100 MPa at 600°C (Figure 5.1). However, though similar trend is present in FVS1212, the tendency is to greater strength at lower temperatures in association with greater softening at elevated temperatures. For 8009, we observed peak stresses reaching approximately 450 MPa at 300°C; at 400°C, σ ranged from 350 MPa at 0.1 s^{-1} to 400 MPa at 4.0 s^{-1}; at 500°C, an average of 175 MPa and finally at 600°C, a low 50 MPa at 0.1 s^{-1} but 100 MPa at 4.0 s^{-1} as shown in Figure 5.1.

These peak stresses plotted versus temperature in Figure 5.2, show that there is almost linear softening for 8009 with the increase of temperatures from 300°C to 500°C for all strain rates. However at 600°C, the stress declines more slowly and appears less strain rate sensitive. The FVS1212 alloy shows somewhat different behavior. The peak stress does not drop so rapidly from 300 to 400°C and then very rapid softening takes place down to 150 MPa for all three strain rates at 500°C. As the temperature increases

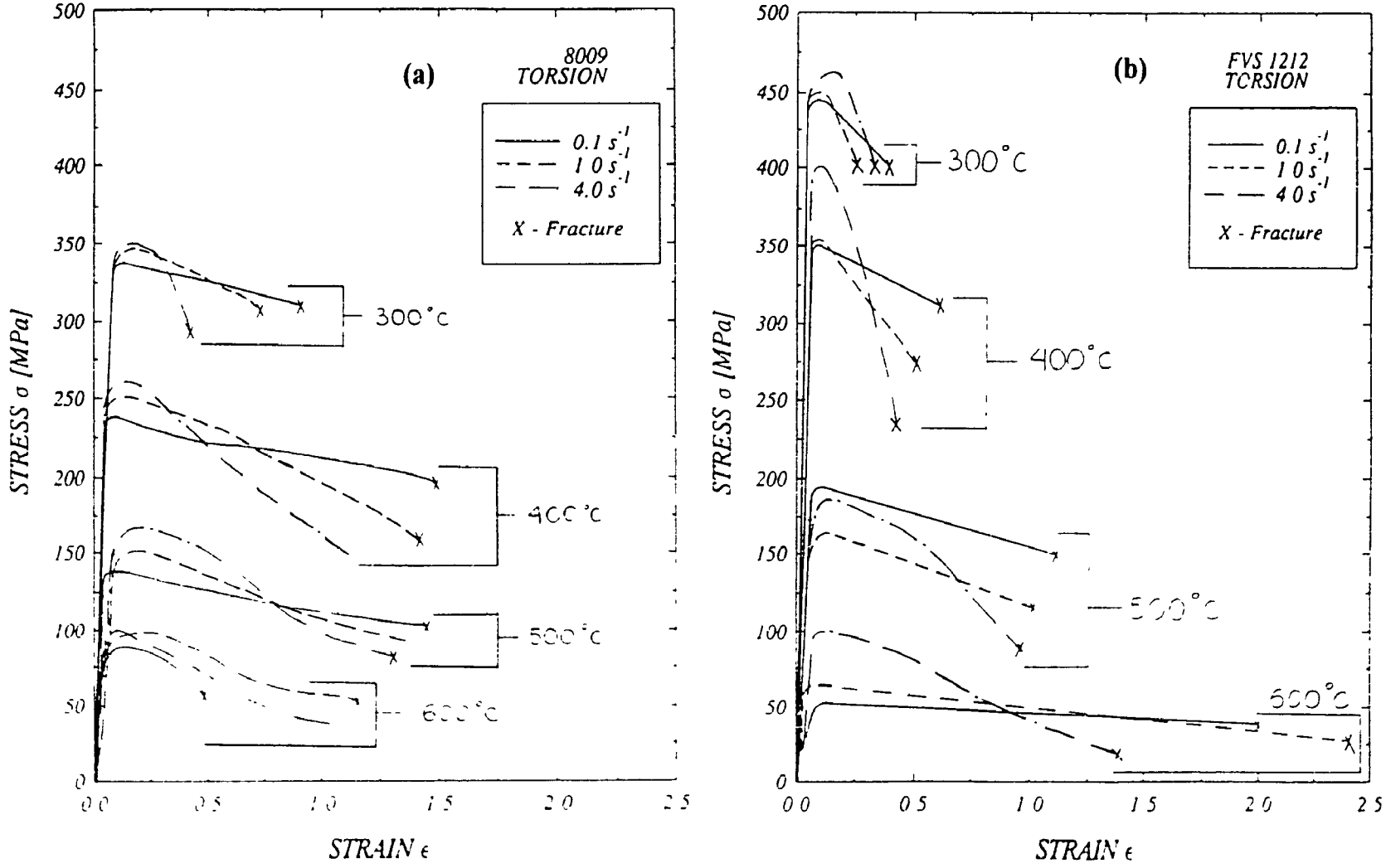

Figure 5.1 Stress-Strain Curves: (a) 8009 and (b) FVS1212

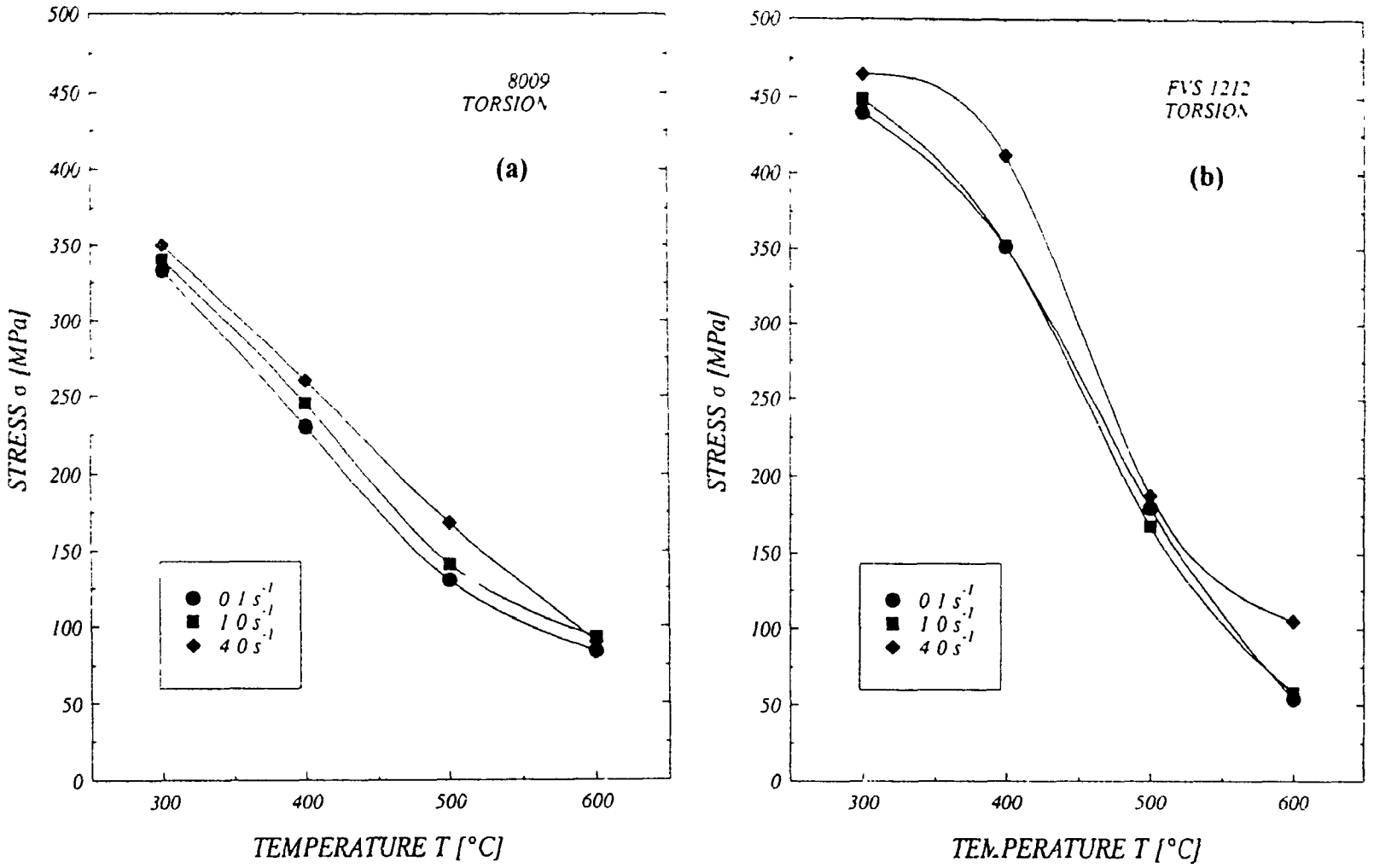

Figure 5.2: Peak Stress vs. Temperature: (a) 8009 and (b) FVS1212

to 600°C, the high strain rate 4.0 s^{-1} decreases the peak stress less than the low strain rates (Figure 5.2)

5.2 Ductility

Figure 5.3 shows plots of the strain-to-fracture versus temperature for each alloy. For 8009, as the temperature rises from 300 to 500°C, there is a trend towards higher fracture strain, maximum of 1.5 at 500°C. In this temperature range, increase in the strain rate yields a decrease in the fracture strain. This trend reverses itself in the range of 500 to 600°C so that for 0.1 s^{-1} fracture occurs ≈ 0.5 while for 0.1 s^{-1} and 1.0 s^{-1} the strain exceeds 1.25. Unlike 8009, the FVS1212 alloy shows an increase of fracture strain with temperature increase. From 300 to 375°C the increase in strain is gradual in relationship to the gradual decrease in stress. In general there is a definite trend for increase in strain rate to cause a decrease in the fracture strain. From 375 to 600°C the ductility rises rapidly except at 4.0 s^{-1} which shows slower rate of increase in relation to slower drop in strength.

5.3 Constitutive Plots

Based on the hyperbolic sine analysis, the optimum value of α should result in the constant temperature lines on the plots of log $\dot{\varepsilon}$ versus log sinh($\alpha\sigma$) being close to parallel. However, it is common to analyze with the value of α from other alloys as described in the literature since this permits comparison of activation energies and of data by graphical

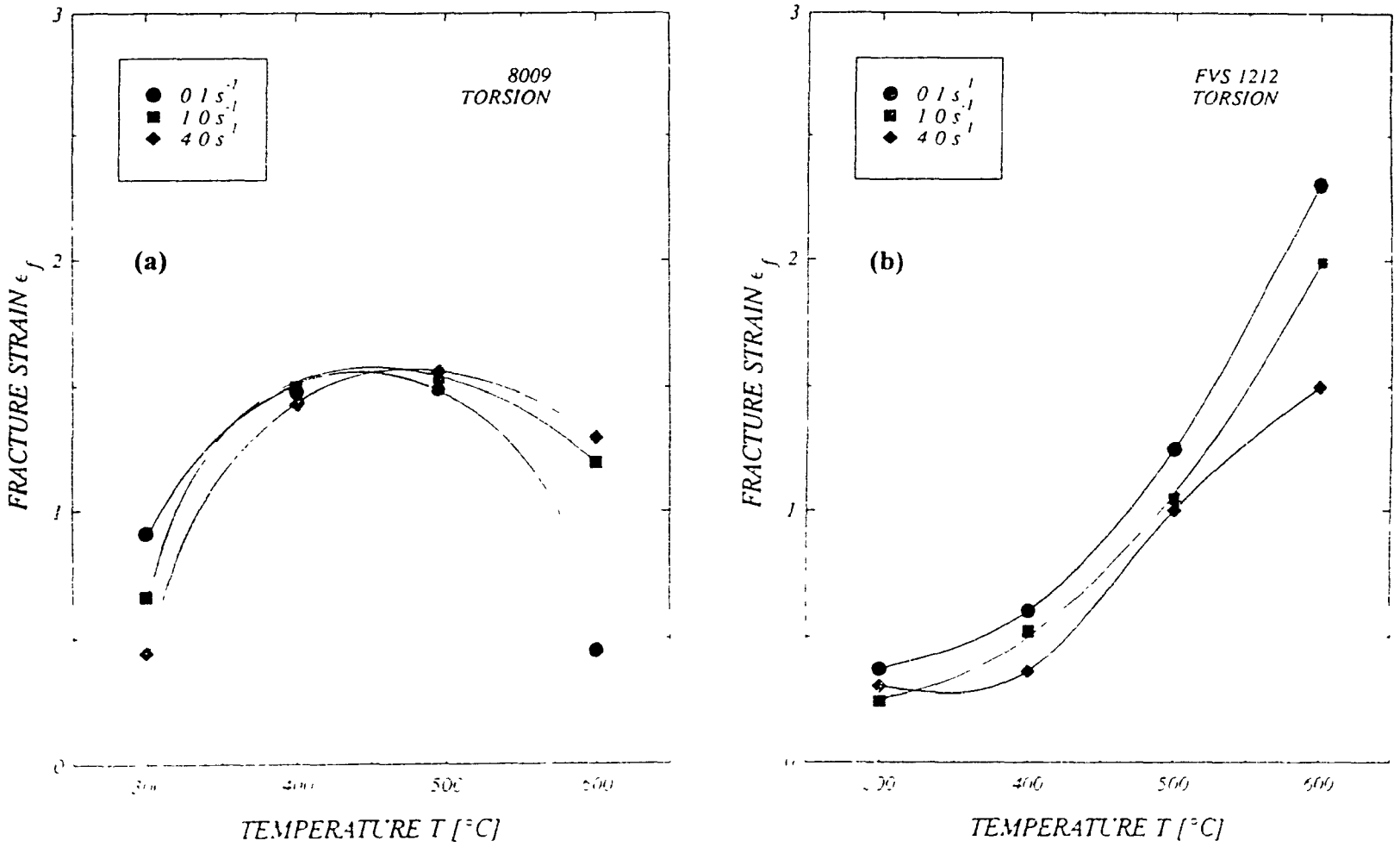

Figure 5.3: Strain-To-Fracture versus Temperature: (a) 8009 and (b) FVS1212

means The value of $\alpha = 0.052$ MPa^{-1} is usually used for aluminum alloys From the plots log sinh($\alpha\sigma$) versus 1/T, we calculate Q using the following relationship

$$Q = 23 \cdot R \cdot n \cdot s \tag{5 1}$$

where n is the stress exponent and s is the slope of log sinh($\alpha\sigma$) versus 1000/T All the values of n, s and Q are summarized in Tables 5 1 and 5.2 for each alloy tested.

Our calculations of the slope s for four different stress multipliers illustrated in Figures 5 4 and 5 5 exhibit very interesting results. In the 8009 alloy, s_{avg} for $\alpha = 0\ 020$ MPa^{-1} was found to be 3 73; by doubling α, we discover that $s_{avg} = 7.43$ is almost twice the value The linear relationship follows suit for $\alpha = 0\ 052$ MPa^{-1} and $\alpha = 0.080$ MPa^{-1} having s_{avg} equal to 9.66 and 14 85, respectively. Similar relationships were confirmed for alloy FVS1212 for the same stress multipliers Hence, the plot of s versus α shows direct proportionality as shown in Figure 5.6, however, the slope s is more sensitive to rising α at 1 0 s^{-1} than at 4 0 s^{-1} but the line for 0 1 s^{-1} falls in the middle. Based on the above results, we may conclude that in the regime of α assigned there exists a relationship between s and α which could be described as.

$$s = b \times \alpha \tag{5 2}$$

where b is a specific slope constant for the alloy In the cases of 8009 and FVS1212, b is approximately 186 MPa and 286 MPa, respectively

As we begin to compare the stress exponent, n, from plots of log strain rate versus log sinh($\alpha\sigma$) (Figure 5 7 and 5.8), for different α we once again observe a simple relationship between α and n The 8009 alloys has $n_{avg} = 8.91$ for $\alpha = 0.020$ MPa^{-1} The n_{avg} for $\alpha = 0\ 040$ MPa^{-1} is 4.56 about half that for $\alpha = 0.020$ MPa^{-1}. For $\alpha = 0.052$ MPa^{-1}

Table 5.1: Constitutive Constants for Alloy 8009

n	0.020 MPa^{-1}	0.040 MPa^{-1}	0.052 MPa^{-1}	0.080 MPa^{-1}
300°C	10.58	5.29	4 07	2.65
400°C	6 15	3 07	2.36	1.54
500°C	4.40	2.21	1.70	1 11
600°C	14.51	7.67	5 91	3 84
Average	**8.91**	**4.56**	**3.51**	**2.29**

s	0.020 MPa^{-1}	0.040 MPa^{-1}	0.052 MPa^{-1}	0.080 MPa^{-1}
0.1 s^{-1}	3.72	7 41	9 63	14.81
1.0 s^{-1}	3.70	7.36	9.57	14.72
4.0 s^{-1}	3.77	7.52	9.77	15.03
Average	**3.73**	**7.43**	**9.66**	**14.85**

Q (kJ/mol)	0.020 MPa^{-1}	0.040 MPa^{-1}	0.052 MPa^{-1}	0.080 MPa^{-1}
300°C	755	752	752	753
400°C	439	436	436	437
500°C	314	314	314	315
600°C	1035	1090	1092	1090
0.1 s^{-1}	634	646	646	649
1.0 s^{-1}	630	642	642	645
4.0 s^{-1}	642	656	656	658
Average	**636**	**648**	**648**	**650**

Z Plots	0.020 MPa^{-1}	0.040 MPa^{-1}	0.052 MPa^{-1}	0.080 MPa^{-1}
A (s^{-1})	8.1×10^{33}	1.3×10^{33}	6.0×10^{32}	3.3×10^{32}
n	8.82	4.52	3 48	2.27
r	0.996	0.996	0 996	0.996

Table 5 2 Constitutive Constants for Alloy FVS1212

n	0.020 MPa^{-1}	0.040 MPa^{-1}	0.052 MPa^{-1}	0.080 MPa^{-1}
300°C	6 29	4 16	3 00	2 03
400°C	4 60	1 67	1 19	0 83
500°C	6 28	4 29	3 00	2 03
600°C	5 00	2 28	1 49	0 95
Average	**5.54**	**3.10**	**2.17**	**1.46**

s	0.020 MPa^{-1}	0.040 MPa^{-1}	0.052 MPa^{-1}	0.080 MPa^{-1}
0.1 s^{-1}	5 73	11.33	14 72	22 64
1.0 s^{-1}	5 87	11 62	15 10	23 23
4.0 s^{-1}	5 56	11 10	14 42	22 19
Average	**5.72**	**11.35**	**14.75**	**22.69**

Q *(kJ/mol)*	0.020 MPa^{-1}	0.040 MPa^{-1}	0.052 MPa^{-1}	0.080 MPa^{-1}
300°C	688	903	846	881
400°C	510	362	336	360
500°C	687	931	846	881
600°C	547	495	420	412
0.1 s^{-1}	607	672	611	632
1.0 s^{-1}	622	689	627	649
4.0 s^{-1}	589	658	598	620
Average	**606**	**673**	**612**	**633**

Z Plots	0.020 MPa^{-1}	0.040 MPa^{-1}	0.052 MPa^{-1}	0.080 MPa^{-1}
A (s^{-1})	1.7×10^{34}	1.0×10^{37}	2.8×10^{33}	2.4×10^{34}
n	5 19	2 91	2.03	1 37
r	0 969	0 969	0.969	0 969

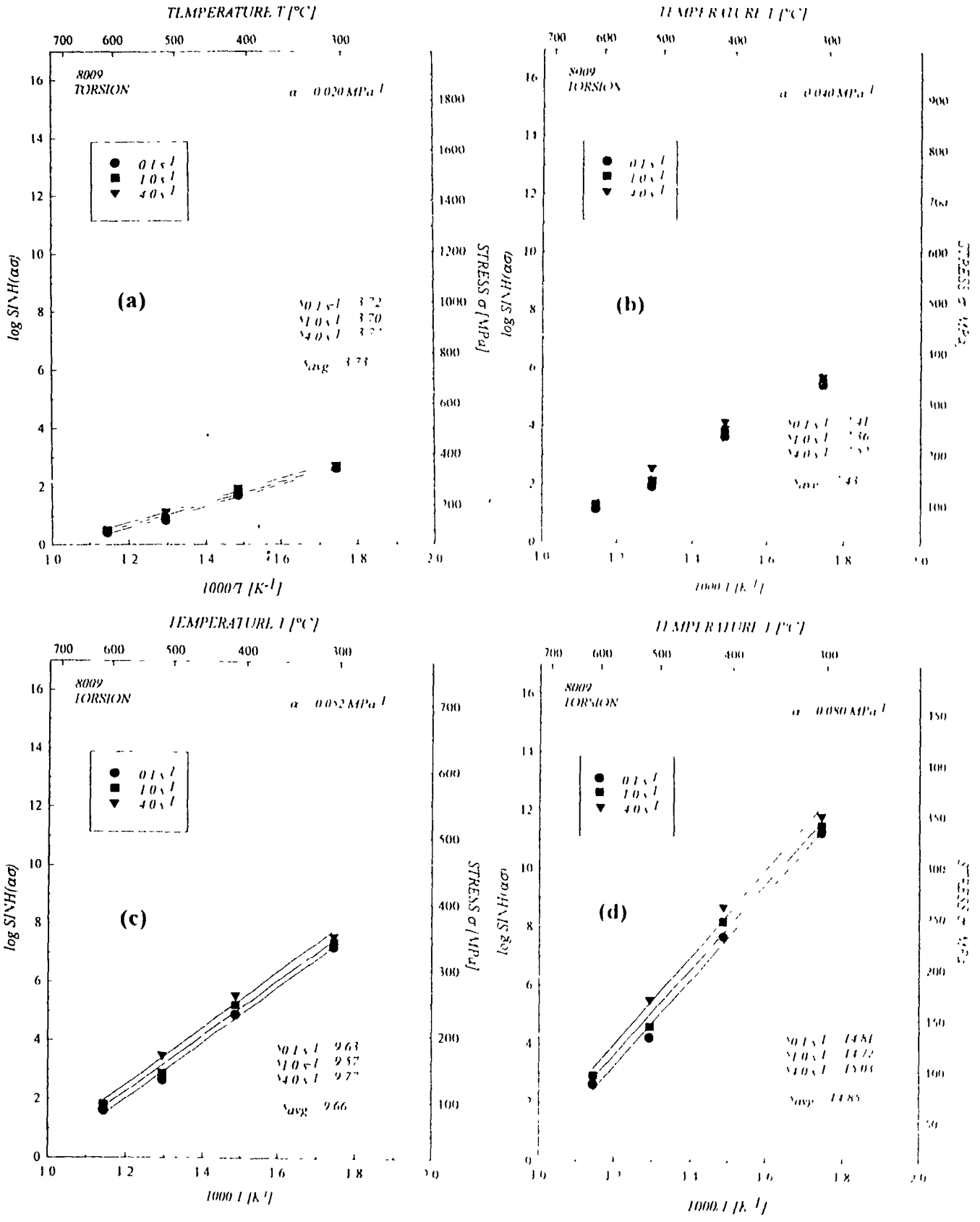

Figure 5.4: Arrhenius Plots for 8009 at (a) $\alpha = 0.020$ MPa^{-1}; (b) $\alpha = 0.040$ MPa^{-1}, (c) $\alpha = 0.052$ MPa^{-1} and (d) $\alpha = 0.080$ MPa^{-1}

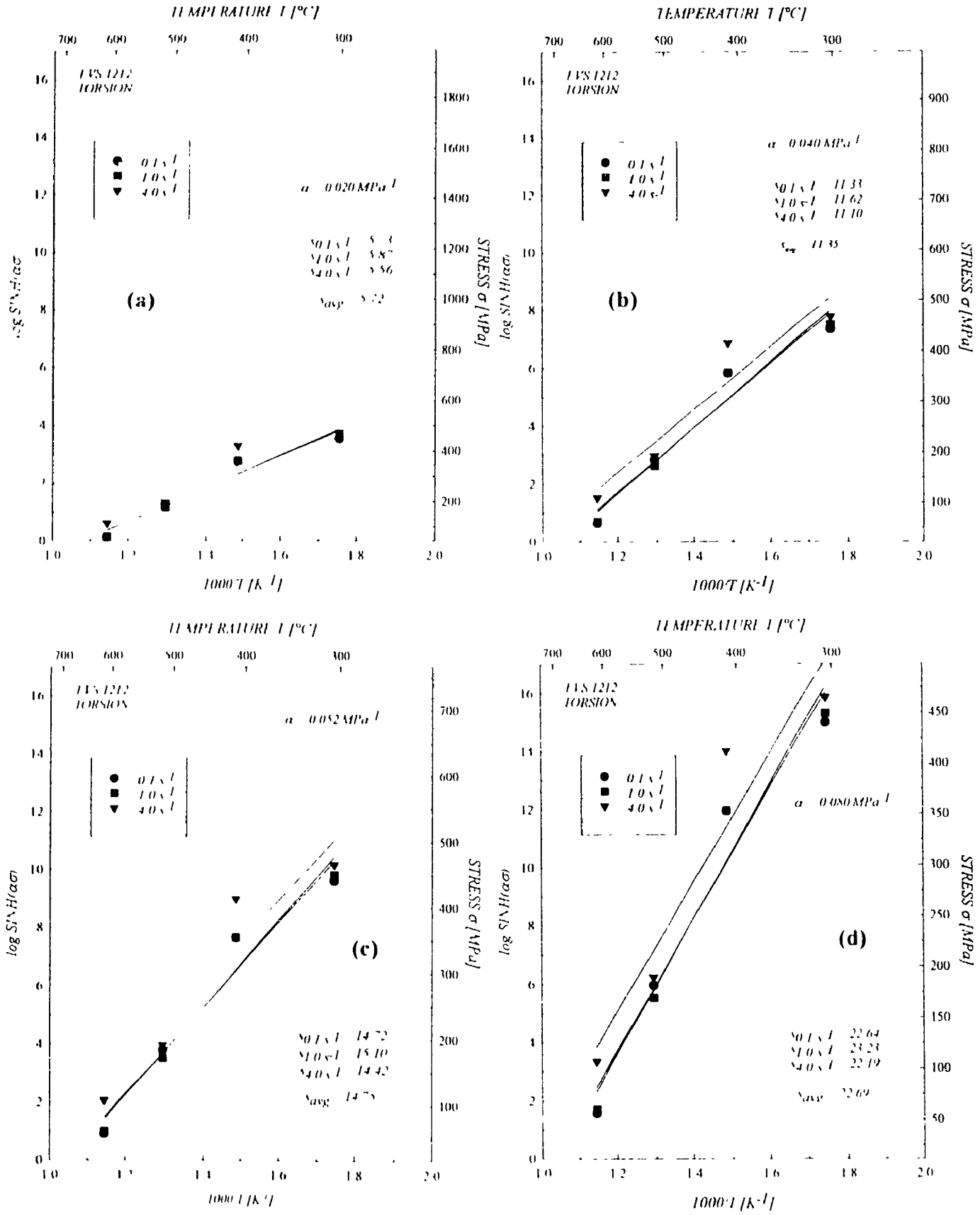

Figure 5.5: Arrhenius Plots for FVS1212 at (a) $\alpha = 0.020$ MPa^{-1}; (b) $\alpha = 0.040$ MPa^{-1}; (c) $\alpha = 0.052$ MPa^{-1} and (d) $\alpha = 0.080$ MPa^{-1}

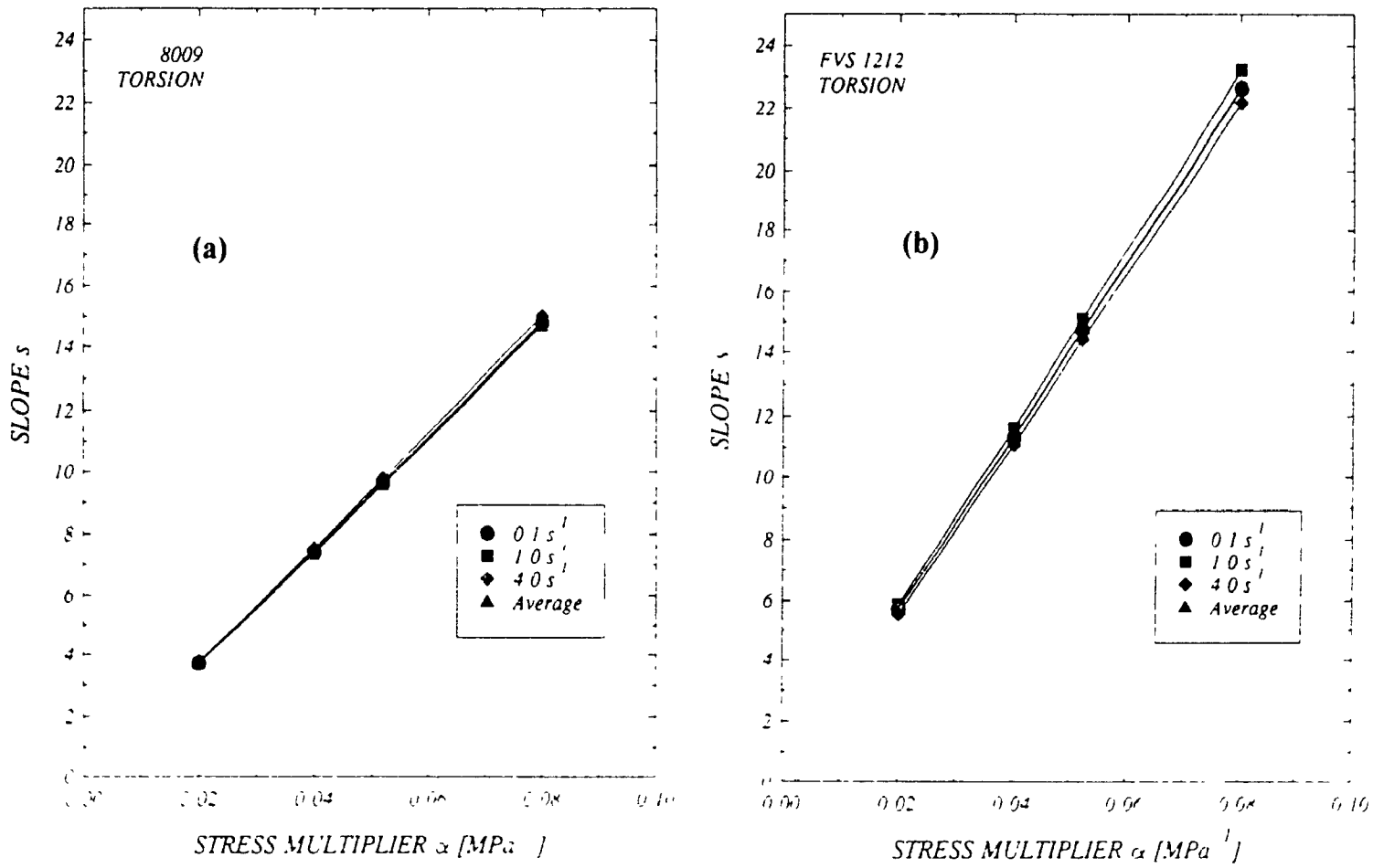

Figure 5.6: Slope versus Stress Multiplier: (a) 8009 and (b) FVS1212

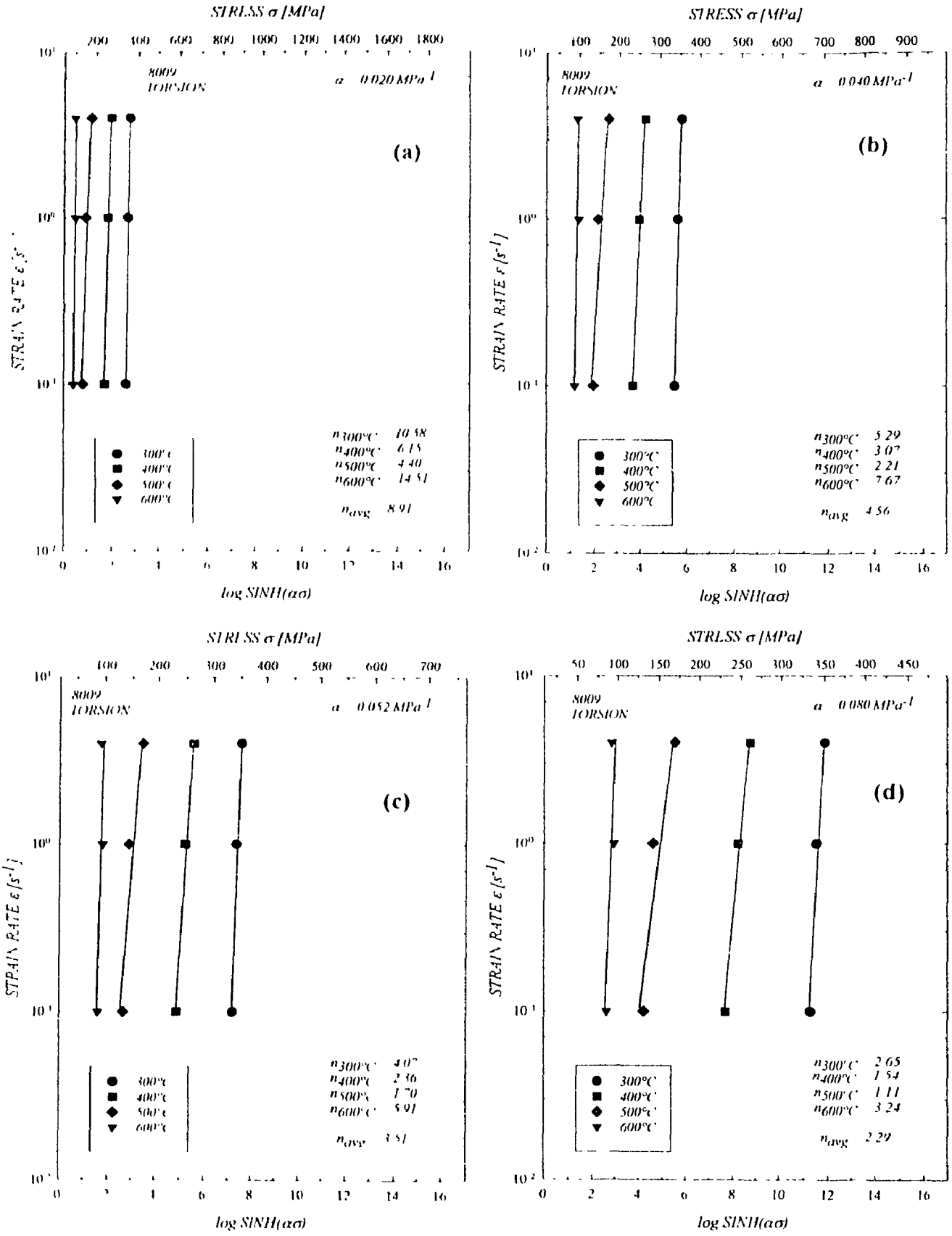

Figure 5.7: Log Strain Rate Versus Log Sinh(ασ) for 8009 at (a) $\alpha = 0.020\ MPa^{-1}$; (b) $\alpha = 0.040\ MPa^{-1}$; (c) $\alpha = 0.052\ MPa^{-1}$ and (d) $\alpha = 0.080\ MPa^{-1}$

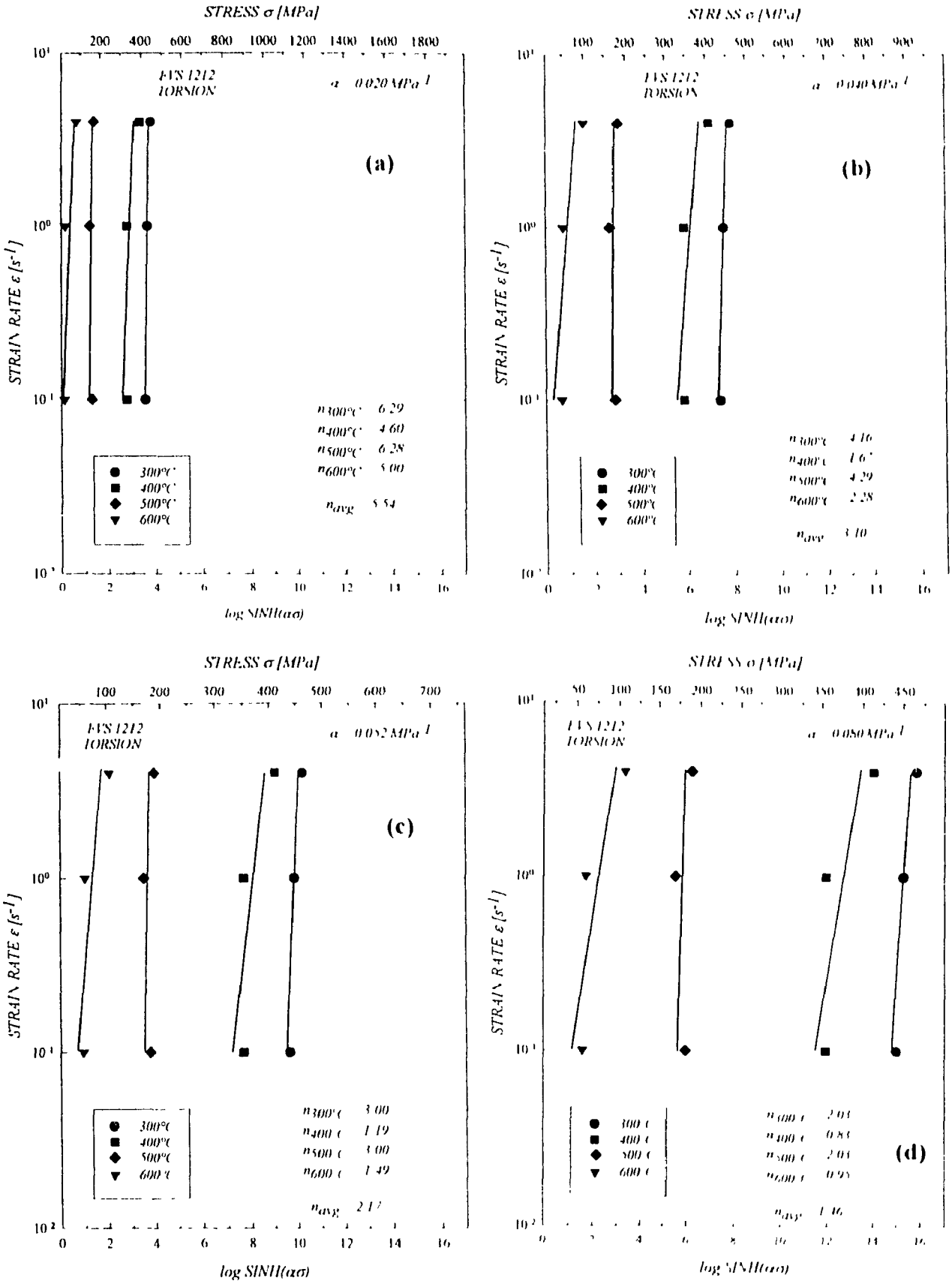

Figure 5.8: Log Strain Rate Versus Log Sinh(ασ) for FVS1212 at (a) $\alpha = 0.020$ MPa^{-1}; (b) $\alpha = 0.040$ MPa^{-1}; (c) $\alpha = 0.052$ MPa^{-1} and (d) $\alpha = 0.080$ MPa^{-1}

the reciprocal relationship gives n to be 3.91 comparing well with the measured n_{avg} = 3 51 Finally, for α = 0.080 MPa^{-1} we calculate n to be 2.23 whereas experimentally n_{avg} is 2 29. Similar relationships is observed with the FVS1212 alloy where n_{avg} ranges from 5 54 for α = 0.020 MPa^{-1} to 1 46 for α = 0.080 MPa^{-1}. When n is plotted as a function of α for four different test temperatures for 8009 alloy, we see that n decreases more gradually as α rises consistent with a reciprocal relationship:

$$n = a \times (1/\alpha) \qquad (5\ 3)$$

where a is specific stress constant for the alloy. In the case of alloy 8009 and FVS1212, a = 0.180 MPa and 0.0675 MPa, respectively In the case of FVS1212 alloy, in comparison to 8009, the temperature has more effect on the n versus α relationship For 8009, we find the highest values of n at 600°C while n is highest at 300°C and 500°C for FVS1212 (Figure 5 9) Since s increases lineraly and n reciprocally with rising α, Q remains almost invariant as shown in Figure 5 10

The flow stress is related to a function (Equation 3.5) of the strain rate and the reciprocal Arrhenius term exp(-Q/RT), which is a temperature compensated strain rate called the Zener-Hollomon parameter (Z) At greater values of Z (i e. a lower temperature or the shorter time as a result of high strain rate), higher stress is developed as a result of fewer thermally activated events per unit strain From the values of Q determined for various α, the plot of log Z versus log sinh($\alpha\sigma$) is charted, thus drawing the data into single lines with slopes of n and intercept values of A (Figure 5.11).

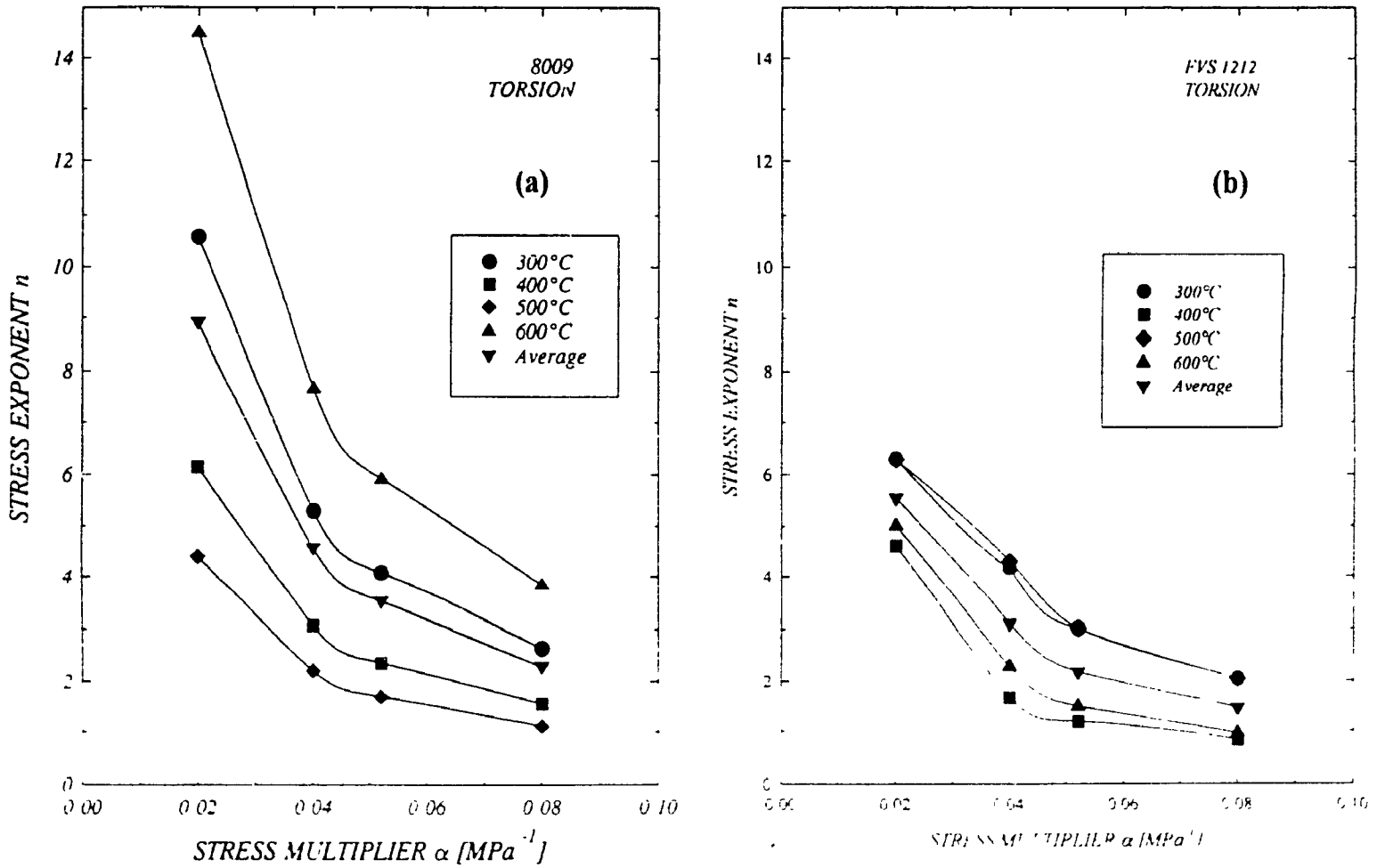

Figure 5.9: Stress Exponent Versus Stress Multiplier; (a) 8009 and (b) FVS1212

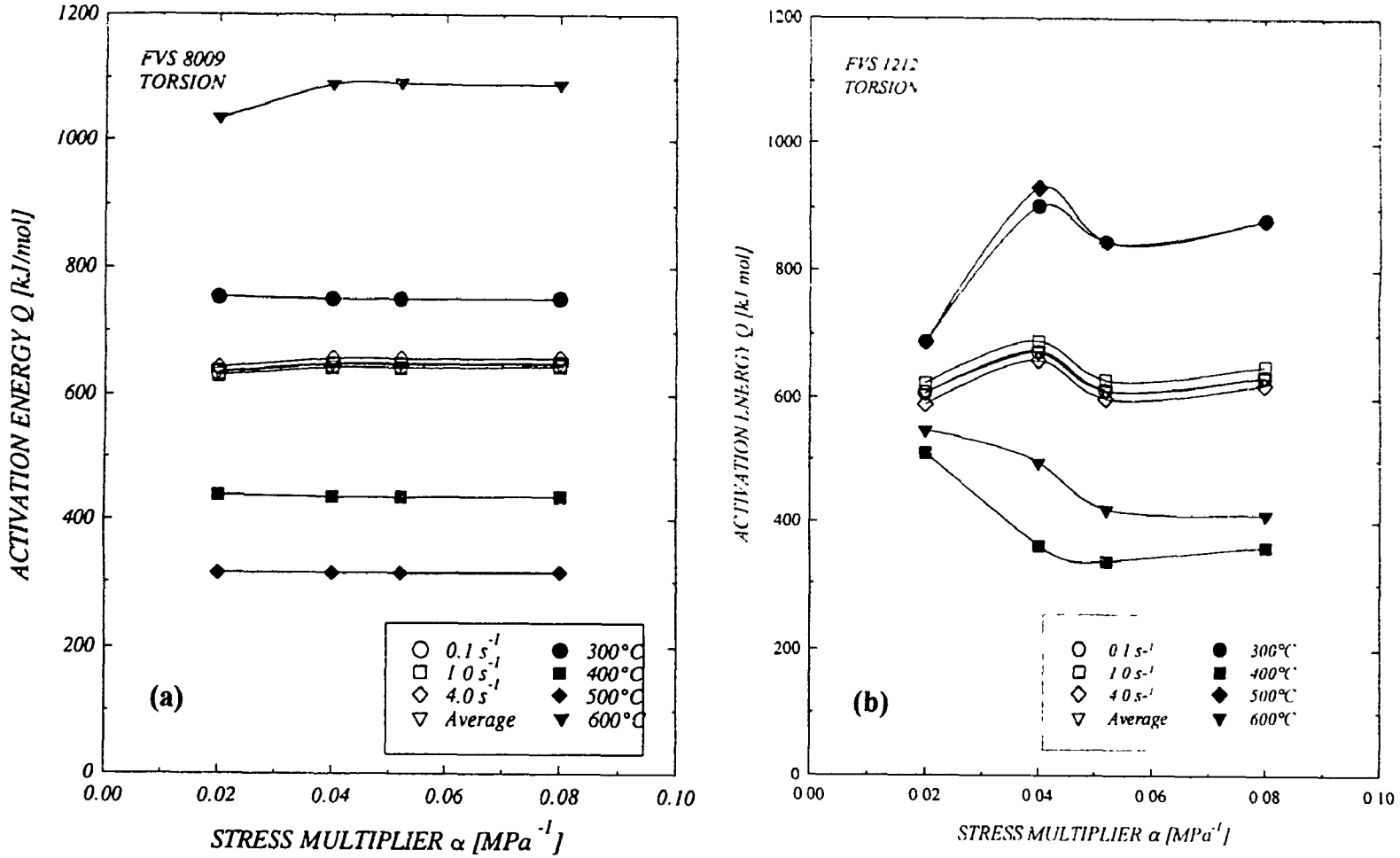

Figure 5.10: Activation Energy Versus Stress Multiplier; (a) 8009 and (b) FVS1212

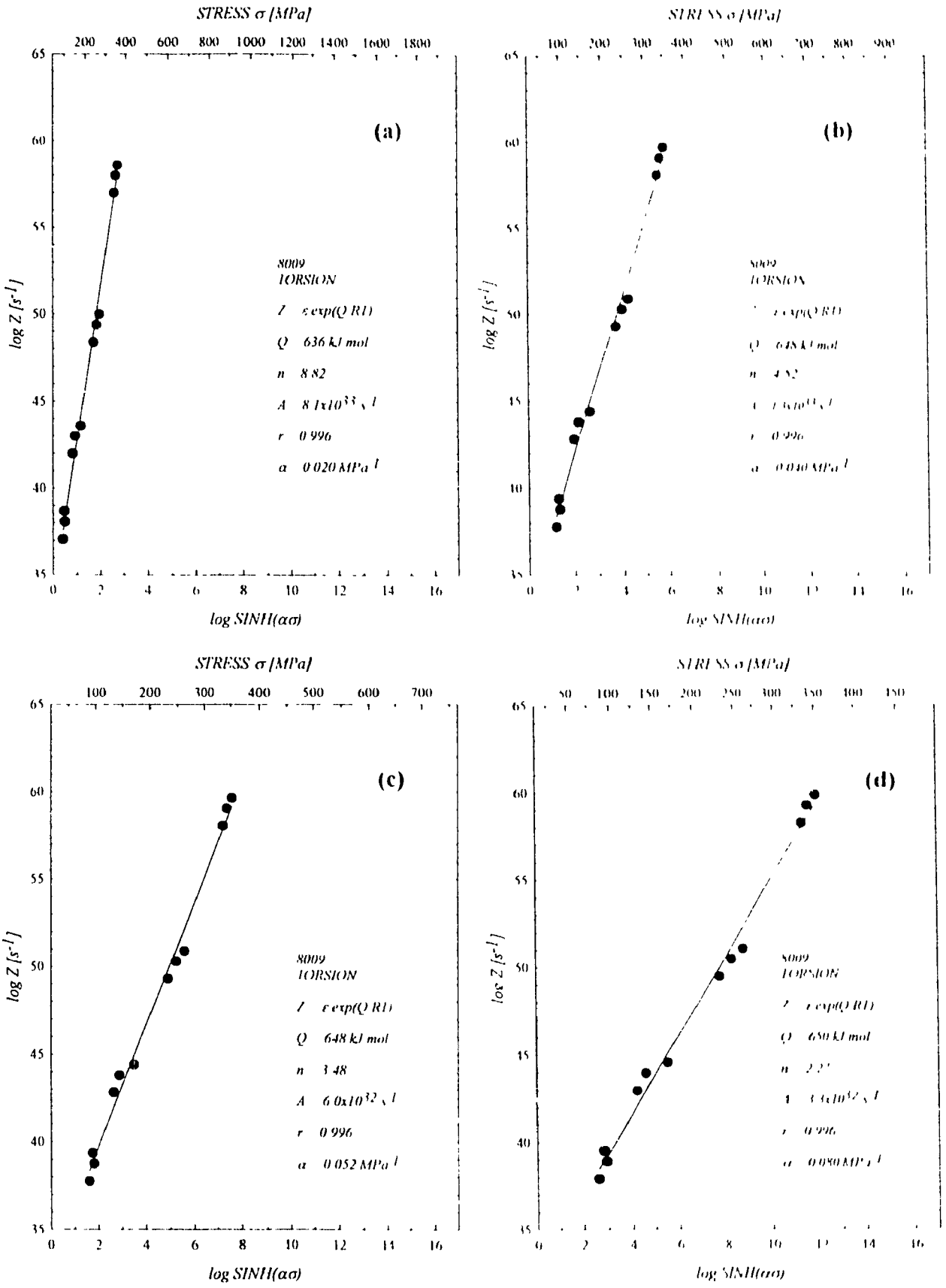

Figure 5.11 Log Zener-Hollomon Parameter versus Log Sinh(ασ) for 8009 at (a) α = 0.020 MPa^{-1}; (b) α = 0.040 MPa^{-1}, (c) α = 0.052 MPa^{-1} and (d) α = 0.080 MPa^{-1}

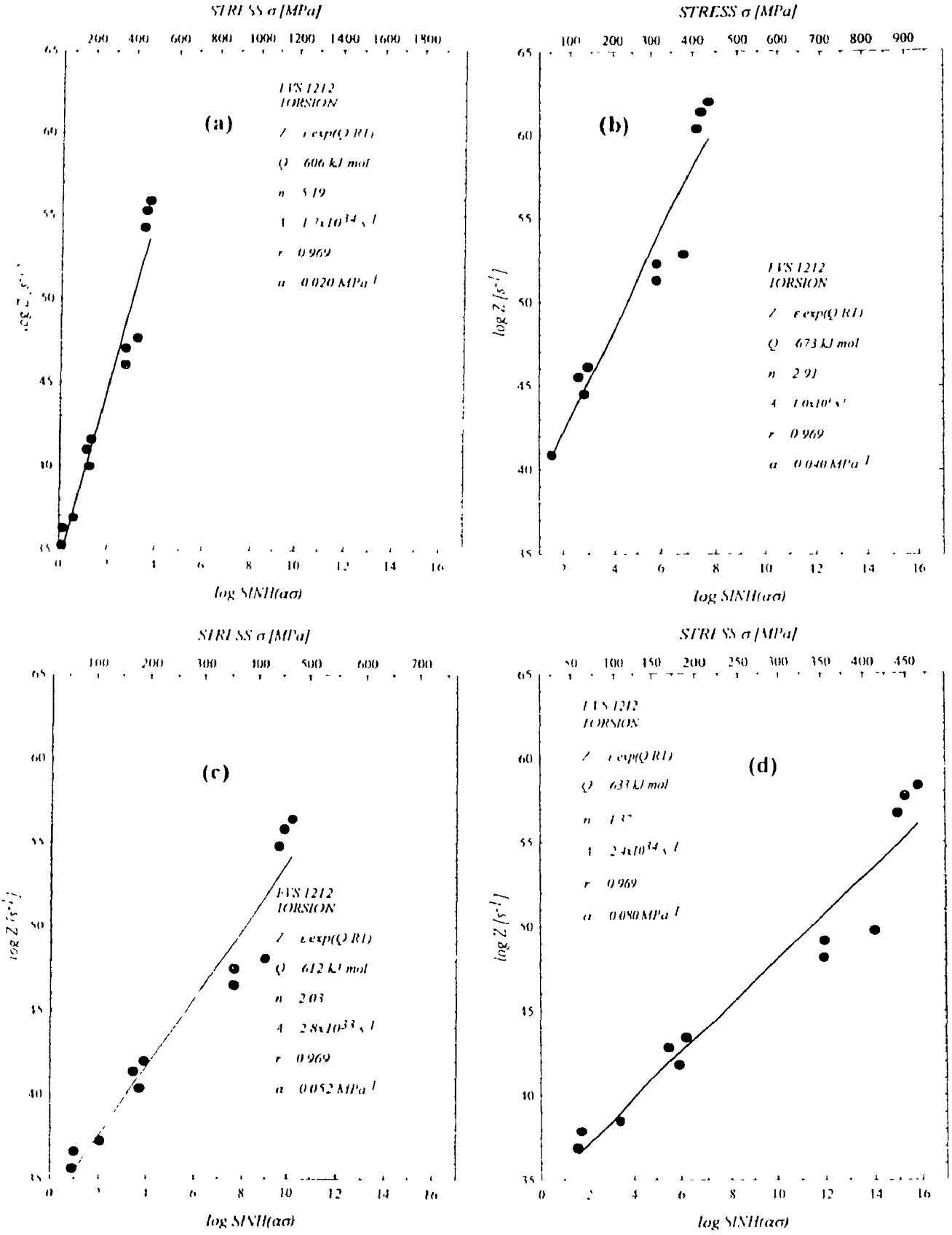

Figure 5.12 Log Zener-Hollomon Parameter versus Log Sinh($\alpha\sigma$) for FVS1212 at (a) α = 0.020 MPa^{-1}, (b) α = 0.040 MPa^{-1}, (c) α = 0.052 MPa^{-1} and (d) α = 0.080 MPa^{-1}

6. DISCUSSION

6.1 Stress-Strain Curves

During the experiments we were able to obtain stress-strain curves that were derived from torque-twist relationships at different twist rates and temperatures. By carefully studying the stress-strain curves we have observed distinct stress peaks followed by considerable softening. This was especially noticeable at lower temperatures and higher strain rates. The materials have been work hardened in the initial stage of deformation followed by considerable softening; only at low strain rate of 0 1 s^{-1} and high temperature of 600°C, the characteristic stress peak flattened particularly in FVS1212 It could be observed that the degree of softening beyond the stress peak was a function of temperature and strain rate applied, being higher at lower temperatures and higher strain rates.

The above feature of alteration of dominance from work hardening to softening is a most notable characteristic of the curves obtained from the experiments Such deformation behavior is very rarely observed in tests of conventional aluminum alloys. For those, a gradual increase and then a plateau in stress, until fracture, is the characteristic relationship in the stress-strain curves. It is usually attributed to the balance between work hardening and softening by dynamic recovery. There is very little strain hardening due to the speed at which softening processes operate A stress peak is an indicator of the softening by deformation heating or structural changes during deformation. Under the above conditions studied, there is enough thermal energy that

atomic diffusion mechanisms over time can contribute to the softening process. There appears to be two possibilities for this process: recovery without recrystallization much as in hot creep or dynamic recrystallization. The DRX softening mechanism usually does not operate in aluminum alloys with high stacking fault energies which enables dislocations to cross slip and climb easily so that full DRV can occur.

Both of the materials judged by the flow curve shape are restored primarily by DRX. The basic shapes of the curves observed is similar to the ones observed in torsion tests of Al-5Mg-0.8Mn alloy which is known to restore by both DRV and DRX (64). Flow curves with peaks as a result of DRX have been observed in hot working behavior of another powder metal alloy (Al-20Si-7.5Ni-3Cu-1Mg) by hot torsion (59). At lower temperatures and higher strain rates, the dislocation concentrations in the alloy being built up to sufficient heights due to relatively slow recovery thus developing a substructure good for nucleation of recrystallization. Particles larger than 0.5 μm can play a significant role in developing high local dislocation densities and then initiating nucleation (61,62,64,65). At the low temperatures of 300 to 400°C and high strain rates, dynamic recrystallization may be assisted by temperature rise resulting from deformation heating. In materials 8009 and FVS1212, the characteristic peaks decrease at low strain rates and high temperatures. One may conclude that under these conditions the stress-strain curves appeared to be typical of material that was restoring only by DRV, i.e. work hardening followed by steady-state deformation. In order for DRX to occur, a condition of high concentration of dislocations has to be present for the nucleation of new crystals.

However at high temperature and low deformation rate, the decrease in dislocation density by DRV is enough to prevent the nucleation of recrystallization

As a result of deformation heating, thermal softening takes place in the gauge section. At the high strain rates it is especially evident since the deformation under these conditions approaches an adiabatic process Since the peak stress of the present material was found to be highly temperature dependent, a small increase in temperature measurably lowers the stress Because the flow stress of this alloy is so high compared to traditional alumninum alloys, this effect may be fully responsible for the observed stress peaks shown under all testing conditions. To support this argument one may study the stress-strain curves at 400°C and 500°C in 8009 and 400°C and 600°C in FVS1212, the 0 1 s^{-1} curve has a higher peak but softens faster to drop below the low strain rate ones and the 1 0 s^{-1} curve is higher but then drops below the 0 1 s^{-1} one However, at the low strain rate of 0 1 s^{-1}, when deformation heating would be of minor importance there is still work softening which leads one to believe that other factors might be involved that are structural in nature. However, it should be pointed out that the decline at low temperature, particularly at 300°C in FVS1212 may result from propagation of cracks

There are a number of structural changes that could take place during deformation such as precipitation, transformation and second phase coarsening It has been shown that significant strain-induced precipitation or transformation does not occur (66) On the other hand, there is a distinct possibility that coarsening of second phase particles is taking place during the hot torsion tests. This phenomenon is responsible for the stress peak observed in the other alloys such as 2024 Al alloy (67,68) In Al-20Si-7 5Ni-3Cu-1Mg

alloy during hot torsion testing among there are several phases dispersed in the aluminum matrix which could undergo coalescence Some, like silicon crystals, Al_3Ni, $Al_3(NiCu)_2$ and Al_7Cu_4Ni have been shown to be thermally stable at the testing temperatures (63,65) However, the coarsening of Mg_2Si phase might be relevant to the observed peak, though it has not been microscopically ascertained Relevant to the tested alloys, it has been shown that controlled nucleation and growth of metastable second phases (e.g. Al_6Fe) during extension of splatcooled Al-Fe alloys leads to increase in flow stress because of the obstacles provided to dislocation motion by dispersoids, however, the high levels are retained at 350°C due to the relative resistance of the Al-Fe dispersoids to Oswald ripening (72-74) Enhancement of both mechanisms at a high testing temperature and a lower strain rate could partially account for the flattening of the stress peak at 500°C and 600°C for 0 1 s^{-1}

In conclusion, it appears that the synergy of the above three effects working together are responsible for the softening beyond the stress peak It is most likely though that the principle contributors are deformation heating accompanied by localized recrystallization In classical DRX, it has been typical to observe that the strain to the stress peak decreases progressively with rising temperature and decreasing strain rate (64). Such a mechanism is thermally activated and strain and strain rate controlled. Hence it should appear at a lower strain when temperature is higher and strain rate is lower. However in FVS1212, 8009 and Al-20Si-7 5Ni-3Cu-1Mg (59), one observes very slight variation of the strain to the stress peak with temperature and strain rate The observed stress peak is attributed mainly to the occurrence of deformational heating and small

amounts of recrystallization. Such low sensitivity of peak strain to temperature may be due to the fact that with the decrease of temperature, dynamic recrystallization becomes less influential while deformation heating become increasingly important The disturbing effect of temperature rise on the strain to the stress peak at high strain rate has been observed in torsion tests on Cu-P alloys (81) and Al-20Si-7 5Ni-3Cu-1Mg (31,59) Finally, the results also confirm that the involvement of temperature rise in torsional deformation is more marked then in tension or compresion because of the greater strains before fracture

6.2 Ductility

The tests have shown that the 8009 and FVS1212 compared to conventional aluminum alloys possess very low ductilty By carefully observing the variation of the strain-to-fracture with temperature and strain rate, we are able to see the trend typical of other aluminum alloys With the increase of temperature and lower strain rate, DRV reduces the stress concentrations at triple points and at second phase particles where initiation and propagation of micro-cracks take place Such a trend has been regarded as an indication that DRV is a significant restoration mechanism in aluminum alloys, in contrast for dynamically recrystallized materials, strain to fracture increases with rising strain rate as crack propogation is slowed down (70) It may be suggested that the strain rate dependence arises from a combination of DRX and DRV as in another aluminum alloy Al-5Mg-0.8Mn (64)

It is also important to note that the ductility of an aluminum alloy is dependent not only upon restoration mechanisms but also upon fracture mechanisms In the tests that

were conducted on 8009 and FVS1212, fracture may have been initiated by the decohesion between the aluminum and dispersed-phase particles (mainly intermetallic $Al_{12}(Fe,V)_3Si$) which are enhanced by deformation at a high rate. The volume fraction of the dispersed particles with various sizes in the aluminum matrix is nearly 37% for FVS1212 and 24% in 8009, give a very high interfacial area and easy path to the linkage of micro-cracks. These values compare to 30% of dispersoids by volume in Al-20Si-7.5Ni-3Cu-1Mg in which particles of different kinds and sizes have different effects especially when the temperature rises the stress concentration decreases. It is therefore likely that the increased density of recrystallization nuclei, resulting from deformation at a higher strain rate, was not able to cope with the enhanced decohesion at the earlier stages of deformation. For 8009, the lower volume fraction of dispersoids contributed to the higher ductilty then FVS1212 between 400°C and 500°C. The reason for higher ductility in the latter at 600°C is not clear; one can speculate that the higher dispersed content leads to a finer grain size and superplasticity.

6.3 Strain Rate Sensitivity and Superplasticity

In tensile, extrusion and compressive tests on other hypereutectic Al-Si based alloys produced by powder metallurgy, very high m (strain rate sensitivity) values were obtained. In Al-20Si-7.5Ni-3Cu-1Mg (59) for example, it was found to be as follows: m = 0.13 at 375°C, m = 0.2 at 400°C and m = 0.24 at 425°C, thus being much higher than the range of 0.026 to 0.227 at 300 to 500°C in conventional aluminum alloys (52,54,72,82). The values of m for 8009 and FVS1212 are shown in Figure 6.1 and are

not significantly high. Thus it is not important as in other high silicon rapidly solidified alloys where reducing the deformation rate such as ram speed in extrusion can significantly reduce the flow stress permitting reduced temperature.

In the Al-Si based alloys the high m values may be attributed to the presence of high volume fraction of silicon crystal phase (about 20%) Since the linear thermal expansion coefficient of silicon is about one-eighth that of aluminum, stresses are imposed on the adjacent aluminum matrix when the material is heated. It has been shown experimentally that the imposition of random internal stresses does assist the plastic flow of the aluminum matrix and lead to a low stress exponent and a high m value especially when applied stresses are low (73). The present alloys may differ because the silicides are different from silicon and the strain rate employed is rather high

In some alloys, superplasticity gives rise to m > 0 3 (usually 0 4 to 0.7) and a large elongation is observed. For 8009 and FVS1212, they do not exhibit the tendency to superplasticity except perhaps in the latter at 600°C where m reaches 0 165 (Figure 6.1) However, superplasticity has been obtained and the value of m has been enhanced by adding silicon carbide whiskers and imposing thermal cycles (81) Hence the stresses induced by the silicon carbide crystals are likely to be relevant to the high m values of the material as consistently found in Al-Si alloys due to silicon crystals (50,52,80,82). The present test results generally establish very low ductility of FVS1212 and 8009 in the torsion test. The low ductility is probably due to cracking of the dispersed-phase particles and interfacial decohesion acting as the major fracture mechanism that accelerates the failure of the material. However, the highest equivalent strain to fracture of 2 5 at 600°C

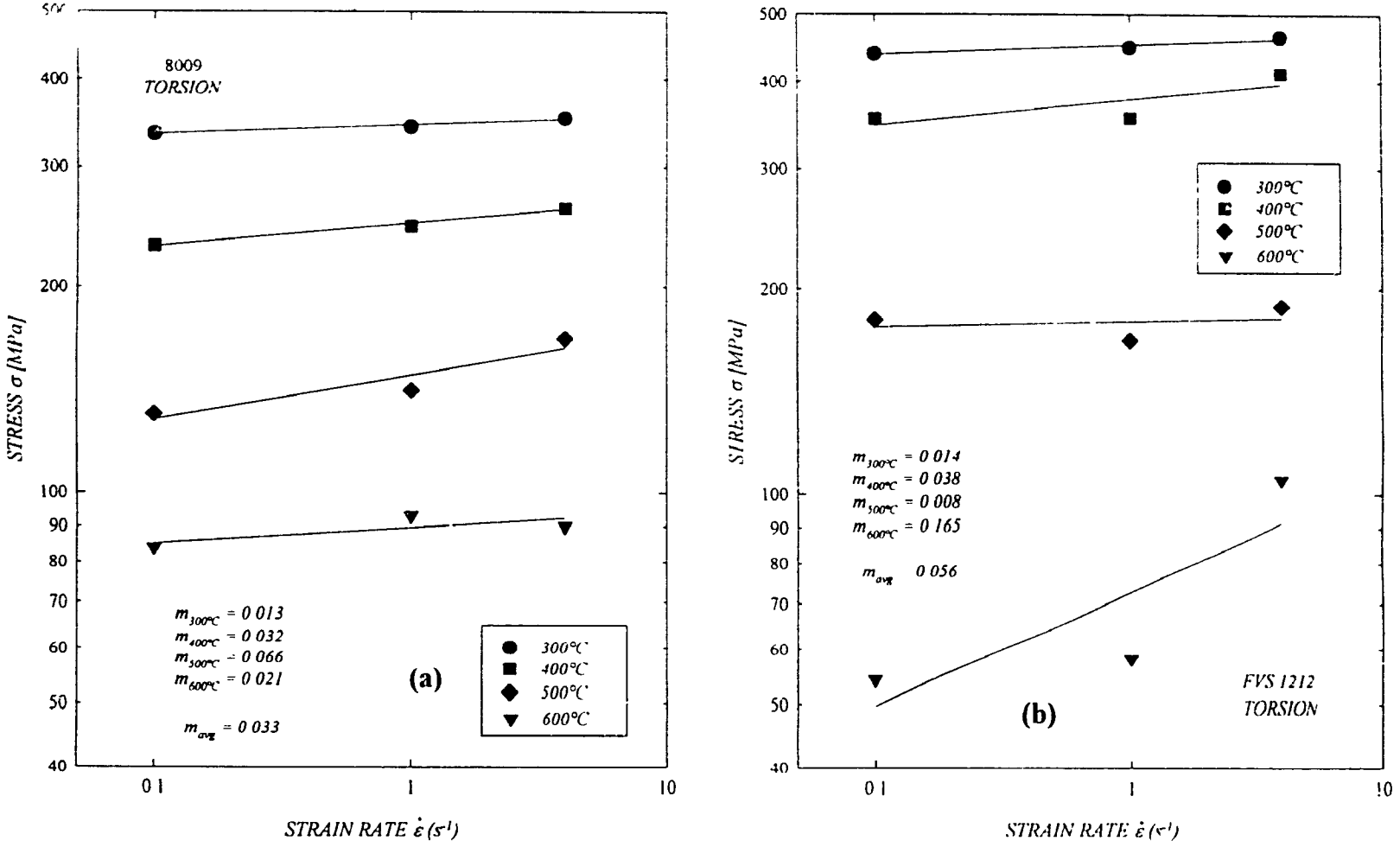

Figure 6.1: Strain Rate Sensitivities for (a) 8009 and (b) FVS1212

and strain rate of 1.0 s^{-1} for FVS1212 may indicate new mechanisms Therefore a high m is not necessarily associated with a high ductility (71)

The results show another very interesting feature of m values of the tested materials. There is a strong temperature dependence of m values; to double the peak stress of FVS1212 requires an increase in strain rate of 200 times at 400°C but only 20 times at 600°C. In practice the forces to shape the material can be effectively reduced by lowering the deformation rate at a higher temperature A strong m value dependency on temperature has been reported in Al-Fe and Al-Fe-Co alloys as a result of deformation heating at low temperature (56,59).

In the research conducted on Al-20Si-7 5Ni-3Cu-1Mg (59), the attempt was made to explain the large m value variation with temperature by use of an equation that is most commonly used to link the material properties with the deformation conditions However, it was established that the present experimental data fail to correlate to this equation Therefore, the following additional factors might have been taken into consideration in our analysis of the results of torsional testing of 8009 and FVS1212 if the microstructures were thoroughly examined.

1 Volume fraction and size of the second-phase particles (which decrease uniformity of substructure)

2. Size of subgrains (influenced by temperature and strain rate)

3. Internal stresses (those are imposed by the second-phase particles, like, the silicide dispersoids, $Al_{12}(Fe,V)_3Si$)

In pure aluminum, factor [1] is virtually absent. Essentially, the velocity of dislocations affected by pinning, is dependent upon the strain rate imposed At higher temperatures, when node unpinning as a recovery mechanism is operative, one would expect a higher m as has been consistently found in dispersion strengthened aluminum alloys (56) A strong dependence of the degree of dynamic recovery upon temperature as measured by [2] is also related to the presence of second phase particles. Factor [3] is a unique for the present alloys with a high volume fraction of silicide crystals. We have discussed earlier, that internal stresses arising from the difference in thermal expansion coefficient between the silicon crystals and the aluminum matrix, reduce the effective stress needed to drive dislocations leading to a higher m (85)

6.4 Interdependence of Stress, Strain Rate and Temperature

It was found that the hyperbolic sine equation gave the best fit to the data obtained in the hot torsion experiments It was therefore taken as the basic formula for a constitutive equation suitable for use at various temperatures to satisfy a condition that α and n in Equation 3 4 are independent of temperature over the experimental range. We have plotted logarithmic strain rate against logarithmic $\sinh(\alpha\sigma)$ at different temperatures We found that the best fit was for α = 0 020 MPa^{-1} and n_{avg} = 5 54 for FVS1212 The best fit for 8009 was again at α = 0 020 MPa^{-1} and n_{avg} = 8.91. The linearity displayed in the plots confirm the validity of Equation 3.4 empirically describing the relationship between the peak stress and strain rate at a constant temperature.

From our tests we have established that the material is much stronger than aluminum at a lower temperature hence the much higher value of Q It is interesting to quantitatively compare the calculated Q values for 8009 and FVS1212 with other aluminum alloys. Activation energy for self-diffusion of aluminum was estimated and reported to be 138 kJ/mol (86). Other sources reported it to be 126 to 142 kJ/mol (87) while the commercial purity aluminum has a Q value of 155 kJ/mol (88) A wide range of Q values of various grades of aluminum alloys in different states have been reported in literature ranging from 116 to 285 kJ/mol (55,59,89-91). Because of the great compositional and microstructural variabilty, no satisfactory explanation of such great variance have been given. However, it is understood and accepted widely that Q reflects the energy barriers over which deformation takes place. In case of pure aluminum Q is an indicator of energy barriers for self-diffusion which largely governs the dislocation motion In general, Q is affected by solute concentrations in a complex way Usually these concentrations in addition to particle distribution and volume fractions act as additional barriers to the free motion of dislocations (57,92).

Our two quaternary, heavily alloyed materials (8009 Al-8 5Fe-1 3V-1.7Si, FVS1212: Al-11.7Fe-1.2V-2.4Si) could have a part of the alloying elements dissolved in the aluminum matrix at the testing temperatures. This could decrease the stacking fault energy of the matrix, increasing the stacking fault width and thus the energy for cross slip of screw dislocations (93). However, the solution level could have an opposing influence on the activation energy since the atomic misfits between the solutes and aluminum matrix could generate additional vacancies to promote dislocation climb proceeding by a diffusion

mechanism. However, the individual solute levels are very low at 500°C. Dispersion of second phase particles is another very important factor that influences the value of Q. For Al-Si binary as-cast alloy (Al-13Si), Q ranges from 132 to 139 kJ/mol at the stresses of 4 to 7 MPa (94) For another aluminum alloy, Al-20Si-3Cu-1Mg, Q ranges from 145 to 163 kJ/mol at stress of 80 to 90 MPa using tensile tests (52). The values of Q are higher yet for material consolidated from rapidly solidified powder; for a quinary alloy Al-20Si-7.5Ni-3Cu-1Mg at a stress of 40 to 238 MPa, Q is equal to 233 kJ/mol (59). The above data suggests that with increasing complexity in alloying the volume fraction of second-phase particles, the activation energy increases from that of aluminum self-diffusion which governs the climb of edge dislocations. Such increase is due to the interactions between particles and dislocations.

Characteristically for material consolidated from rapidly solidified powder Al-Fe-V-Si alloys (FVS1212 and FVS0812 (8009)), the microstructure of which consists of very fine nearly spherical $Al_{13}(Fe,V)_3Si$ (silicide) dispersoids uniformly distributed throughout the aluminum matrix These silicide dispersoids are extremely stable at elevated temperatures and they are essentially insoluble upon heating to testing temperatures. These dispersoids are acting as obstacles to the cross slip and climb of dislocations. To by-pass these obstacles, additional energy is required to close extended dislocations and then allow them to leave their original glide planes which definitely increase the Q value. In addition one may expect an increase of 20% in the Q value due to the participation of dynamic recrystallization in the process of deformation (75,78). The additional factor is due to the fact that dynamic recrystallization proceeds by grain boundary movement

instead of vacancy movement (64). The combined effect of the factors discussed above contribute to the high values of Q found for 8009 636 to 650 kJ/mol and FVS1212 606 to 673 kJ/mol.

We now have established constitutive equations for the deformation of the alloys tested:

[8009]: $\varepsilon = (8.1\times10^{33})[\sinh(0.020\sigma)]^{8.91}\exp(-636000/83147T)$ (6.1)

[FVS1212]: $\varepsilon = (1.7\times10^{34})[\sinh(0.020\sigma)]^{5.54}\exp(-606000/83147T)$ (6.2)

If one would compare the values obtained above with commercial purity aluminum (A 2.35x10^{10} s^{-1}, α = 0.030 MPa^{-1} and n = 4 to 4.2) (86) and with those of various grades of conventional aluminum alloys (A = 3.45x10^{8} to 3.8x10^{11} s^{-1}, α 0.012 to 0.037 MPa^{-1} and n = 2.22 to 5.3) (93,94). Higher Q values of Al-Fe-V-Si alloys reflect that dislocations have to overcome higher obstacles (to move in unit time) (81,89)

On the simple basis of the mechanical data, the two alloys appear fairly similar The Q value for FVS1212 is slightly lower than that of 8009 as one would expect from the much heavier alloying. However, one might wonder why the difference is so small for such a large increase in volume fraction of silicides (37% to 24% respectively) In the absence of microscopy, the difference in initial particle distributions or matrix grain structure are not known, nor are their evaluations during deformation The alloys do differ in that FVS1212 has much higher temperature and strain rate dependence (lower n values) which might indicate a much finer microstructure Upon closer examination, one notices the small change in flow stress from 400°C to 300°C (Figure 5.2(b)) for FVS1212 which tends to decrease the linearity of the Arrhenius plot (Figure 5.5) One might be

inclined to draw two lines through the data, one for 600°C to 400°C (hot working) and one for 400°C to 300°C (and lower, cold working) If one determines the slope for the hot working only, then the Q value would be about 900 kJ/mol This is more consistent with the change in volume fraction of silicides (50% increase). However, the values being considered (> 650 kJ/mol) are extremely high compared to conventional alloys (160 to 300 kJ/mol) This indicates scientifically on one hand a marked interference on the restoration mechanisms by the high concentration of dispersoid and technologically the difficulties that would be encountered in forging as the materials cool for the final shaping stage These high Q values suggest that isothermal forging be considered

7. CONCLUSIONS

- The hot working behavior of 8009 and FVS1212 aluminum alloys differed from that of conventional aluminum alloys by exhibiting a distinct stress peak in the stress-strain curves during torsional deformation The stress peak appears as a result of various factors such as deformational heating and localized dynamic recrystallization
- At very high temperatures and low strain rates, deformation proceeded by interaction between work hardening and softening by dynamic recovery
- The ductility of the materials was generally very low in comparison with conventional aluminum alloys, especially at low temperatures and high strain rates Hence, special caution is to be exercised in choosing deformation conditions to prevent cracking during deformation and shaping
- An average strain rate sensitivity (m) of the materials was found Hyperbolic sine equations have been used to give the best fit to the data It shows that these m values are primarily associated with a high activation energy for deformation Since the flow stress of the material is strain rate dependent (increasingly so at higher temperatures), attention should be paid to the settings of deformation parameters to be applied
- Temperature had a profound effect on the stress of the material Arrhenius equations have been derived to describe the peak stress relationship to the temperature The activation energy for deformation was found to be much higher than that of pure aluminum, traditional alloys and other consolidated, rapidly-solidified aluminum alloys

This may have been due to a high volume fraction of silicide dispersoids as major barriers to metal flow.

- There is a linear correlation of the stress multiplier values (α) and slope s values for both alloys in the Arrhenius plots and an inverse correlation between the stress exponent n and α. This gives the net result of Q values independent of α.

REFERENCES

1. Osborn, G.H., Stross, W., 'Analysis of Aluminum Alloys', Chemical Publishing Co., New York, 1953, p.1.

2. Callaioli, G., 'Trends in Technology of Aluminum and Aluminum Alloys', from "The Science of Materials Used in Advanced Technology", edited by Parker, E.R., Colombo, U., A. Wiley - Interscience Publication, John Wiley & Sons, New York, 1973.

3. Gatto, F., 'Research and Development of Aluminum', From same publication as (2).

4. Hunsicker, 'Aluminum Alloys' Symposium on Weight Saving', Material Sciences Laboratory, Lockheed-Georgia Company, April 21-26, 1966, p.43.

5. Steinberg, M.A., 'Materials for the New Generation of Aircraft', From same publication as (2).

6. George, J., Boggs, W., 'Solution to Problems of Aircraft Corrosion and Stress Corrosion', Collected papers of joint Lockheed/Air Transport Association Symposium on long life aircraft, Marrietta, GA, Nov. 12-13, 1968.

7. Shultz, R.A., 'Alcoa Alloys 7075-T76 and 7178-T76', Applications Engineering Division, Aluminum Company of America, Jan 1970.

8. Liedl, G.L., 'The Science of Materials', Scientific American, Volume 255, Number 4, Oct. 1986, p.131.

9. Myshlyaev, M.M., Fedorov, V.M. and Kamalov, M.M, "New High Temperature Powder Metal Alloys", Technology, Publication of Russian Scientific Research Institute of Interdisciplinary Information, Series on Economical Processes Equipment, Materials, Moscow, 1993, pp 38-39.

10. Steinberg, M., "Materials for Aerospace", Scientific American, October 1986, p. 70.

11. Grant, N., 'Rapid Solidification Technology: Particulate Production and Consolidation', From "Industrial Materials Science and Engineering", edited by Murr, L.E., Marcel Dekker, Inc., New York, 1984, p.243-271.

12. NASA Fact Sheet RSC 191-80, 'A Primer on Propellants', Nov. 1980.

13. Adam, C.M., 'Rapid Solidification Processing Method', from "Mechanical Behavior of Rapidly Solidified Materials", proceedings of a symposium by Mechanical Metallurgy

Committee of TMS-AIME and the Flow and Fracture Committee of ASM held at the AIME Annuel Meeting, New York City, New York, Feb. 24-28, 1985, edited by Sastry, S.M.L., MacDonald, B.A., a publication of Metallurgical Society, Inc.

14. Pond, R.B., U.S. Patent 2,825,108; 4 March 1958.

15. Bedell, J., U.S. Patent 3,862,568, Jan. 28, 1975.

16. Narasimhan, M.C., U.S. Patent 4,142,571, March 6, 1979.

17. Gilman, J.F., 'Metallic Glass Materials', from "Industrial Materials Science and Engineering", edited by Murr, L.E., published by Marcel Dekker, Inc., New York, 1984, p.1-27.

18. Olson, G.B., Bourdeau, R.G., DAS, S.K., Kear, B.H., and Adam, C.M., (eds.) 'Rapidly Solidified Crystalline Alloys', Metallurgical Society of AIME, Warrendale, PA, 1985, p.185.

19. Slaughter, E.R., Das, S.K., Mehrabian, R., Kear, B.H., and Cohen, M., (eds.) Proc. 2nd International Conference on Rapid Solidification Processing; Principles and Technologies, Reston, VA, March 23-26, 1980, Claitor's Publishing Division, Baton Rouge, LA, 1980, p.354.

20. Bye, R.L., Kim, N.J., Skinner, D.J., Raybould, D., Brown, A.M. Froes, F.H., and Savage, S.J. (eds.) 'Processing of Structural Metals by Rapid Solidification', American Society for Metals, Metals Park, OH, 1987, p.283.

21. Adam, C.M., Kear, B.H., Giessen, B.C., and Cohen, M. (eds) 'Rapidly Solidified Amorphous and Crystalline Alloys', Materials Research Society Symp. Proc., Vol. 8, Elsevier, New York, 1982, p.411.

22. Jones, H., Mater. Sci. Eng., 5 (1969-1970) 1.

23 Tonejc, A., Bonefacic, A., J. Appl. Phys., 40 (1969) 419.

24. Thursfield, G., Stowell, M.J., J. Mater. Sci., 9 (1974) 1631.

25. Jacobs, M.H., Dogett, A.G., Stowell, M.J., Mater. Sci. Eng., 9 (1974) 1631.

26. Das, S.K., Davis, L.A., 'High Performance Aerospace Alloys via Rapid Solidification Processing', paper presented at the 6th International Conference on Rapidly Quenched Metals, Montreal, August 3-7, 1987, Material Science and Engineering, 98 (1988) 1-12.

27. Hildeman, G.H., U.S. Patent 4,379,719, April 12, 1983.

28. Skinner, D.J., Bye, R.L., Raybould, D., Brown, A.M., Scr. Metall., 20 (1986) 867.

29. Tech. Brief, 1986 (Alcoa).

30. Adam, C.M., Simon, J.W., Langenbeck, S, Mehrabian, R., (ed.) Proc. 3rd International Conference on Rapid Solidification Processing; Principles and Technologies, Gaithersburg, MD, December 1982, National Bureau of Standards, Washington, DC, 1982, p.629.

31. Tech. Bull., 1987 (Allied-Signal Inc., Morristown, NJ).

32. Gilman, P.S., Zedalis, M.S., Peltier, J.M., Das, S.K. AIAA-88-4444 'Rapidly Solidified Aluminum-Transition Metal Alloys for Aerospace Applications', Allied-Signal Inc., Corporate Technology, Morristown, NJ, presented at AIAA/AHS/ASEE Aircraft Design, Systems and Operations Conference Sept. 7-9, 1988/Atlanta, Georgia

33. Angers, L., Chen, Y., Fine, M.E., Weertman, J.R., Zedalis, M.S. Instarke Jr., E.A., Sanders, T.H., (eds.) 'Aluminum Alloys - Physical and Mechanical Properties', Engineering Materials Advisory Services, Warley, 1986, p.321

34. Zedalis, M. Raybould, D., Skinner, D., Das, S.K. in Froes, F H, Savage, S J, (eds.) 'Processing of Structural Metals by Rapid Solidification', ASM, Metals Park, OH, 1987, p.347.

35. Skinner, D.J., Unpublished Data, 1987.

36. Adam, C.M., and Lewis, R E., In Das, S.K., Kear, B.H., and Adam, C.M. (eds.) 'Rapidly Solidified Crystalline Alloys', Metallurgical Society of AIME, Warrendale, PA, 1985, p.157.

37. Lewis, R.J., presented 1989 TMS-AIME Annual Meeting, Las Vegas, NV (1989)

38. Skinner, D.J., Zedalis, M.S., Gilman, P., 'Effect of Strain Rate on Tensile Ductility for a Series of Dispersion-Strengthened Aluminum Based Alloys', Materials Science and Engineering, A119 (1989) 81-86.

39. Pharr, G.M., Zedalis, M.S., Skinner, D.J., Gilman, P.S., Rice Uni, Department of Material Science, P.O. Box 1892, Houston, Texas, 77251, Allied-Signal Inc., Metals and Ceramics Lab., P.O. Box 1021R, Morristown, NJ 07960

40. Mukherjee, A.K., Bird, J.E., Dorn, J.E., in 'Quantitative Relations Between Properties and Microstructure', Brandon, D.G., Rosen, A., (eds.), Israel Univ Press, Jerusalem, 255 (1969).

41. Lewis, R., 'Elevated Temperature Creep Deformation of a Rapidly Solidified Al-Fe-V-Si Alloy', (in press).

42. Gilman, P.S., Zedalis, M.S., Peltier, J.M., Das, 'The Joining of Rapidly Solidified Aluminum-Iron-Vanadum-Silicon Alloys for Aerospace Applications', from 1989 Advances in Powder Metallurgy, Volumes 1-3, Metal Powder Industries Federation, Princeton, NJ.

43. From 'Aluminum Alloy Development will Improve Performance', Aviation Week and Space Technology, Oct. 3, 1988, p.57.

44. Sheridan, J.J., 'High Temperature Aluminum Applications', Allied-Signal Aerospace Section Review, 27 March 1990.

45. Raybould, D., Ubvardy, S., Zedalis, M.S., Das, S.K., presented 2nd International Conference on Rapidly Solidified Materials, San Diego, CA, March 7-10, 1988.

46. Adam, C.M., Das, S.K., presented Fourth Conference on Rapid Solidification Processing Principles and Technologies, Univ. of CA, Santa Barbara, Dec. 15-18, 1986.

47. Skinner, D J., presented 1988 TMS Annual Meeting, Phoenix, AZ, January 25-28, 1988.

48 Zedalis, M.S., 'Rapidly Solidified High Temperature Aluminum Composites', Metals & Ceramics Laboratory, Research & Technology, Morristown, NJ 07962, March 27, 1990.

49. "PM and Spray Deposition of Al-Si-Fe-2Ni Alloy", Metal Powder Report, vol. 45, p. 403, 1990.

50 Smith, P , Powder Metallurgy, vol. 33, p. 202, 1990.

51. Zhou, J. and Duszczyk, J., Journal of Materials Shaping Technology, vol. 6, p. 241, 1989.

52. Zhou, J., Duszczyk, J. and Korevaar, B.M., Journal of Materials Shaping Technology, vol 8, p 91, 1990.

53. Zhou, J., Duszczyk, J. and Korevaar, B.M., "Advanced Technology of Plasticity 1990", Proceedings of the 3rd International Confernce on Technology of Plasticity, Kyoto, Japan, July 1990, vol. 2, p. 957.

54. Hirai, Y., Kanayama, K., Nakamura, M., Sano, H. and Kubo, K., Aluminium, vol. 66, p. 389, 1990.

55. Pickens, R., Langan, T.J., England, R.O. and Liebson, M., "A Study of the HotWorking Behaviour of SiC-Al Alloy Composites and Their Matrix Alloys by Hot Torsion Testing", Metallurgical Transactions A, vol. 18A, February 1987, pp 303-312.

56. Conrod, K. and McQueen, H.J., "Hot Working Characteristics of Al-0.65%Fe and Al-0.5%Fe-0.5%Co Conductor Alloys", Proceedings of the International Conference on Aluminum Alloys, Their Physical and Mechanical Properties, Charlottesville, VA, USA, June 1986, edited by Starke Jr., E.A. and Sanders Jr., T H , vol. 1, pp 435-447.

57. Espedal, A., Gjestland, H., Ryum, N. and McQueen, H.J., "Hot Deformation of Al-Mg-Si Alloys", Scandinavian Journal of Metals, vol. 18, 1989, pp 131-136

58. Evangelista, E., Forcellesee, A., Gabrielli, F. and Mengucci, P., "Hot Workability of Some Heat Treatable Aluminum Alloys, Hot Deformation of Aluminum Alloys, TMS-AIME, Warrendale, PA, 1991, pp 121-139.

59. Zhou, J., Duszczyk, J., Korevaar, B.M. and Verlinden, B , "Characterization of the Hot Working Behaviour of a P/M Al-20Si-7.5Ni-3Cu-1Mg Alloys by Hot Torsion", Journal of Material Science, vol. 27, 1992, pp 4247-4260

60. Kassner, M.E., Myshlyaev, M.M. and McQueen, H J . Material Science and Engineering, vol. 108A, 1989, p. 45.

61. McQueen, H.J., Evangelista, E. and Kassner, M.E., "The Classification and Determination of Restoration Mechanisms in Hot Working of Al Alloys", Zeitschrift fur Metallkunde, vol. 82, no. 5, 1991, pp 336-345.

62. McQueen, H.J. and Conrod, K., "Recovery and Recrystallization in the Hot Working of Al Alloys", Microstructural Control in Al Alloy Processing, TMS-AIME, Warrendale, PA, 1986, pp 197-220.

63. Zhou, J., Duszczyk, J and Korevaar, B.M., Journal of Material Science, vol 27, 1992, p. 3.

64. McQueen, H.J., Evangelista, E., Bowles, J. and Crawford, G , Metal Science, vol. 18, 1984, p. 395.

65. McQueen, H.J., "Micromechanisms of Dynamic Softening in Aluminum Alloys During Hot Working", Hot Deformation of Aluminum Alloys, TMS-AIME, Warrendale, PA, 1991, pp 31-54.

66. Orsund, R. and Nes, E., Annealing Processes - Recovery, Recrystallization and Grain Growth, Proceedings of the 7th Riso International Symposium on Metallurgy and

Materials Science, Rosklide, Denmark, September 1986, edited by Hansen, N., Juul Jensen, D., Leffers, T. and Ralph, B., p. 475.

67. Verlinden, B, Wouters, P, McQueen, H.J., Aernouldt, E., Delaey, L. and Cauwenberg, S., Material Science and Engineering, vol. 123A, 1990, p. 229.

68 Wouters, P., Verlinden, B, McQueen, H.J., Aernouldt, E., Delaey, L. and Cauwenberg, S., Material Science and Engineering, vol. 123A, 1990, p. 239.

69. Monldofo, L.F., "Aluminum Alloys, Structure and Properties (Butterworths, London, 1976) pp 509.

70. Evangelista, E. Mengucci, P., Di Russo, E., Fiorini, P. and McQueen, H.J., Proceedings of the 8th International Light Metals Congress, Leoben, Vienna, Austria, June 1987, edited by Jeglitsch, F., p. 544.

71. Zhou, J. and Duszczyk, D., Journal of Material Science, vol. 25, 1990, p. 4541.

72. Altan, A. Oh, O. and Gegel, H., "Metal Forming, Fundamentals and Applications", (ASM, Metals Park, OH, 1983), p. 65.

73. Wu, M Y. and Sherby, O D., Scripta Metallurgica, vol. 18, 1984, p. 773.

74 Hamilton, C.H. and Ghosh, A.K., Metallurgical Transactions A, vol 11A, 1980, p. 1494.

75. McQueen, H.J., "Deformation Mechanisms in Hot Working", Journal of Metals, vol. 18, no. 4, April 1968, pp 31-38.

76. McQueen, H.J., Wong, W.A. and Jonas, J.J., "Deformation of Aluminum at High Temperature and Strain Rates", Canadian Journal of Physics, vol. 45, 1967, pp 1225-1234.

77 McQueen, H J. and Tegart, W.J.M., "The Deformation of Metals at High Temperatures", Scientific American, vol. 232, no. 4, April 1975, pp 116-124.

78 McQueen, H.J , "Dynamic Recovery and Its Relation to Other Restoration Mechanisms", Metallurgia I Odlewnictwo, vol. 5, no. 3, 1979, pp 421-451.

79. Luton, M J., "Workability Testing Techniques", edited by Dieter, G.E. (ASM, Metals Park, OH, 1984) p. 95.

80. Fulop, S., Cadien, K., Luton M.J. and McQueen, H.J., "A Servo-Controlled Hydraulic Torsion Machine for Hot Working Studies", Journal of Testing and Evaluation, vol. 5, 1977, pp 419-426.

81. Yiu, H.L. and Sheppard, T., Material Science and Technology, vol. 1, 1985, p. 209.

82. Sano, H., Abo, M. And Yamauchi, S., Sumitomo Light Metals Technology Report, vol 30, 1989, p. 24.

83. Bernstein, M.L. and Zaimovsky, V.A., Mehanical Properties of Metals, MIR Publishers, Moscow, 1983, pp 203-206.

84. Chung, D.W. and Cahoon, J.R., Metal Science, vol.13, 1979, p. 635.

85. Alden, T.H., Acta Metallurgica, vol. 37, 1989, p. 1683.

86. Nowick, A.S., Journal of Applied Physics, vol. 22, 1959, pp 1182-1186

87. Sherby, O.D., Klundt, R.H. and Miller, A.K., Metallurgical Transactions A, vol. 8A, 1987, p. 843.

88. Wong, W.A. and Jonas, J.J.,Trans. Metallurgical Society, AIME, vol 242, 1968, p. 2271

89. Ayres, R.A., Metallurgical Transactions A, vol. 8A, 1977, p. 487.

90. Olla, P. and Virdis, P.F., Metallurgical Transactions A, vol 18A, 1987, p 293.

91. Avramovic-Cingara, G., McQueen, H.J., Salama, A. And McNelley, T.R , Scripta Metallurgica, vol. 23, 1989, p. 273.

92. Cotrell, A.H., "Creep and Ageing Effects in Solid Solutions", From Creep and Facture of Metals at High Temperatures, National Physics Laboratory, Fro Proceedings on the Creep and Fracture of Metals at High Temperatures, 1954, Teddington, Middlesex, p 143

93. Rao, K.P. and Prasad, Y.V.R.K., Aluminium, vol. 60, 1984, p 184.

94. Chung, D.W. and Cahoon, J R., Metal Science, vol 13, 1979, p 635

95. Bailey, J.A., Haas, S.L. and Shah, M.K., International Journal of Mechanical Science, vol 14, 1972, p. 735.

96. Sheppard, T., "Extrusion, Scientific and Technical Developments", eds Lang, G , Castle, A.F., Bauser, M. And Scharf, G., (Deutsche Gesellschaft fur Metallkunde), 1981, p 17.